Acoustofluidic Manipulation for Diagnosis and Drug Loading

by

Zeyu Wang

Department of Mechanical Engineering & Material Science
Duke University

Date:_____
Approved:

_____
Tony Jun Huang, Advisor

_____
W. Daniel Stamer

_____
Xiao-Fan Wang

_____
Benjamin Biron Yellen

_____

Dissertation submitted in partial fulfillment of
the requirements for the degree of Doctor
of Philosophy in the Department of
Mechanical Engineering & Material Science in the Graduate School
of Duke University

2021

ABSTRACT

Acoustofluidic Manipulation for Diagnosis and Drug Loading

by

Zeyu Wang

Department of Mechanical Engineering & Material Science
Duke University

Date:_____
Approved:

_____
Tony Jun Huang, Supervisor

_____
W. Daniel Stamer

_____
Xiao-Fan Wang

_____
Benjamin Biron Yellen

_____

An abstract of a dissertation submitted in partial
fulfillment of the requirements for the degree
of Doctor of Philosophy in the Department of
Mechanical Engineering & Material Science in the Graduate School of
Duke University

2021

Copyright by
Zeyu Wang
2021

Abstract

Showing increased application in biological and medical fields, acoustofluidics is a combined technology between acoustics and microfluidics. The core function of acoustofluidics is a label-free and contact-free manipulation of particles in the fluid, which can be applied as active separation, active mixing, and active concentration. Since in therapeutic and diagnostic applications, contamination in the samples can significantly interference analysis results and treatment outcome, proper per-screening of the sample can significantly decrease the target detection threshold and avoiding interferences come from noise and misreading. The acoustofluidic technology derive a particle manipulation based on physical properties of the particles and fluids, specifically, the size of the particle, densities for the particles and fluid, and the viscosity of the fluid, which generate a screening system that can separate particles with different sizes and densities. By utilizing this property, acoustofluidics has been applied on separating multiple biological particles and objects including circulating cancer cells, red blood cells, and multiple populations of vesicles. These reagent-free and contact-free separations have been demonstrated biocompatible for cells and vesicles and can conserve the cell viabilities and vesicle cargoes including DNA, miRNA, and proteins. However, current achievements on acoustofluidic manipulation focus on general analysis of the separated components, which are not disease specific biomarkers, and the body fluid using for separation are

limited to blood and artificial isotonic solutions including phosphate-buffered saline. Although these works demonstrated acoustofluidic technology is eligible for separating bio-particles that have diagnosis and therapeutic functions, lack of real cases related applications and diseases specific investigations still make the technology's application abilities being restricted to possibilities but not promised functions.

To deeply investigate and demonstrate the acoustofluidic technology's potential on diagnostic application, the technology was evaluated by using samples related with multiple specific diseases. Since the acoustofluidic technology has been demonstrated eligible for isolating exosomes, which are 50-200 nm vesicles secreted from cells, pathology related exosomes were selected for diagnostic application investigation. Exosomes' vesicle structures make them ideal candidate for diagnosis, since vesicles formed by lipid bilayer membrane contain both proteins or nucleic acids as cargoes inside and transmembrane or membrane proteins and polysaccharides on the surface. Furthermore, the forming and secreting pathologies of exosomes are highly dependent on endocytosis and exocytosis pathologies, which are influenced by cellular metabolism. Exosomes' cargoes have been found specifically correlated with secreting cells populations, indicates depending on types of cells, like tumor cells or stem cells, the secreted exosomes will contain different molecules that can be used as biomarkers for reversed identifying secreting cells. Except high values on biological and medical research and applications, exosomes' small size makes the vesicles difficult for isolation and

increase the cost on both equipment and time aspects. Since acoustofluidics provides an active approach for separating nanometer sized particles and the isolation is a continuous procedure, the simple and rapid exosome isolation the acoustofluidics can provide makes the technology high valuable. Considering these improvements, the acoustofluidics can provide on exosome related fields, demonstrating acoustofluidic devices separated exosomes containing disease biomarkers and could be used for diagnostic applications become a necessary step for validating the technology's ability.

In this dissertation, the first attempt for validating acoustofluidic exosome separation's diagnostic potential was made for isolating salivary exosomes aimed at human papillomavirus (HPV) induced oropharyngeal cancer diagnosis. Different with previous research that worked on blood exosome separation, a unique property of this study is achieving exosome separation from saliva, which is a more unstable system on components and physical properties than blood. By isolating salivary exosome using the acoustofluidic technology and processing down-stream digital droplet polymerase chain reaction (PCR) analysis, HPV-16 virus, which has been found can induce oropharyngeal cancer, was found majorly distributed in isolated exosome fractions. Since saliva has complex components that cause inaccuracy analysis result, the application of acoustofluidic technology can increase the diagnostic sensitive and enable saliva based liquid biopsy for early screening of oropharyngeal cancer.

In the next work, we further demonstrate the acoustofluidic technology's advantage on rapid isolation of exosomes benefits the time sensitive diagnosis. The acoustofluidic devices were applied for isolating exosomes from mice models that were induced to traumatic brain injury (TBI), which can develop to chronic diseases or deteriorate in short term. Since these outcomes induced by improper or untimely treatments, fast screening of TBI becomes critical for achieving ideal therapeutic outcomes. By collecting plasma from mice and deriving exosome isolation through the acoustofluidics devices, isolated exosome samples with less contamination were found compared with original plasma. Protein analysis further indicates isolated exosomes keeps several exosome specific and neuron damage specific proteins, indicates the acoustofluidic technology is biocompatible and low harmful for exosome structures and components. High isolation purity achieved by the acoustofluidic technology also benefits downstream analysis by decreasing detection noise. In flow cytometer analysis, the acoustofluidic devices isolated exosomes demonstrated TBI disease biomarker increasing in 24 h after the mice were induced to TBI, while the plasma sample cannot demonstrate this tendency. The success of revealing early stage TBI biomarker changes indicates the acoustofluidic technology not only can benefit diagnosis, but also eligible for achieving diagnosis in a very early stage of the pathology.

Since the acoustofluidic technology had demonstrated a promising performance on biocompatibility and rapid separation, other time-sensitive samples, including live

virus was applied for evaluating the device's performance. To achieve better control and eliminate irrelevant variable, we use cultured reverse transcription virus that is used for mammal cells transfection as target for isolation. The acoustofluidic technology showed reliable isolation of the murine leukemia virus and majority of the virus particles were separated out from the original sample. Virus viability was further validated robust based on the transfection experiments that using acoustofluidic separated virus and original virus samples demonstrated similar level transfection rates. This work indicates except vesicles like exosomes, the acoustofluidic technology is also eligible for isolating virus and keeping its viability, which significantly expands the application of the technology.

Next, to expend the acoustofluidic technology's functions, we utilized the concentration and manipulation ability of the device for deriving high efficiency membrane degradation. By generating strong microstreaming and microstreaming derived shear stress, the acoustofluidic devices can generate strong vertex flow fields in channel that can capture and lyse mammal cells. Since the acoustofluidic cell lysis is totally a physical process without participation of any chemical reagent and demonstrates a high lysis efficiency, this acoustofluidics application has potential for achieving high efficiency cell analysis.

Since the acoustofluidic technology has demonstrated potential for concentration and lysis effect by generating high flow rate microstreaming vertex, we further investigated whether similar effect can derive exosome concentration and lysis. By

generating acoustofluidic vertex in droplet containing exosome, nanoparticles, and small molecule drugs, exosome concentration and lysis effects were utilized for high efficiency drug loading and carrier encapsulation. Derived by the acoustofluidic concentration effect, the porous nanoparticles and drug molecules are concentrated in small area of the fluid system and this active concentration increasing induces a high drug loading rate. Simultaneously, the acoustofluidic vertex disrupts exosome membrane and concentrates exosomes with the nanoparticles, which induces exosome encapsulation. These exosome encapsulated drug-loaded nanoparticles demonstrate high intake rate of cells and derive more efficient drug delivery rate. Since the drug loading and exosome encapsulation are physical processes, the acoustofluidic technology derived particle manipulation has potential for deriving loading and encapsulation for large varieties of drugs, particles, and vesicles, which significantly expand the technology's application.

Dedication

The dissertation is dedicated to my family and lab members.

Contents

Abstract iv

List of Tables xvi

List of Figures xvii

Acknowledgements xx

1. Introduction 1

1.1 Background of microfluidics 1

1.2 Acoustofluidics: integration of acoustics to microfluidics 11

1.2.1 Types of acoustofluidic separation technology 14

1.2.2 Mechanisms of acoustofluidic manipulation 20

1.3 Application of acoustofluidic technology 23

1.3.1 Acoustofluidic apheresis 23

1.3.2 Acoustofluidics cell manipulation 28

1.3.3 Acoustofluidic extracellular vesicle separation 33

1.4 Objectives and dissertation outline 37

2. Acoustofluidic salivary exosome separation 41

2.1 Motivation 42

2.2 Mechanism and system 44

2.3 Experiment methods 46

2.3.1 Device fabrication and simulation 46

2.3.2 Saliva sample collection 47

2.3.3 Acoustofluidic separation of particles and saliva samples 48

2.3.4 Downstream validation 49

2.4 Results and discussion 51

2.4.1 High viscosity fluid influence on acoustofluidic separation 51

2.4.2 Salivary exosome isolation and validation 54

2.4.3 Acoustofluidic salivary exosome isolation yield 56

2.4.5 Analysis of HPV virus from exosome separated from HPV-OPC patient samples 57

2.5 Conclusion 59

3. Acoustofluidic exosome separation for TBI diagnosis 65

3.1 Motivation 66

3.2 Mechanism and system 69

3.3 Experiment methods 71

3.3.1 Acoustofluidic device fabrication 71

3.3.2 TBI animal preparation and plasma collection 72

3.3.3 Acoustofluidic separation and isolated exosome validation 73

3.3.4 TBI pathology related exosome detection 75

3.4 Results and discussion 76

3.4.1 Isolated exosomes validation 76

3.4.2 Astrocytes TBI exosome intake 77

3.4.3 Validate the feasibility of TBI exosome detection using flow cytometer 78

3.4.4 TBI related exosomes population change after TBI 81

3.5 Conclusion 86

4. Acoustofluidic live virus separation 91

4.1 Motivation 92

4.2 Mechanism and system 97

4.3 Experiment methods 100

4.3.1 Acoustofluidic device fabrication 100

4.3.2 Live virus culture 101

4.3.3 Virus separation and downstream validation 101

4.4 Results and discussion 102

4.4.1 Distribution of acoustic field in the channel 102

4.4.2 Virus separation validation 105

4.4.3 Virus infection analysis 108

4.5 Conclusion 109

5. Acoustofluidic homogenizator for cell lysis 111

5.1 Motivation 111

5.2 Mechanism and design 116

5.3 Experiment methods 119

5.3.1 Acoustofluidic sharp-edge homogenizator fabrication 119

5.3.2 Acoustofluidic cell lysis and staining 120

5.3.3 Lysis efficiency analysis 121

5.3.4 Lysis product validation 123

5.4 Results and discussion 125

5.4.1 Acoustic microstreaming and shear stress distribution 125

5.4.2 Validate role of sharp-edge in homogenization 126

5.4.3 Lysis efficiency influenced by device power 129

5.4.4 Flow rate influence on lysis efficiency 131

5.4.5 Downstream lysis product analysis 132

5.4.6 Malaria infected RBCs lysis and analysis 133

5.5 Conclusion 135

6. Acoustofluidic drug loading 141

6.1 Motivation 142

6.2 Mechanism and system 145

6.3 Experiment methods 146

6.3.1 Device fabrication 146

6.3.2 *Silicon nanoparticle synthesis* 147

6.3.3 Acoustic droplet rotation encapsulation and drug loading 148

6.3.4 Vesicle encapsulation evaluation 149

6.3.5 Cell intake experiment 150

6.4 Results and discussion 151

6.4.1 Acoustic streaming and shear stress distribution in the device 151

6.4.2 Acoustofluidics induced concentration effect 152

6.4.3 Acoustic rotation increases drug loading rate 154

6.4.4 Acoustic rotation derived vesicle encapsulation 156

6.4.5 Acoustofluidic exosome encapsulation enhances endocytosis 159

6.4.6 Drug intake improvement and proliferation inhibition achieved by acoustofluidic droplet rotation derived drug loading and vesicle encapsulation .. 162

6.4.7 Pathway of acoustofluidic droplet rotation derived drug delivery 166

6.5 Conclusion 167

7. Conclusions 170

7.1 Achievement 170

7.2 Prospect 173

References 175

Biography 195

List of Tables

Table 1 Comparision between passive and active microfluidics 10

Table 2 Types of acoustofluidic manipulation technologies..... 18

Table 3 Primers for PCR validation 124

List of Figures

Figure 1-1: The generic design of the SPLITT platform. 8

Figure 1-2: Mechanism of acoustic wave generation by piezoelectric materials. 16

Figure 1-3: Schematics of bulk wave and standing wave separation techniques. 18

Figure 1-4: Acoustofluidic apheresis technologies. 26

Figure 1-5: Schematics of acoustofluidic manipulation technologies. 32

Figure 1-6: Acoustofluidic CTC separation technologies. 32

Figure 1-7: Acoustofluidic technologies for nanometer scale particles separation. 35

Figure 1-8: Acoustofluidic exosome isolation technologies. 37

Figure 2-1: Schematics and mechanism of the device 45

Figure 2-2: Particle isolation using different size polystyrene particles mixture. 62

Figure 2-3: Fluid viscosity's influence on particles separation. 53

Figure 2-4: Characterization of acoustofluidic chip exosome isolation. 55

Figure 2-5: Size distribution of saliva isolation products from different outlets. 56

Figure 2-6: Comparison of yields of exosome from acoustofluidic separation technology and ultracentrifugation (UC) method. 57

Figure 2-7: Detection of HPV16 DNA in acoustofluidic separated saliva exosome of HPV16 positive OPC patients. 59

Figure 3-1: Schematics detailing the process of detecting exosomal biomarkers for TBI from the blood of animal models. 70

Figure 3-2: Isolated samples validation. 77

Figure 3-3: C8-D1A astrocytes cultured with isolated exosomes from mice plasma. 78

Figure 3-4: Single staining of exosomes isolated from plasma collected 24 h after TBI treatment. 80

Figure 3-5: CD63+/GFAP- exosomes population change after TBI treatment. 83

Figure 3-6: CD63+/GFAP- exosomes population change after TBI treatment of mouse 2. 84

Figure 3-7: CD63+/GFAP- exosomes population change after TBI treatment of mouse 3. 85

Figure 3-8: Comparison of CD63+/GFAP+ events of acoustofluidics isolated exosomes and plasma samples. 86

Figure 4-1: Schematics of normal IDTs and dummy finger IDTs difference when deriving acoustofluidic separation. 99

Figure 4-2: Simulation of acoustic field generated by different IDT designs. 103

Figure 4-3: Experimental validation of acoustic field distribution in the acoustofluidic devices. 105

Figure 4-4: Validation of acoustofluidic virus isolation by NTA and TEM. 107

Figure 4-5: Virus viability validation. 108

Figure 5-1: Overview of the homogenizator structure and working pattern. 119

Figure 5-2: In-channel microstreaming and shear stress distribution. 126

Figure 5-3: Temperature during device working and comparison between no-sharp-edge device and sharp-edge device when acoustic transducer is on and off.. 128

Figure 5-4: Acoustic transducer power influence on lysis efficiency. 130

Figure 5-5: Flow rate influence on lysis efficiency. 132

Figure 5-6: Downstream lysis product analysis results 133

Figure 5-7: Characterization of malaria infected cell lysis product 135

Figure 6-1: Schematics of the acoustofluidic droplet rotation drug loading device. 148

Figure 6-2: Microstreaming in the droplet induce shear stress 152

Figure 6-3: Microstreaming in the droplet induce concentration 153

Figure 6-4: Acoustic droplet rotation enhances DOX loading rate to porous silicon nanoparticles. 155

Figure 6-5: Exosomes encapsulate different sizes and shapes silicon nanoparticles after acoustic droplet rotation 157

Figure 6-6: Exosome encapsulation morphological and protein validation 159

Figure 6-7: HeLa endocytosis of 50 nm silicon rod nanoparticles is enhanced after acoustic droplet rotation induced exosome encapsulation. 160

Figure 6-8: HeLa endocytosis of 100 nm silicon rod nanoparticles is enhanced after acoustic droplet rotation induced exosome encapsulation 161

Figure 6-9: HeLa endocytosis of 200 nm silicon rod nanoparticles is enhanced after acoustic droplet rotation induced exosome encapsulation 161

Figure 6-10: Acoustic droplet rotation derived exosome encapsulation and drug loading enhance DOX intake rate and inhibit cell proliferation 163

Figure 6-11: Acoustic droplet rotation derived exosome encapsulation and drug loading enhance DOX intake rate and inhibit cell proliferation 164

Figure 6-12 Acoustic droplet rotation derived exosome encapsulation and drug loading enhance DOX intake rate and inhibit cell proliferation 165

Figure 6-13: DOX loaded in exosome encapsulated silicon nanoparticles through acoustic droplet rotation is intake by endocytosis. 166

Acknowledgements

First and foremost, I would like to express my most sincere appreciate to my Ph.D. advisor, Prof. Tony Jun Huang, for his guidance and support. The completion of this dissertation is under his well guidance and he provide me trust for conducting my research in an ideal environment. During my Ph. D. journey, his encouragement is important and supports me deal with multiple challenges in the research and academic fields.

I would like to thank my dissertation committee, Prof. W. Daniel Stamer, Prof. Xiao-Fan Wang, Prof. Benjamin Yellen, and Prof. Tony Jun Huang for their valuable suggestions on my dissertation work. I would also like to acknowledge Prof. David T. Wong, Prof. Daniel T. Laskowitz, Prof. Feng Li, and Prof. Haichen Wang for their insightful suggestions and strong support to my research.

Additionally, I would like to thank all the past and present members of the Acoustofluidics group. My sincere thanks to Dr. Po-Hsun Huang, Dr. Zhenhua Tian, Dr. Mengxi Wu, Dr. Nanjing Hao, Dr. Peiran Zhang, Joseph Rufo, Shujie Yang, Yuyang Gu, Chuyi Chen, Shuaixiang Zhao, Haodong Zhu, Geonsoo Jin, Jianping Xia, Zhehan Ma, Kaichun Yang, Ruoyu Zhong, Ty D. Naquin, Ryan Becker and Joseph T. Rich for their helps.

I would also want to thank the Department of Mechanical Engineering and Materials Science at Duke University for offering me the opportunity to work and study here. I also want to thank various funding agencies that supports my study and research.

1. Introduction

Acoustofluidics is a combination of acoustics and microfluidics for integrating unique functions in these two different fields. Once developed, this technology has demonstrated great potential and widely application in life science. Currently acoustofluidics technology has been applied for cell screening, tissue manipulation, vesicle isolation, and chemical detection, which has covered the majority aspects in the biomedical analysis field (Ozcelik et al., 2018). As an interdisciplinary technology that integrates technology from two fields, to understand the importance and future role of this technology, it is necessary for understanding the initial motivation and the development tendency of acoustofluidics. In this chapter the background of microfluidics and acoustofluidcs will be introduced, and for understanding the reason for integrating acoustics into microfluidics, current developed acoustofluidic devices and their functions will be introduced.

1.1 Background of microfluidics

The beginning of microfluidics development is the requirement of constructing and observing micro-reaction, which can reveal rapid reaction processes and demonstrate quantitative relationship between participants and products of the reactions (Gravesen et al., 1993). To meet the strict requirements of building and observing micro-reaction processes, the design of the reaction systems developed from chemical aspects, which mainly focused on molecular level including molecular dynamics, to physical aspects that

aim at stable the reaction and observation environment (Jensen, 2001). Since a stable reaction system required each participants of the reaction contacts in a small and stable rate, and observation requires reaction area limited to microscale level for integrating sensitive detection technologies including optical and electrical methods, the micro-reaction systems were developed to small reactions in micro rooms and channels, which are also called 'lab-on-chips' (Abgrall et al., 2007). The first of and the most important reason of using microscale channels is the extreme controllable ability on fluid manipulations, since in large scale fluid system, partial instability is inevitable and frequently happened (Landahl et al., 1989). These turbulence and random processed could cause uneven contacts rates between substrates and the derived uneven reaction rates further caused uneven releasing of reaction energy, which further interferes the fluid dynamics in the reaction system (Jones et al., 1982). Different with the large-scale reaction system, in the microchannel the fluid field is more stable and predictable, and the stable laminar flow induces substrates solved in different flow can generate reaction in a controllable and stable rate (Löwe et al., 1999). The stability derived by the microscale of the microfluidic devices enables the precise and efficient control of the reagents and samples, and micrometer channels or reactors sealed in tiny transparent materials benefit observation and analysis. Benefits from these unique advantages, microfluidics quickly emerged as an important technology in analytical chemistry, medicine, biomedical engineering, biochemistry, and molecular biology fields since the technology was

introduced in 1990s (Yamada et al., 2004, Yamada et al., 2005, Sethu et al., 2006, VanDelinder et al., 2006, Choi et al., 2007). Benefited from the advantage of accuracy and efficiency derived from tiny volume reaction system precise manipulation, microfluidic technology has made great contribution to analytical areas and successful commercialized in multiple well known analytical projects including human genome project (Volpatti et al., 2014).

Beyond the tremendous successes in micro-reaction and analytical fields, microfluidic technology further utilized its groundbreaking stable and precise manipulation features in particle manipulation and screening fields, which are cell manipulation and screening more specifically. In recent decades, application and study of microfluidics demonstrated obvious tendency that changing from molecular analysis to cellular level separation including circulating tumor cells, immune cells, and stem cells separation (Zhang et al., 2012, Chokkalingam et al., 2013, Dong et al., 2013). This shifting of research focus of microfluidics shows an internal consistency with the develop direction of biology and biomedicine in the postgenomic era. Different with genomic era, when studies are aimed at genome sequence analysis and basic metabolic mechanisms widely appear, researches in postgenomic era are focused on the regulation mechanisms and the function diversity that derived from gene expression differences like apparent genetics (Kaput et al., 2004). Continues to this day, postgenomic era demonstrating a tendency that study the organism as a whole system. Since cells are the basic unit of the

organism, cellular studies that can explain the mechanisms of growing, developing, and pathology events become the major direction (Peltonen et al., 2001, Loscalzo et al., 2007, Nishikawa et al., 2007). This focus shifting further induce the research and application direction change in the microfluidic field and the microfluidic systems for cellular biology research have developed to the integrated platforms that contain multiple function units for separation, preparation, and analysis. Among these different modules, microfluidic separation modules that isolate specific targets and eliminate contamination have been developed to a critical unit as important as detection unit (Bhagat et al., 2010, Gossett et al., 2010). This change of development focus is also due to the requirement from application side, since with the development of cellular biology, it is found that the cells that trigger critical biological events usually belong to the less abundance populations. In cancer progress, the metastasis and drug resistance have been founded due to small number of cancer stem cells, and in immune reactions, small population of immune cells including dendritic cells and helper T cells regulate the complex immune response pathways (Clarke et al., 2006, Chaplin, 2010). However, in majority of the biological samples, compared with large amount of total cell populations, these target cells only have low abundance levels and induce difficulties for investigation. Furthermore, the signals from least abundance cell populations may covered by the high populations and cause the difficulty of downstream analysis. For example, CTC has been demonstrated deriving critical role of tumor metasitasis, which directly cause cancer deterioration and

poor therapeutic outcomes (Paterlini-Brechot et al., 2007). However, compared to billions of cells in patient peripheral blood, CTCs only have extreme small percentage. Although the study of CTC can reveal tumor heterogeneity and provide more accurate prognosis, which can both guide to more efficient treatment, CTC based clinical applications are still in a starting stage. To face the necessary of collection and analysis rare population targets, which initiated by the new requirement in postgenomic era, the separation function of microfluidic technology becomes important.

With the development of biomedical and biological studies, microfluidics has also been utilized on subcellular scale structures separation and analysis. Subcellular structures, especially extracellular vesicles, has emerged as important participants in intracellular communication and regulation events (Pickett et al., 2006, Verhage et al., 2008). Since these structures enable the material exchange between cells and containing specific cargo and biomarker depending on secreting cells, they have attracted increasing attention in biological research. Large amount of work has revealed subcellular vesicles' great potential for deriving tissue regeneration, cancer early diagnosis, and immune activation (György et al., 2011, Andaloussi et al., 2013, Robbins et al., 2014). However, like the difficulty of rare population cells studies, subcellular vesicles samples are also contaminated by vast components in biofluids including cell debris, platelets, apoptosis bodies, and lipoproteins. Lack of isolation method for collecting specific population of subcellular vesicles has become the major obstacle for bring subcellular vesicles to clinical

therapeutic and diagnostic applications (Tkach et al., 2018). Since microfluidic technology's significant advantage on precise manipulation and small volume sample processing, which naturally meet the requirements of low population subcellular vesicle study, this situation further promote the study that develop microfluidics as a separation method.

The requirement of separating specific population of cells or subcellular vesicles promotes the development of acoustofluidic technology as an innovative separation tool. This tendency also leads the microfluidic separation approaches developing from passive separation, which utilizes channel structure generated fluid field and hydrodynamic force, to active separation that integrates new physical effects, including optical, magnetical , and electrical force, for achieving separation (Sajeesh et al., 2014, Shields IV et al., 2015). The main separation mechanism of the passive microfluidic separation is hydrodynamic force, which can be generated from laminar flow and geometry structures in the channel. By applying the mechanism that different physical properties particles will migrate to different layer of laminar flow and micro-structures in the channel divide the laminar flow layers and achieve particles separation. By utilizing the structure-flow-particle interaction, passive microfluidic separation technology has been able to isolate particles and cells from biosamples based on density, size, shape, deformability, and other features. Currently passive microfluidic separation includes hydrodynamic filtration, cross-flow filtration, pinch flow fractionation, deterministic lateral displacement, micro

centrifugation, inertial microfluidics, and not limited to these (Huang et al., 2004, Yamada et al., 2004, Yamada et al., 2005, Sethu et al., 2006, Choi et al., 2007, Chen et al., 2008, Mach et al., 2010, Hou et al., 2013). Since there is not need for introducing external force or effects into the system except the force for driving the flow field, the most obvious advantages of passive microfluidic technologies are free from giant energy supplying units and simple design and setup. However, only replying on hydrodynamic effects also cause passive microfluidic technologies need long specifically designed channels for deriving structure-fluid interactions that are obvious enough for generating separation effects. Furthermore, passive separation also been disrupted by low resolution problems, which means the separated particles by the technology should demonstrate very significant differences on physical properties. These problems induce low efficiencies of the passive microfluidic technology and bring the necessary of introducing external effects that can enhance the separation outcomes, which lead to the development of the active microfluidic separation technologies.

The purpose of integrating external effects in microfluidic system is improving separation efficiency and flexibility, since extra fields in the channels derive more field-fluid and field-particle interactions that can derive higher precise manipulation. The external mechanisms have been utilized on microfluidic channel includes electrical force, dielectrophoretic force, optical force, and magnetic force (MacDonald et al., 2003, Narayanan et al., 2006, Kim et al., 2008). Compared with passive microfluidic separation

technologies, active separation methods are less relied on microstructures in the channel but focusing on the stable fluid in microfluidic devices. The most common design of the active microfluidic separation platform is the split-flow lateral-transport thin (SPLITT) platform developed by Giddings (Giddings, 1985). As Figure 1-1 show, a SPLITT platform has multiple inlets for sample and sheath flow injections and the splitter is used for dividing different flows. To isolate target particles, the SPLITT platform has a part of channel that is not divided but has external field distribution. The external field can general different level of force on particles with different features and generate a vertical migration to the flow direction. Particles migrate to sheath flow will then be separated since the sheath flow and original sample flow are divided by downstream splitter. By adjusting external force field and target particles the active microfluidic separation device can derive high flexible and precise separation, which induce higher efficiency. Introducing external force further increases the mechanism for particle manipulation and enables the active microfluidic separation technologies have a wider application than passive microfluidic technologies.

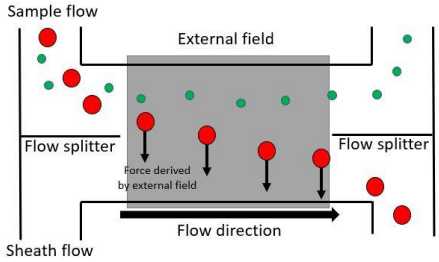

Figure 1-1: The generic design of the SPLITT platform. External effect is utilized for isolating different particles and particles separate in different Laminar flows which are separated by the flow splitter in the channel.

To demonstrate the differences between the passive and active microfluidic separation technologies, their separation performances are summarized in Table-1. Separation mechanism, separation markers, throughput, channel size, application are the parameters for comparison. Although both advantages and limitations exist for both passive and active microfluidic separation technology, active microfluidic separation technologies show wider application potential. The major limitation of passive microfluidic separation, which is limited separation mechanism, cause the passive methods relied on channel structures and structure derived flow patterns. This feature brings high throughput advantages to the passive microfluidic technologies, but increases the channel length and induces low separation resolution. The main separation marker for passive microfluidic separations is the size difference between particles, and for generating size-based separation, the difference is usually micrometer level, which cause the difficulty for separation particles with low size difference (Bhagat et al., 2009, Warkiani et al., 2015, Yoon et al., 2016). The main advantages of active microfluidic is the ability for low number or single particle manipulation. Although this feature can decrease the throughput, higher precise manipulation can increase the separation resolution and enable the separation of rare population targets or targets demonstrate small parameter differences. Since the external field bring significant improvement on separation flexibility and resolution, which are the main limitations for downstream analysis, continuous efforts have been made for integrating new separation mechanism in the

microfluidic device for achieving high efficiency. Among various of efforts, the integration of acoustic field has been found successful and improved the separation outcomes. Acoustics integrated microfluidic technology have been modified to a series of device with wide applications and shown a potential for benefit a wide research community.

Table 1 Comparision between passive and active microfluidics

	Mechanism	Separation markers	Throughput	Channel size	Application	Reference
Passive	Hydrodynamic force, inertial of particles	Size, deformability, shape, density	High, majorly above 50 μL/min	Long channel, majorly above 5 cm	Bacterial separation, apheresis, leukapheresis	(Huang et al., 2004, Yamada et al., 2004, Yamada et al., 2005, Abgrall et al., 2007, Choi et al., 2007, Mach et al., 2010)
Active	Optical force, homogeneous electric field, electric field gradient, magnetic force	Size, refractive index, polarizability, charge, magnetic,	Various, optical separation majorly less than 50 μL/min,	Short (compared with passive device),	Cancer cell separation, fetal cell separation, embryo manipulation,	(Stone et al., 2001, Kim et al., 2005, Kelly et al., 2006, Çetin et al., 2011, Wang et

		fluorescence, surface modification	magnetic and electrical usually higher	500-1000 μm	immune cell screening, transfection screening	al., 2011, Zhang et al., 2017)

1.2 Acoustofluidics: integration of acoustics to microfluidics

The category of acoustic study is the mechanical waves' behaviors and interactions in both fluid and solid mediums. Since the propagation of the acoustic wave can occur in large varieties of materials and the propagation patterns are deeply influenced by materials' physical properties and acoustic waves' features, acoustics has still been a robust studied field over decades (Pierce, 2019). The strong preparation ability brings acoustic wave unique advantages, which is deep and non-contact interaction with targets covered by other materials (Drinkwater et al., 2006). The non-contact feature of the acoustic waves enables the generator of acoustic wave not directly contact with the target but still can deliver interference on it. Although other physical effects like optics and electrics also demonstrate the ability of propagation and non-contact, these effects' propagation distances are far less than acoustic waves (Wells, 1999). Higher attenuation during propagation further limited these effects' application in non-contact interaction, since the energy lost during propagation is majorly transferred to heat and can cause damage of the material (Fayad et al., 2001). Another advantage of acoustics is the excitation of acoustic waves can be easily achieved by transducers that transfer other form

of energy to mechanical forces that 'shake' the propagation media (Safari et al., 2008). Furthermore, the propagation manners of the acoustic waves are various and can generate different effects including reflection, diffraction, absorption and so on. The easy generation and various form characteristics provide acoustics wide application in both scientific and industrial fields, including navigation, ranging, underground detection, and-nondestructive evaluation (Vary et al., 1979, Popper et al., 2001, Eustice et al., 2007, Peng et al., 2007). Benefit from the deep propagation and gentle energy release features, acoustic waves are also appliable on bio-samples like ultrasonography. These properties make acoustics great potential candidates for integrating with microfluidics.

Since the previous successes of acoustics in biological and biomedical fields, recently the attempt of integrating acoustics to microfluidics has grabbed great attention. By adjusting frequency, the piezoelectric transducers can generate low wavelength acoustic fields (micrometer and millimeter level) that are matched with the scale of microfluidic device channel. Since in this scale the acoustic waves can form stable acoustic field in the microfluidic channel, these external field can induce active separation of particles. Despite the interaction with particles, acoustic field further derive strong interaction as resonance with fluid in the microfluidic devices. Since both field particle interaction and field fluid interaction can be generated by acoustic waves, acoustics can generate strong manipulation effects in microfluidic devices. Furthermore, acoustics is a well-developed field with solid theory accumulation and application experiences, which

make acoustics a tool that can be easily used. Based on practical requirement, the mature theoretical basement of acoustics can provide reliable guide for achieving designed functions. Although in acoustofluidic application it is necessary for modifications of the coupling of acoustics and microfluidics to achieve ideal outcomes, well studied physical principles of acoustics significantly decrease the difficulty of design and evaluation of the acoustofluidic platforms. Being able to manipulate both particles and fluids, acoustofluidics can achieve separation, fluid pumping, droplet jetting and moving, mixing, atomization, mixing and rotation, concentration, and alignment, which nearly cover all requirements in microfluidics (Friend et al., 2011, Lenshof et al., 2012, Wiklund et al., 2012).

Among the various applications that the acoustofluidic technology is eligible, the most impactive and attractive direction is the particle manipulation (Lenshof et al., 2012). Efficient particle manipulation is basic for particle separation, which is the essential step for multiple biological and biomedical research. The mechanisms of achieving acoustofluidic particle manipulation are various, including direct manipulation by acoustic wave and acoustic wave derived microstreaming manipulation. These mechanisms can function individually or coupling, induce acoustofluidics based manipulation technology have high efficiency, simplicity, and versatility advantages. Furthermore, acoustofluidic manipulation can function without participating of chemical labels, induces acoustofluidic manipulation biocompatible and label-free features. These

important advantages enable the preservation of biosamples' function and structure integrity during acoustofluildic manipulation and separation. Currently acoustofluidic manipulation technology has been successfully applied for separating platelets, red blood cells, neutrophils, cancer cells, and bacteria (Laurell et al., 2007, Antfolk et al., 2015, Li et al., 2015, Augustsson et al., 2016, Chen et al., 2016, Li et al., 2016, Ahmed et al., 2017). To further develop acoustofluidic manipulation and separation technology, types of acoustic waves that can interact with microfluidic system and the mechanisms of acoustic manipulation will be introduced in following subsection.

1.2.1 Types of acoustofluidic separation technology

External acoustic waves are the active approach used by acoustofluidics for influencing fluid fields and particles in fluids. With development of acoustics various of transducers have been developed for generating acoustic wave. Among these transducers, piezoelectric transducers, which can be constructed by polycrystalline ceramics, single crystals, or polymers, are the most convenient candidates for integrating with microfluidic channels. The mechanism of piezoelectric transducers generating acoustic wave is the unsymmetrically distributed electrical charge on the transducers. These electric dipole moments induce a regular and reciprocating deformation of the transducer, results the electrical energy be transformed to mechanical energy. Since the piezoelectric transducers' simple structures, these transducers could be designed small for fitting the small scale of the microfluidic technology.

Depends on properties of material, configurations, and mechanism of generating vibration, the piezoelectric transducers could be various. Net electrical dipole induced acoustics usually could be found in materials with natural crystal structures which enables yielding and generating piezoelectric effects; more common approaches of generating acoustic waves is deriving electric polarization externally. Vibration mode of the transducers is decided by material properties and polarization methods, and vibration mode further decide the propagation pattern of the acoustic wave in material. Thickness compression and shear is the most common mode for transducer vibration, which are shown in Figure 1-2. The electrodes in transducers deliver alternating current signals and induce vibration of piezoelectric materials. During the thickness compression and expansion, acoustic waves are generated inside the piezoelectric material and is spreading in the body of the material. This type of acoustic wave is called bulk acoustic wave (BAW). When the piezoelectric material is vibrating in a shear pattern, the acoustic wave will be generated and propagated on the surface of the material. This type of acoustic wave is called surface acoustic wave (SAW). Interdigitated transducers are used for generating SAWs and the generate acoustic waves' frequency and wavelength is depending on the coupling of the frequency of alternating currency and the distance between electrodes.

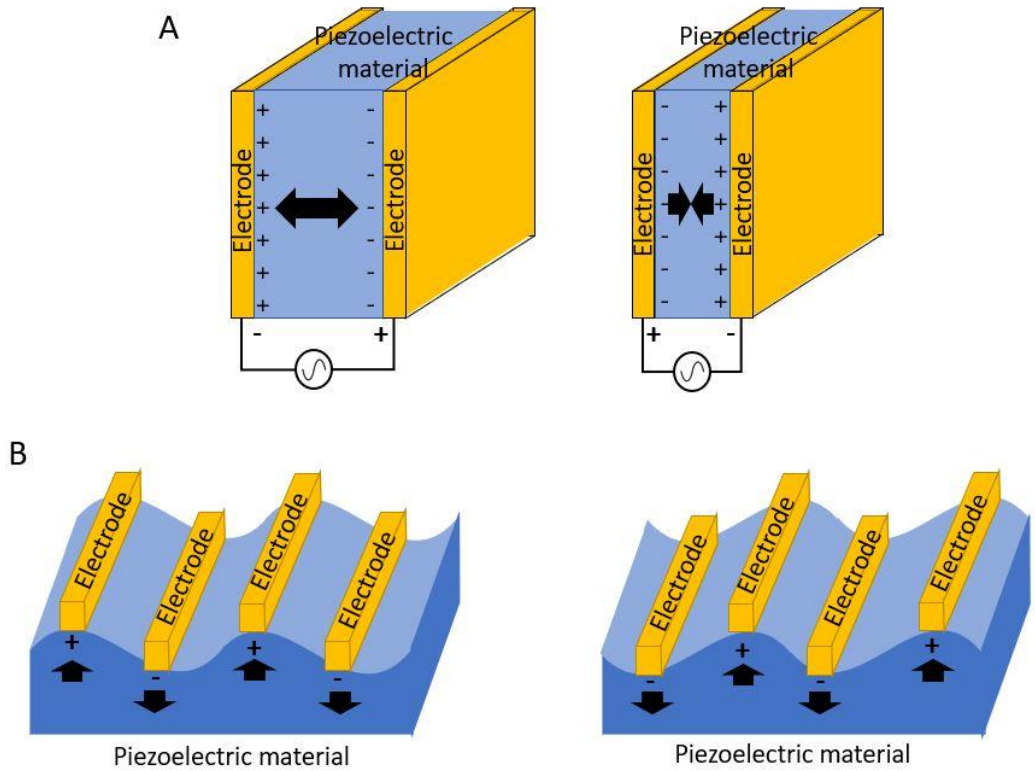

Figure 1-2: Mechanism of acoustic wave generation by piezoelectric materials. (A) Generation of bulk acoustic wave, when there is alternating voltage on the electrodes, continuous compression and expression of the piezoelectric material will generating acoustic wave in the body of the material. (B) Generation of surface acoustic wave, IDT is activated by alternating electric voltage and induce vibration on the surface of the material.

Both BAW and SAW could be used in acoustofluidic devices as Figure 1-3 shows. Bulk wave based acoustofluidic devices usually contain channel made by high acoustic impedance materials like metal and glass. During functioning, generated bulk wave propagates in a direction as transducer-channel-fluid. Since the liquid has lower acoustic impedance than channel material, this impedance mismatch induces the reflection of acoustic wave on the channel wall. To enhance the manipulation effect of the acoustic

wave, the depth and width of the channel need to be specially designed for fitting the half wavelength of the acoustic wave. When the transducer functioning at designed frequency, it will initiate channel oscillations and the reflecting effect of the channel wall will induce acoustic wave forming standing waves in the channel. Bulk standing wave can also be generated between two transducers working in same frequency. The mechanism of SAW manipulation can be divided to standing wave and traveling waves. Since in the SAW device, the channel structure is normally formed by piezoelectric substrate bounded with soft material like polydimethylsiloxane (PDMS). The acoustic wave propagates on the surface of the substrate and the manipulation is achieved by leaky wave transferred from substrate to the fluid. However, the PDMS material shows low reflection of acoustic wave, inducing weak standing wave in the vertical direction. To generating standing wave by SAW, two interdigitated transducers (IDTs) generating same frequency SAWs need to be placed in two sides of the channels. In the channel area two acoustic waves propagating in opposite directions can result a standing wave field. In standing wave fields formed by both bulk wave and surface wave, interval distributed pressure nodes and anti-pressure nodes can form periodic arranged high acoustic pressure area and low acoustic pressure area, which can manipulate particles by pressure difference. The traveling wave SAW device only has one IDT, resulting no stable standing wave in the channel.

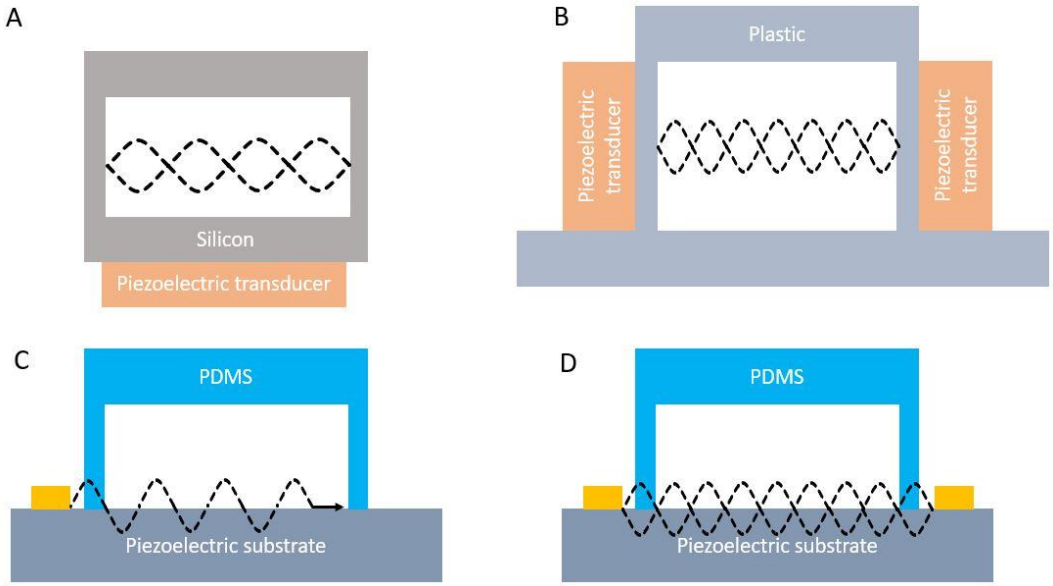

Figure 1-3: Schematics of bulk wave and standing wave separation techniques. (A) Standing wave generated by channel resonation of the bulk wave. (B) Standing wave generated by two bulk wave transducers. (C) Travelling SAW generated by one IDT. (D) SAW standing wave generated by two IDTs.

The most common acoustofluidic manipulation technologies are summarized in Table 2. The frequencies of bulk wave devices and surface wave devices have different optimized ranges, which is mainly depended on the transducer structures. The bulk wave transducers have a flexible frequency of generated acoustic waves, since the compression and the expansion rates of the piezoelectric material is depended on the frequency of alternating current signals. By adjusting the frequency of input current signals bulk wave transducer can adjust output acoustic wave frequency. The surface acoustic wave transducer, IDT, only generate fixed frequency acoustic wave which depends on the IDT structure. Since the acoustic wave frequency is defined by the sound propagation speed on the piezoelectric material surface and the wavelength that is four times of the spacing

between IDT electrodes, one IDT only have a stable working frequency. However, benefited from the development of photolithography technology, spacing of IDT electrodes could be tiny for generate higher frequency waves than bulk wave transducer, which will influence their application in acoustofluidics since the acoustic frequency is one important factor for manipulation mechanism introduced in following section.

Table 2 Types of acoustofluidic manipulation technologies

Category	Mechanism	Frequency	Reference
BAW	Piezoelectric transducer and channel generated resonation standing wave; standing wave generated radiation force	< 10 MHz	(Petersson et al., 2005, Chen et al., 2016, Li et al., 2016, Antfolk et al., 2017)
Traveling SAW	Single IDT generated traveling acoustic wave; leak wave from travelling wave generated radiation force	Up to 5 GHz	(Au et al., 2012, Destgeer et al., 2013, Destgeer et al., 2014)
Standing SAW	Pair of IDT generated standing wave; leak wave from standing wave generated radiation force	Up to 5 GHz	(Nam et al., 2011, Au et al., 2012, Wu et al., 2017)

1.2.2 Mechanisms of acoustofluidic manipulation

The two main mechanism for achieving acoustofluidic manipulation is the acoustic radiation force and acoustic streaming. In the acoustic fields, interactions like absorption, scattering, reflection, interference, and dampening generate gradient in the field and result radiation force and streaming (Torr, 1984, Doinikov, 1996).

Acoustic radiation force is derived by the gradient acoustic pressure field, which cause unbalanced acoustic pressure on objects including particles, bubbles, cells, and vesicles. Except acoustic radiation force generated by particles and acoustic field, which is the primary acoustic radiation force, since particles also reflecting and scattering acoustic waves, there exist particle-particle interactions that is called secondary acoustic radiation force. Since standing wave have stable distribution of high acoustic pressure areas (pressure nodes) and low acoustic pressure areas (pressure antinodes), particles influenced by primary acoustic radiation force will migrate to these pressure nodes or pressure antinodes. The secondary acoustic radiation force derives inter-particles interferences, which cause particles aggregations or assembling. In a standing acoustic field, acoustic radiation force analysis can be built on Doinikov's theory (Doinikov, 1996). Generally, a spherical compressible particle in a standing acoustic field will be suffered a primary acoustic radiation force given by (Yosioka et al., 1955):

$$F_r = -\left(\frac{\pi p_0^2 V_p \beta_f}{2\lambda}\right)\phi(\beta,\rho)\sin\left(\frac{4\pi x}{\lambda}\right) \quad (1)$$

$$\phi(\beta,\rho) = \frac{5\rho_p - 2\rho_f}{2\rho_p + \rho_f} - \frac{\beta_p}{\beta_f} \quad (2)$$

In these equations, p_0 represents the acoustic pressure, V_p represents the particle volume, λ is the wavelength of acoustic wave, x is the distance between the particle and the pressure node, ρ_p and ρ_f are the density of the particle and the fluid, and β_p and β_f represent the compressibility of the particle and the fluid. According to the equation 1, particle size is one of the major factor for deciding the strength of the acoustic radiation force. Depending on the acoustic contrast factor of the objects and fluids, particles with positive acoustic contrast factor will be pushed to pressure while negative acoustic contrast factor particles will be pushed to pressure antinodes. The compressibility of the fluids and the particles influences the acoustic radiation force magnitude. Because of these relationships, physical properties and size can cause significant difference of acoustic radiation force on the different particles including cells and vesicles, inducing manipulation and separation results.

Acoustic streaming is another critical mechanism for supporting acoustofludic technology operation. Different with acoustic radiation force, which is the effect derived by acoustic field on the objects, acoustic streaming is derived by fluid's viscous attenuation. Since the liquid viscosity derived dragging effect also depends on the particle volume, the oscillating particles displacements will not show a same amount. Depending on the wave attenuation scale and process, acoustic streaming can demonstrate different patterns including boundary-driven streaming, which is derived by acoustic wave dissipation on a solid boundaries (Nyborg, 1958, Wiklund et al., 2012). Since rotation

streaming could be achieved by designing the propagation direction of acoustic waves, acoustic streaming has been utilized in active mixing, vertex, and microcentrifugation . The coupling of acoustic radiation force and acoustic streaming for achieving object manipulation has also demonstrated achievable (Zhang et al., 2020).

Acoustic radiation force and acoustic streaming derived particle movement has been analyzed by Barnkob in a bulk wave system (Barnkob et al., 2012). In this model acoustic radiation force is the main effect for deriving particle manipulation, while the acoustic streaming suspends the fluid and induces a fluid derived Stokes drag force. The ratio of acoustic radiation force and acoustic streaming induced particle movement could be demonstrated by a function:

$$\frac{u_y^{rad}}{u_y^{str}} = \frac{1}{6s}\frac{\rho_f \Phi}{\eta}\,\omega\, a^2 \qquad (3)$$

Where a, ω, η, Φ, and ρ_f demonstrate the particle radius, angular frequency, viscosity, acoustic contrast factor, and fluid density, and u_y^{rad} and u_y^{str} demonstrate the acoustic radiation force derive migration and acoustic streaming derived migration. The channel structure and geometric features influence liquid thermo-viscus property and determine the s which is the streaming coefficient. Through this equation, it is obvious that there exists a size threshold of the particle that determine whether acoustic radiation force of acoustic streaming is the main effect for determining the particle movement. Generally, large particles in low frequency acoustic field are majorly controlled by drag

force derived by acoustic streaming, while opposite size and frequency cause acoustic radiation force in the dominate position.

Acoustic radiation force and acoustic streaming could demonstrate interference, coupling, or domination, respectively. Since in biological and biomedical applications there are comprehensive requirement of manipulation and separation, the utilization of acoustic radiation force and acoustic streaming for manipulation is influenced by the manipulation target.

1.3 Application of acoustofluidic technology

Acoustofluidic manipulation technology has been deeply studied and has various applications in multiple biological and biomedical fields including apheresis, cancer cell separation, and vesicle separation. In this section several most representative applications of acoustofluidic technology will be introduced for evaluating the advantages and existing limitations.

1.3.1 Acoustofluidic apheresis

Body fluids are important components for constructing the internal environment of multi-cellular organisms. Material transportation and information exchange are support by body fluids and induce complex components. The most important body is the blood, which is the basic biofluid for support circulation system. Since it participates the majority metabolic processes in the body, blood has comprehensive components but provides valuable targets for diagnostic and therapeutic applications. The complex

components and study requirement make blood separation or apheresis technology important.

Conventional blood separation technology is complicate and time-costing. Centrifugation is the most widely used approach for separating blood components (Zhu et al., 2013). However, to separating target components multiple steps are necessary. Red blood cells (RBCs) and white blood cells (WBCs) formed the majority cell population in the blood, which are 4 – 6 million RBCs and 4,500 to 11,000 WBCs per microliter. To separate these cells, a centrifugation under 1500 - 3000 g for several minutes is necessary. After separating the cell components, there are still platelets (160,000 to 460,000 per microliter) and vesicles including apoptosis bodies and extracellular vesicle. The removal of platelets requires 5000 – 6000 g centrifugations, and the removal of extracellular vesicles even need ultracentrifugation. This multi-step centrifugation cost long period and induce potential damage for cells, proteins, or nuclei acid components in the blood (Chen et al., 2008). Another method for blood components separation is filtration. However, like the centrifugation, filtration is also required for multi-steps since single filtration cannot provide high separation resolution. Furthermore, blood cell damage during filtration can induce disease including hemolysis and thrombus (Sapatnekar et al., 2005, Kaplan, 2012). Since the analysis and clinical blood transfer application require rapid separating blood components for reducing contamination and sample degradation, developing efficient new approach is necessary.

The attempts of using acoustofluidic technology for blood components separation are successful with advantages including high efficiency and biocompatibility. Both bulk wave and surface wave acoustofluidic devices has demonstrated successful separation of blood cells for plasma, blood cells from platelets, and white blood cells from red blood cells. The bulk acoustic wave blood cell separation was firstly reported by Petersson in 2005, as Figure 1-4A shows (Petersson et al., 2005). Activated by piezoceramic transducer attached on the silicon chip, standing wave was generated by the resonation in the channel and form stable pressure nodes. When blood and sheath flow plasma were injected by different outlets, stable laminar flow was firstly formed. The stretch from acoustic radiation force then inducing blood cells migration to the pressure node and enter the laminar flow formed by sheath flow. The isolation yield of blood cells by this device achieves more than 95% and the throughput of blood sample is 0.17 mL/min. By derive precise temperature control for balancing the thermal generated by the transducer, the power of piezoelectric transducer could be further increased for achieving a throughput higher than 15 mL/min (Adams et al., 2012).

Except separating blood cell from plasma, acoustofluidic technology can also derive separation between leukocytes and platelets. The surface acoustic wave platelet separation was firstly introduced by Nam. By deriving standing acoustic wave field using a pair of IDTs, leukocytes will migrate to sheath flow on each side of the channel while platelets stay in the center as Figure 1-4B shows (Nam et al., 2011). Although the

throughput of this SAW device is not ideal with a sample flow rate of 0.25 μL/min, it can remove 99% of blood cells and the isolate platelet purity can achieve 98% by flow cytometry analysis. Different with the high purity and low throughput features of surface acoustic wave devices, acoustofluidic technology using bulk wave can achieve significant higher throughput for platelet separation. The bulk wave acoustofluidic technology developed by Chen can achieve 10 mL/min throughput for platelet, as Figure 1-4C shows (Chen et al., 2016). However, the removal rate of leukocytes is only 80% and the separation yield of platelets is 85%.

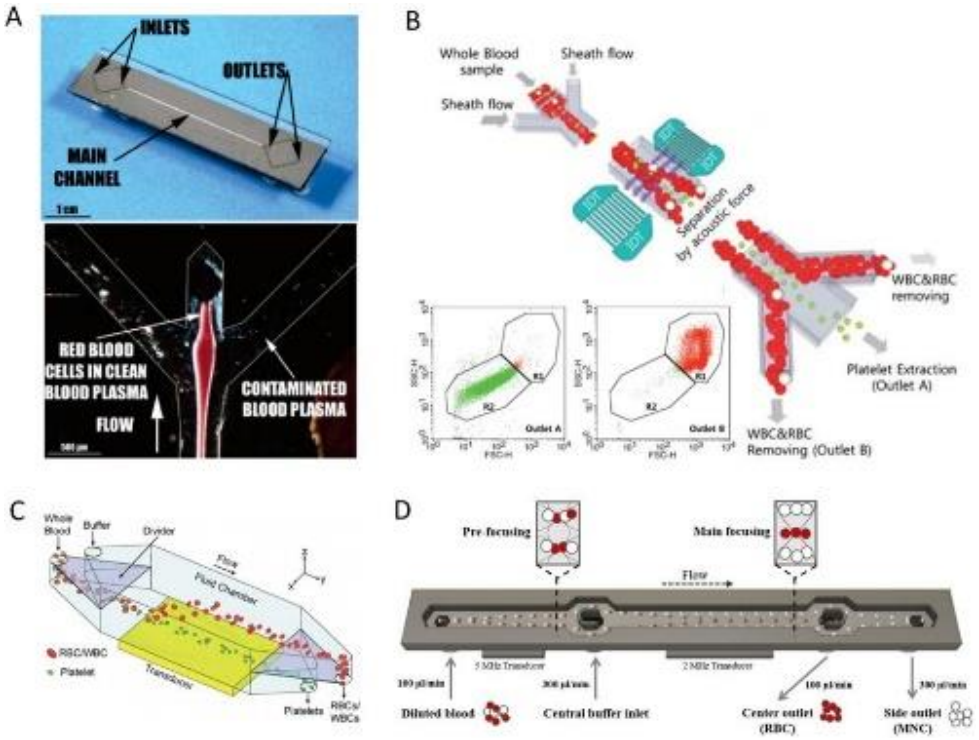

Figure 1-4: Acoustofluidic apheresis technologies. (A) Plasmapheresis by bulk wave acoutofluidic technology (Petersson et al., 2005). (B) Platelet and blood cell separation by surface acoustic wave (Nam et al., 2011). (C) Bulk wave platelet separation (Chen et al., 2016). (D) Mononuclear cells acoustofluidic separation by two stages with different frequency acoustic fields (Urbansky et al., 2017).

With the requirement of increasing separation accuracy and resolution, which allow the separation of subpopulation of blood cells including red blood cells and lymphocytes, complicated acoustofluidic devices that use multiple acoustic fields with different frequencies have been developed. Figure 1-4D demonstrates Urbansky's work on separating monocytes and red blood cells by using a two-stage device (Urbansky et al., 2017). By adjusting ratio of Stock Isotonic Percoll buffer and transducer frequency, the standing wave fields demonstrate different pressure node patterning and induce monocytes and red blood cells migrate to different laminar flows.

Acoustofluidic apheresis technologies have been proven eligible for various blood component isolation in a biocompatible way, which has been demonstrated by cell viability and platelet activation ability . Among these successes, bulk wave-based acoustofluidic separation and surface wave-based separation demonstrated different limitations and advantages. Acoustofluidic technologies based on bulk wave can achieve high throughput separation but shows low resolution that induce low purity and yield. The internal reason of these features is the mechanism of generating acoustic field in the channel. By generating bulk standing wave, it is necessary for generating reflection of acoustic waves on the channel wall for generating resonance. However, the pattern of pressure nodes needs to fit the geometric size of the channel, which limits the acoustic wave frequency to a low level. Furthermore, the transducer of the bulk wave device induces vibration of the whole chip, which bring difficulties for integrating multiple

transducers with different frequencies in one chip. Since for achieving higher separation resolution, multiple stage isolation is necessary, the mechanisms of acoustic wave propagation and stand wave formation become major obstacles for improving the performance of bulk wave acoustofluidic technologies. The main problem of surface wave based acoutofluidic separation technology is the throughput limitation caused by transducer power and no resonance. Despite this drawback, since multiple IDTs can be integrated in one chip and can generates high frequency acoustic waves that are eligible for precise manipulation, surface wave based acoustofluidic separation technology has great potential in vast biological and biomedical research and applications.

1.3.2 Acoustofluidics cell manipulation

Cell manipulation is an important technology for investigate intracellular communication mechanism, which has been found critical for multiple biological activities including immune activation or deactivation, proliferation control, development regulation, and cancer metastasis. Intracellular communication is derived by receptors on membrane surface receiving activations and transform extracellular signals to intracellular signals through various of signal pathways then regulate cell behaviors including gene expression and protein modifications. These comprehensive regulation systems are supported by the entire cells, indicates the manipulation technology should be biocompatible for keeping the integrity of structure and function of the cells. Furthermore, since the protein dynamics is one important branch of intercellular

communication study, the cell manipulation technologies need consider low interference to the observation methods. Currently the main trend is using fluorescence for revealing short term protein dynamic events, including fluorescent modification for protein tracking and fluorescence resonance energy transfer (FRET) for protein interactions, which are sensitive to light. Conventional cell manipulation technologies include micro tweezer, electric tweezer, and optical tweezers, which all have limitations. Micro tweezer is eligible for precise manipulation of cells, but the manipulation is achieved by direct contact that can cause physical stimulation or even damage to the cells. Electric tweezer derives voltage on cells for manipulation, but can cause heat or break down the cell membrane by discharge. Optical tweezer also has thermal limitation, the manipulation derived by light is another obstacle for integration with fluorescent detection methods.

Different with conventional methods, acoustofluidic technology provide a non-contact approach for cell manipulation. By using surface acoustic wave, Shi demonstrated using two vertical acoustic fields with same wavelength can distribute cells in a square pattern as Figure 1-5A shows (Shi et al., 2009). The main advantage of surface acoustic wave is compared bulk wave, it can generate higher frequency and lower wavelength acoustic field in the channel with less attenuation. Since single or small amount cells manipulation need precise control, lower wavelength means short distances between pressure nodes and higher manipulation resolution. Furthermore, the standing wave acoustic field in bulk wave device is generated by the resonation between the channel and

acoustic wave, indicate the wavelength of the acoustic wave field is not adjustable in on device. Although conventional parallel finger IDT also can only generate a stable frequency acoustic wave, utilization of slanted-finger interdigital transducer (SFIT), which is a variation of IDT that has continuous electrode distance change from one side to the other side as Figure 1-5B shows, can derive multiple wavelength acoustic fields in one device and achieve adjustable manipulation (Ding et al., 2012). These advantages make surface acoustic wave a better solution than bulk wave technology microfluidic for cell manipulation. A further development of acoustofluidic cell manipulation is the utilization of acoustic streaming. Since the propagation of surface acoustic wave is on the surface of piezoelectric substrate and the leak wave which shows highest strength at pressure nodes derives the manipulation, the leak wave induced acoustic streaming could also be utilized for manipulation. As Figure 1-5C shows, Guo developed a 3D acoustofluidic cell tweezer by coupling the acoustic radiation force and acoustic streaming (Guo et al., 2016). In this device acoustic streaming generates manipulation on vertical direction and acoustic radiation force derives horizontal direction manipulation. By achieving precise 3D manipulation, single cell could be pick up, move, and placed at targeted positions for creating 2D and 3D patterns.

Acoustofluidic cell manipulation technology also achieved continuous rare population separation, including isolate circulating tumor cells from blood. The developing of CTC is one important process during tumor metastasis, since CTCs are

tumor cells migrated from primary tumor. During transportation in the circulation system, CTCs have possibility for entering other tissues and cause secondary tumor development. Since their important role in the pathology of cancer, CTCs can provide important information about cancer development and are valuable biomarkers for diagnosis, prognosis, and providing therapeutic guideline. The first attempt of isolating CTCs from other blood cells is achieved by Augustsson by an acoustofluidic separation device that has two separation modules for cell alignment and separation as Figure 1-6A shows (Augustsson et al., 2012). This platform can separate cultured cells from WBCs with a throughput of 70 μL/min, purity of 79.6% to 99.7%, and yield of 72.5% to 93.9%. Further attempt using blood sample for CTC isolation was achieved by Wu, which demonstrated acoustofluidic technology can both separating cultured cancer cells from peripheral blood and separating CTCs from patients' blood samples as Figure 1-6B shows (Wu et al., 2018). In experimental evaluation using cultured cancer cells, this acoustofluidic platform can achieve higher than 86% yield in a 7.5 mL/h throughput with idea biocompatibility. Staining of isolated CTCs from prostate patients further demonstrates the platform keeps CTCs' phenotypic heterogeneities, including various of prostate specific membrane antigens. Since the acoustofluidic manipulation technology can separating cells in rapid and biocompatible way, it can significantly improve diagnosis and therapy.

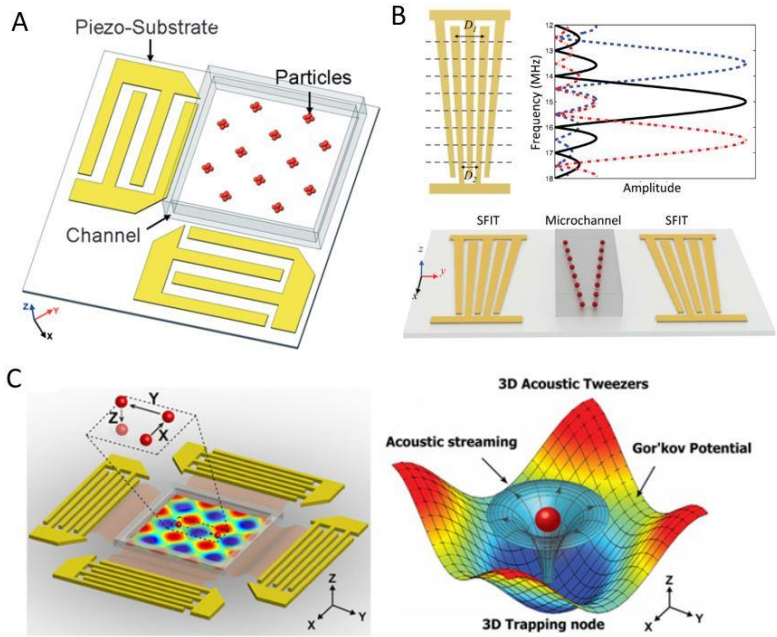

Figure 1-5: Schematics of acoustofluidic manipulation technologies. (A) Surface acoustic wave square patterning (Shi et al., 2009). (B) Frequency adjustable acoustofluidic manipulation by SFIT (Ding et al., 2012). (C) 3D acoustofluidic manipulation by acoustic radiation force and acoustic streaming coupling (Guo et al., 2016).

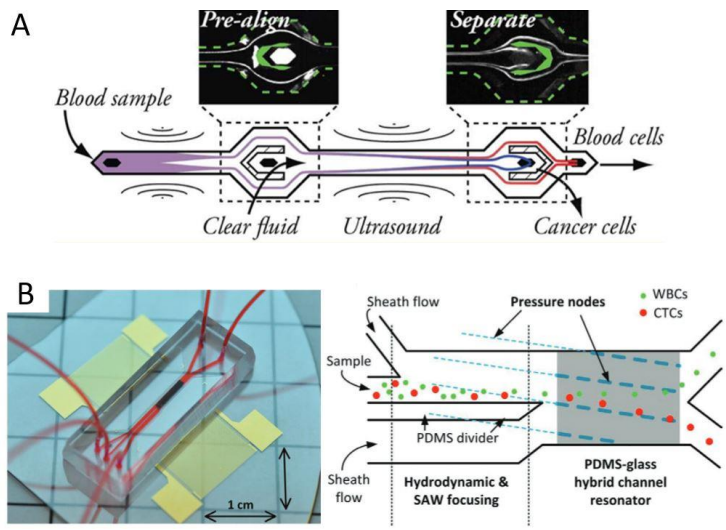

Figure 1-6: Acoustofluidic CTC separation technologies. (A) Two-stage acoustofluidic separation of cancer cells (Augustsson et al., 2012). (B) Acoustofluidic CTC separation from peripheral blood (Wu et al., 2018).

1.3.3 Acoustofluidic extracellular vesicle separation

Extracellular microscale vesicle is another target that quickly gathering researchers' interest in biological and biomedical fields. These vesicles contain various of populations have different origins and biological functions, including apoptosis bodies, macro-vesicles, and exosomes. With the development of biological and biomedical study, these micro particles have been found having important roles in intercellular communications and can influence proliferation and development events. Apoptosis bodies is the product of programmable cell death and have multiple regulation functions including immune activation. Macrovesicles also derive secretion functions in neuron system. Exosome is a new target of study in the past decade, since its complex origin and functions. Exosomes are 50-200 nm vesicles, which are smaller than most of the other extracellular vesicles and derived intercellular communications. The secretion of exosomes is the exocytosis, and the precursor of exosome is the multivesicular body in this process. Since the formation of multivesicular body is also related with the endocytosis process, exosomes not only participate intercellular communication, but also participate cell reaction to intercellular stimulations. Participating multiple cellular activities makes exosomes having varieties of functions including proliferation regulation, immune response, tissue degradation control, and regeneration activation. These functions are critical for multiple biological events and diseases and bring exosomes great value for diagnostic and therapeutic applications. Multiple studies have found cancer cell

secreted exosomes containing specific cancer biomarkers and can derive tumor growth and proliferation. Stem cell secreted exosomes have been revealed can activate tissue repair process and have potential for neuron regeneration applications. However, small size of these particles has become one of the most important obstacles for study their functions. Conventional approach for purifying different populations of extracellular vesicles are ultracentrifugation and density gradient centrifugation. These methods face problems including low isolation yield, long processing times, and low biocompatibility that may cause structure damage of the separated vesicles.

Although acoustofluidic technology is a potential candidate for extracellular vesicle separation, there still exists various challenges. Since the extracellular vesicles are nanosized, to manipulate them the application of high frequency acoustic wave is necessary. Since bulk acoustic wave devices usually operating in 100 kHz to 10 MHz frequency ranges and surface acoustic wave device can reach to GHz level, surface acoustic wave devices are more eligible for nano-sized bioparticle separation. Based on acoustic radiation force generated by SAW, Lee reported nano-size particle separation as Figure 1-7A shows (Lee et al., 2015). Acoustic streaming has also been utilized for nanoparticle size separation. Mao developed acoustic streaming nanoparticle concentration in capillary tube by acoustic vertex in the tube center as Figure 1-7B show (Mao et al., 2017). By utilizing travelling surface acoustic wave, glass capillary can vibrate and generate acoustic streaming focusing to the center of the capillary. Drag force from

vortex streaming and acoustic radiation force then concentrate 80-500 nm nanoparticles to the center. Except acoustic streaming generated by capillary, high frequency travelling surface acoustic wave also has been utilized for nanoparticles separation. Developed by Collins, a microfluidic device using focused IDT that can generate acoustic streaming for pushing nanoparticle to opposite of the channel for nanoparticle separation (Collins et al., 2017). By adjusting acoustic field strength, which influence streaming flow rate, 100, 300, and 500 nm nanoparticles could be separated to different laminar flows regardless their initial position in the channel.

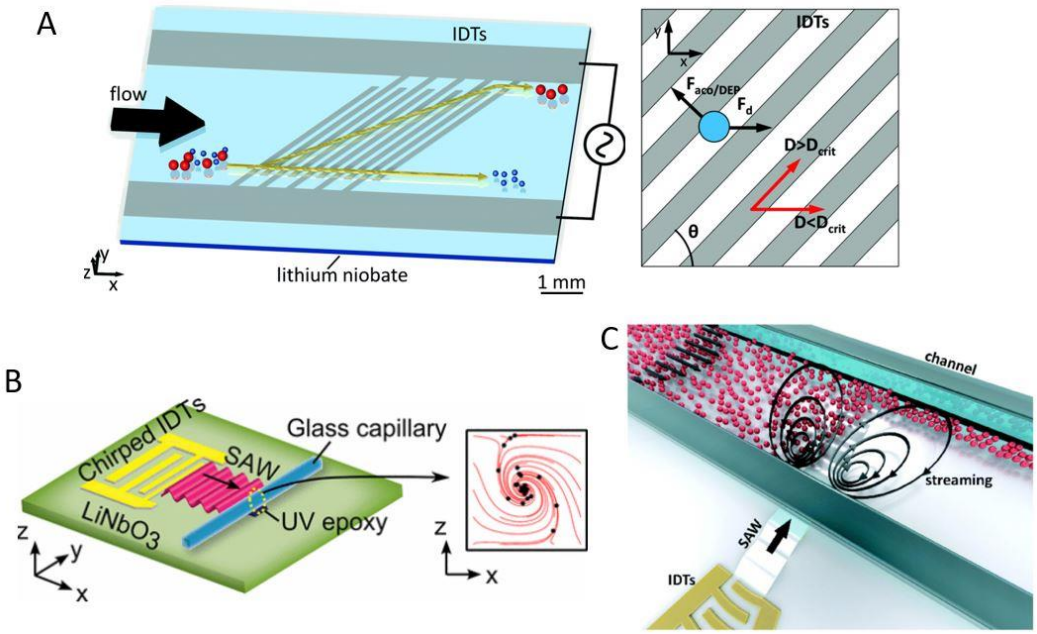

Figure 1-7: Acoustofluidic technologies for nanometer scale particles separation. (A) Separation of nanoparticles by surface acoustic wave generated acoustic radiation force (Lee et al., 2015). (B) Nanoparticle focusing by travelling wave derived capillary vibration generated acoustic streaming (Mao et al., 2017). (C) Nanoparticle separation by focused IDT generated acoustic streaming (Collins et al., 2017).

With the development of acoustofluidic separation technologies using nanoparticles, separation of bioparticles has also been rapidly developed. Shown in Figure 1-8A, Wu reported a two stage acoustofluidic platform for exosomes separation from peripheral blood (Wu et al., 2017). By using two separation modules that can generate 20 MHz and 40 MHs SAW standing wave fields individually, the acoustofluidic exosome separation device generated blood separation in the 20 MHz module and nano sized bioparticle separation in the 40 MHz module. The exosome separation throughput of the device can reach to 20 μL/min with a yield higher than 99% and purity of 98.4%. The most important advantage of this acoustofluidic exosome separation device is the separation is entirely derived by acoustic radiation force. The separation is reagent free and noninvasive for exosome structures, which keeps exosome cargoes and biomarkers for benefiting down streaming analysis. Size-based acoustofluidic exosome separation could also be achieved by coupling acoustic radiation force and acoustic streaming. Shown in Figure 1-8B, Gu developed a droplet vortex based platform for achieving high resolution exosome subpopulation isolation (Gu et al., 2021). By deriving two opposite surface acoustic waves generated by a pair of slanted IDTs, droplets in different positions of the device are driven by different strength and frequency of acoustic waves, cause differences on acoustic radiation force strength and acoustic streaming strength. These differences cause different size particles move to different droplets through a connection

channel between droplets and derive separation of 35 nm exomeres, 60-80 nm small exosomes, and 90-150 nm large exosomes.

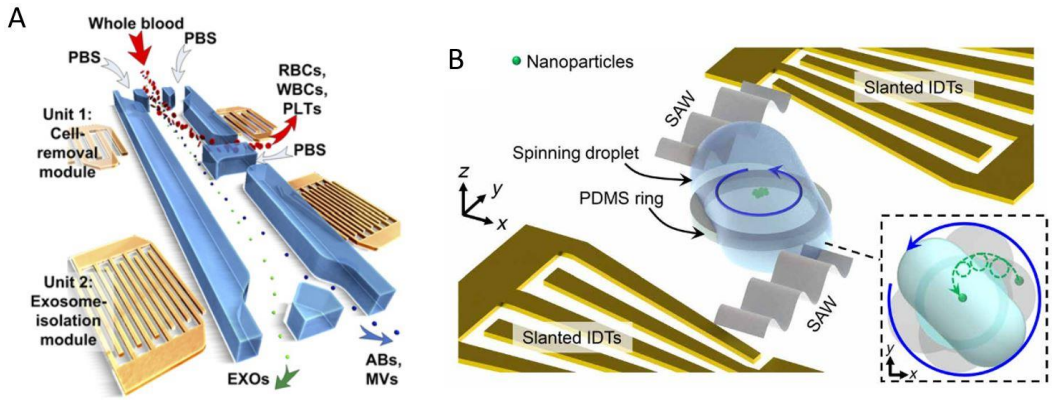

Figure 1-8: Acoustofluidic exosome isolation technologies. (A) Surface acoustic wave based two stage exosome separation technology (Wu et al., 2017). (B) Exosome subpopulation isolation by acoustic streaming and acoustic radiation force coupling (Gu et al., 2021).

1.4 Objectives and dissertation outline

From previous sections, it could be found that the introduction of microfluidics brings a gentle and active manipulation approach for enhancing the separation function of microfluidic system. With the development of acoustofluidic technology, the manipulation and separation targets become smaller, from micrometer level cells to nanometer level vesicles. Recent developed acoustofluidic technologies have been able for isolating bioparticles smaller than 100 nm with a 10 nm resolution, provide acoustofluidic technology great potential for biological and biomedical applications.

The aim of this dissertation is further validating whether acoustofluidic separation technology is eligible for specific diagnostic applications and expand the application of

the technology. Currently the acoustofluidic technology is eligible for isolation exosome from blood, but whether disease biomarkers could be identified from isolated exosome has not been studied. Furthermore, exosomes are widely secreted vesicle from nearly all kinds of cells, indicate exosomes not only exist in blood but exist in other body fluid. Considering the lesion positions of some disease could cause pathology related exosomes have higher expression in body fluids other than exosomes and the collection of body fluids like saliva is easier and noninvasive than blood, studying whether acoustofluidic technology can separation exosomes from other body fluids for research and diagnostic applications is also a valuable topic. Except diagnosis, exosomes also have other applications including drug delivery and therapy. Study the possibility of utilizing the ability of manipulating exosomes for these applications will also be discussed in this dissertation.

Chapter 2 presents the effort for utilizing acoustofluidic exosome separation technology for salivary exosome isolation. Since saliva could be used for oral disease diagnosis but demonstrate different physical properties than blood, which can potentially interference the device performance, it is worthy for validating acoustofluidic technology's performance using saliva samples. We successfully demonstrated acoustofluidic technology provide stable salivary exosome isolation and the isolated samples can be used for diagnostic purpose.

Chapter 3 introduces the potential of utilizing acoustofluidic exosome separation technology for fast diagnosis for traumatic brain injury (TBI). Since TBI is difficult for identify but can cause chronic sequela, fast screening and proper treatment in early stage of TBI can significantly improve the therapeutic outcome. Validation using TBI animal models demonstrates using acoustofluidic exosome separation technology can isolate TBI pathology related exosome in 24 hours after the TBI treatment, indicates the technology can be utilized for fast diagnosis.

Chapter 4 presents the effort of utilizing acoustofluidic technology for virus separation. Virus particles have same size range with exosomes and are valuable target for study. By adjusting the IDT design for increasing the frequency and acoustic field distribution, the acoustofluidic separation platform successfully isolated cultured Moloney murine leukemia virus (M-MLV) from culture medium. The isolated virus keeps ability for infection cells, indicate acoustofluidic separation technology provide a new approach for live virus isolation and study.

Chapter 5 demonstrates acoustofluidic technology could be used for acoustic streaming derived membrane disruption and achieve reagent free cell lysis. By using sharp-edge acoustofluidic device, acoustic streaming derived by sharp-edge vibration generate shear stress for lysis multiple types of cells including HeLa, U937, and red blood cells.

Chapter 6 follows efforts in Chapter 5 and validates whether acoustofluidic technology is eligible for exosome membrane disruption for drug loading application. By using slanted IDTs generate vortex, the acoustofluidic device can derive co-concentration of exosome, porous silicon nanoparticles, and drug molecules. During this process exosome encapsulation and drug loading are synchronously achieved. The products demonstrate higher intake rate by cells and show successful drug delivery.

Chapter 7 is the summary of this dissertation and introduces perspectives for future study.

2. Acoustofluidic salivary exosome separation

Liquid biopsy have potential for achieving oral cancer early diagnosis, which is critical to improve prognosis. Exosomes are important source for genomic and proteomic profiling, but eligible isolation method is required. However, the complex components and flexible physical properties of saliva bring difficulties for physical based exosome separation methods. To develop a rapid and easy to use salivary exosome isolation platform for point-of-care purpose, we developed an acoustofluidic platform to achieve size-based saliva exosome isolation. The platform demonstrated stable isolation on sample with different physical properties and sources. Salivary components bigger than exosomal size were eliminated in isolated sample. Furthermore, downstream analysis demonstrated successful detection of exosome specific biomarker from acoustofluidics isolated samples with an average yield 15-folder higher than that from ultracentrifugation method. By using HPV-associated oropharyngeal cancer patients' saliva samples, the acoustofluidic platform further demonstrated exosome containing HPV DNA could be isolated and detected. These results indicate the acoustofluidic exosome separation technology is an automated and high-throughput isolation approach that can provide a compatible exosome isolation method for liquid biopsy. Results and discussion in this chapter comes from my published first author paper (Wang et al., 2020).

2.1 Motivation

Saliva-based lipid biopsy (sLB) for HPA16 viral sequences represents a non-invasive approach for screening, risk assessment and early detection of OPC.(Hu et al., 2008) Five-year survival rates of OPC patients are lower than 50% and have not shown significant improvement with advanced therapy.(Wang et al., 2015, Sedghizadeh et al., 2016) Poor prognosis is due to presentation of clinical symptoms often occurred in late stage disease, often associated with high recurrence rate and metastasis.(Goy et al., 2009, McGurk et al., 2010) A rising incidence of HPV- related oropharyngeal cancers has been well documented despite the overall decrease in such cancers due to excess smoking. With this rise there has been a shift towards younger, healthier populations with few antecedent risk factors. Despite the fact that many such patients come to medical attention due to the presence of regional cervical metastasic spread, the newer staging systems have been changed to recognize that this does not necessarily portend advanced disease state nor poorer prognosis.(Zhan et al., 2017) Despite this improvement in prognosis and clinical outcome even in light of regional metastatic disease, it is still critical to develop methods for earlier detection of in order to try and minimize post-treatment morbidity and side-effects. Rapid, non-invasive universally-available clinical examination approaches alone cannot easily identify early stage HPV-associated OPC premalignant lesions.(Watanabe et al., 2008, Brocklehurst et al., 2013) Saliva has been shown to contain

tumor biomarkers, making early detection, screening and risk assessment of OPC possible.(Hu et al., 2008)

Exosomes are enriched vesicular sources of tumor-specific genomic and proteomic molecular targets.(Théry et al., 2002) These 50-150 nm nanovesicles are released ubiquitously from cells, including tumor cells, and involved in intercellular communication.(Azmi et al., 2013) The ability to isolate tumor-specific exosomes and identifying the constituent cargo molecular signatures enables exosome-based liquid biopsy with enhanced performance. However, conventional isolation approaches, including differential centrifugation and immune capture, require large volume of samples, are time-consuming, and associated with inherent isolation bias.(Taylor et al., 2015) Since high centrifugal force and/or multiple washing steps are required, these methods also bear potential negative effect on the integrity of exosomes. Label-free, high-throughput isolation technology that can achieve high exosome purity and yield is needed to achieve salivary exosome-based liquid biopsy for early diagnosis of HPV-associated OPC.

Here we demonstrate that the acoustofluidic system that can achieve high purity and yield salivary exosome isolation based on sized differences between exosomes and other salivary components. Our previous efforts have developed an acoustofluidic platforms using standing sequential surface acoustic waves (SAW) to directly isolate exosomes from undiluted blood samples.(Wu et al., 2017) In this study the acoustofluidic

platform has demonstrated proficiency in processing saliva samples with different physical qualities, including high viscosity which can influence isolation efficiency. Applying the optimized acoustofluidic separation for exosome isolation from saliva of patients with HPV-associated oropharyngeal cancer (HPV-OPC), HPV-16 DNA was detected in 80% of the patients' concordance with tissue/biopsy positivity for HPV-16. These results showed the acoustofluidic platform is a rapid and efficient exosome isolation technology for salivary exosome-based liquid biopsy.

2.2 Mechanism and system

Continuous exosome isolation is achieved by the two IDTs design that generate different frequency SAW (Figure 2-1A). The acoustic radiation force F_r push particles from areas with high acoustic pressure to pressure nodes that are parallel to the direction of IDT electrodes. According to Equation 1, increasing of particle volume induces larger F_r, while enlarging the wavelength of the SAW generates lower F_r. Since the acoustic fields on pressure nodes may not uniform, enormous F_r opposite to flow direction could be generated on large particles and derive a dominant capturing effect that causes particle trapping effect as Figure 2-1B shows. Recruiting 20 MHz IDTs at the first stage prevents micrometer sized particles from being trapped by 40MHz IDTs. Submicrometer particles that experience small F_r at the first stage can be discriminated at the second stage with 40 MHz SAW that generate stronger F_r. Considering the complicated components in saliva, two pairs of IDTs allow particles with a wide size distribution to be used. Fluid drag force

F_d generates both positive and negative effects on particle discrimination. Manipulated by F_r and F_d, particles move along pressure nodes of SAW and will be separated. However, F_d also generate a vertical direction force that resist particles manipulated and separated by F_r. Higher drag force is generated by larger fluid viscosity, indicating F_d potentially derive particles escaping from pressure nodes and cause separation failure as Figure 2-1C shows.

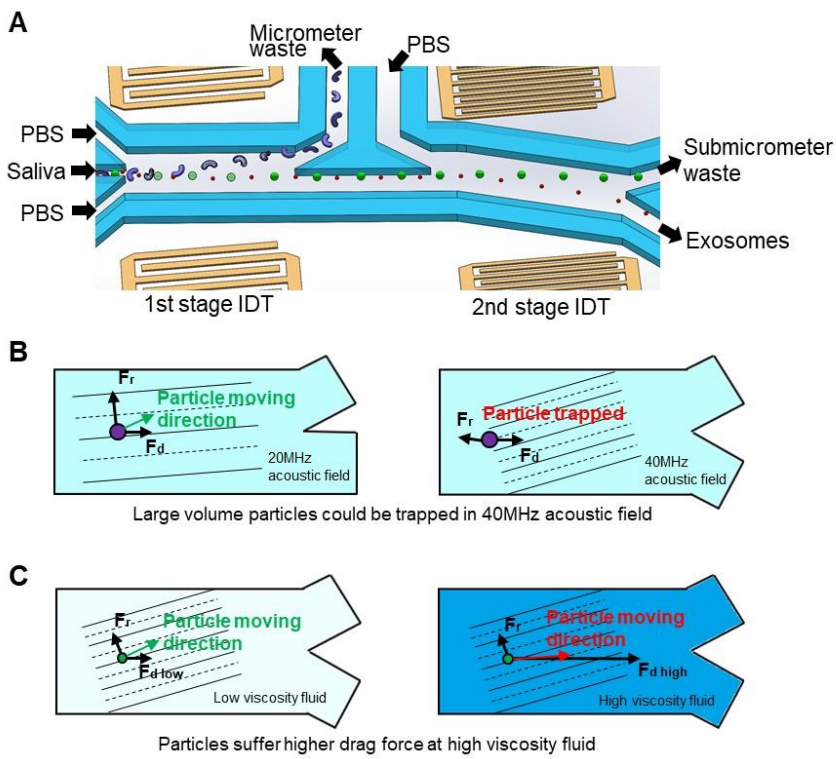

Figure 2-1: Schematics and mechanism of the device. (A) Basic design of the device. The device containing two-stage using 20MHz and 40MHz SAW for micrometer and sub micrometer particles separation. (B) Acoustic radiation force on micrometer sized particles in 20MHz and 40MHz acoustic fields. In high frequency acoustic fields, enormous acoustic radiation force can resist particles flow to the downstream. (C) Drag force influenced by fluid viscosity. Enormous drag force generated by high viscosity fluid may induce separation failure.

2.3 Experiment methods

2.3.1 Device fabrication and simulation

To build the two stage acoustofluidic exosome separation platform, two pairs of interdigital transducers (IDTs) that generate 20 MHz and 40 MHz SAW were deposited on a *Y*+128° *X*-propagation lithium niobate ($LiNbO_3$) substrate through photolithography processes. IDTs' shapes were acquired by a MA/BA6 mask aligner (SUSS MicroTec) and SPR3012 photoresist (MicroChem Corp.). After CD26 developing solution (MicroChem Corp.) removed unwanted photoresist, an e-beam evaporator (Semicore Corp.) was used to deposit a metal double layer (Cr/Au, 50 Å/500 Å) on the substrate. PRS3000 resist stripper (VWR) was applied to form IDTs with electrode widths of 50 and 25 μm on the substrate. Standard soft lithography using SU-8 photoresist (Micro-Chem) created a silicon mold. Sylgard 184 Silicone Elastomer Curing Agent and Base (Dow Corning) were solidified on the mold to form 100 μm height and 800 μm width PDMS microchannel. The microchannel and $LiNbO_3$ substrate were bonded after oxygen plasma coating and incubated at 65 °C overnight.

Simulation of forces and motion of particles in channel were derived by COMSOL. Particles mainly suffer acoustic radiation force from SAW field and drag force from liquid. The acoustic radiation force was simulated by Equation 1 and 2 introduced in Chapter 1. The Drag force is acquired by Stokes drag force:

$$F_d = -6\pi\eta R_p(u_p - u_f) \tag{4}$$

In the equation, η, R_p, u_p, and u_f are viscosity of the fluid, radius of the particle, velocity of the particle, and velocity of the fluid.

2.3.2 Saliva sample collection

Healthy volunteers' salvia collection followed a previous protocol approved by the University of California–Los Angeles (UCLA) Institutional Review Board. Unstimulated saliva samples were obtained from healthy volunteers who were asked to refrain from eating, drinking, smoking, or oral hygiene procedures for at least 1 hour prior to saliva collection. Whole saliva samples were collected without further treatment. Cell free saliva samples were collected through whole saliva centrifuged at 2600×g for 15 min at 4°C. Saliva samples collected by Oasis Diagnostics' saliva collectors were processed by instructions. All collected samples were stored at -80°C and transported in the protection of dry ice.

10 HPV-OPC patients were recruited in the multicenter CompARE trial (14/WM/1170, IRAS161147). The samples were collected using Institutional Review Board–approved protocols at Institute for Head and Neck studies and Education (InHANSE) at the University of Birmingham, UK. The patients were asked to rinse their mouth and gargle with normal saline (0.9% NaCl) for 2 minutes before spitting into a collection pot. The oral fluid samples then were spun at 1500g for 10 mins. The supernatant was removed and stored at -80°C and the pellets were resuspended in 1 mL PBS and stored at -80°C for further exosome isolation and ddPCR analysis.

2.3.3 Acoustofluidic separation of particles and saliva samples

To validate the device performance, beads experiment was firstly used. Polystyrene particles of diameter 50 nm, 500 nm, and 1 μm (Bangs Laboratory) were spiked into Deionized water (DI water) and 30% sucrose solution in DI water, which represent low and high viscosity situation. The acoustofluidic chip was placed on a Peltier cooling system (TEC1-12730, Hebei IT) and powered by a variable DC power supply (TP1505D, Tekpower). Upright microscope (BX51WI, Olympus) combined with CCD camera (CoolSNAP HQ2, Photometrics) was used for recording the separation process. IDTs on acoustofluidic chip were driven by a function generator (E4422B, Agilent) and an amplifier (100A250A, Amplifier Research). 1μm and 500nM bead solutions were used for validating the performance of 20 MHz IDTs and 40 MHz IDTs respectively. Human plasma samples (Zen-Bio Inc.) and saliva obtained were processed by the acoustofluidic chip. Isolated exosome samples, nanometer sized waste, and micrometer sized waste were collected. Particle size distributions were analyzed by Zetasizer Nano (Malvern) and NTA (Nanosight LM10, Malvern) system.

To used as conventional exosome isolation method control group, same volume saliva samples were processed by ultracentrifugation exosome isolation. Saliva samples were processed by centrifugation at 3000g for 15min at 8°C. Supernatants were diluted with PBS to 2.3ml and spun at 120,000g in TLS-55 tubes for 45min at 8°C. Supernatants were then discarded and 120K pellets were resuspend by 2.3ml PBS for another 120,000g

differential centrifugation in TLS-55 tubes for 45 min at 8°C. Pellets were then resuspended by 100μl PBS and stored at -80°C.

2.3.4 Downstream validation

To validate the isolated exosome samples yield, purity, and biomarker level, transmission electron microscopy (TEM), immune-blot, and RT-PCR experiments were utilized. To derive TEM imaging, the isolated exosome sample was fixed by paraformaldehyde. A 300-mesh copper grid support film (Electron Microscopy Sciences) was used to cover 100μl drop of isolated exosome sample for absorption. The grid was then washed by distilled water, followed by uranyl–acetate negative staining. Finally, the grid was washed again using distilled water and left to air dry at room temperature. The sample was then observed under electron microscope (FEI Company).

For deriving immuno-blot analysis, Oasis Diagnostics' saliva collectors were used to collect saliva. Isolated products (including exosomes, nanometer sized wastes, micrometer sized wastes) from similar volume original samples were processed by differential centrifugation. 20μl of each sample was lysed in Pierce Cell Lysis Buffer (Thermo Fisher Scientific) with Halt Protease Inhibitor Cocktail (Thermo Fisher Scientific) mixture. Lysates were processed by SDS/PAGE and transferred to a polyvinylidene fluoride membrane (Bio-Rad). Primary antibodies, including mouse anti-CD63 (Santa Cruz), mouse anti-HSP90 (Abcam), and rabbit anti-TSG101 (Abcam), were separately used for incubating the membrane for 12h at 4°C. Appropriate HRP secondary antibody

incubation, including goat anti-mouse IgG (Abcam) and goat anti-rabbit IgG (Abcam), was used for 1h incubation at room temperature. ChemiDoc XRS+ (Bio-Rad) was used to characterize protein expression levels.

To derive RT-PCR analysis, the exosomal RNA extraction from optimized acoustofluidic separation and ultracentrifugation methods was performed with miRNeasy micro kit (QIAGEN) according to the instruction of the manufacturer. The reverse transcription was conducted with TaqMan MicroRNA Reverse Transcription Kit (Thermo Fisher Scientific). DNA was extracted from salivary microvesicles and exosomes from HPV-OPC patients with Quick-gDNA MiniPrep kit (Zymo Research). The ddPCR was performed by using Droplet Digital PCR (Bio-Rad QX100). A 20μl of a PCR reaction containing 10μl 2×ddPCR supermix (Bio-Rad), 1μl 20× TaqMan probes/primers, 4μl sample DNA or cDNA, and 5μl distilled water was well mixed. The small RNA Taqman assay for miR148a and piR014923 were ordered from Thermo Fisher Scientifc. For HPV-16 assay, primer sequences were adapted from the paper and the probe sequence is: FAM/TGCGTACAAAGCACACACG TAGACATTC/IBFQ (Wang et al., 2015). The PCR reactions were transferred into sample wells of an eight-channel disposable droplet generator cartridge (Bio-Rad). An additional 70μl of droplet generation oil was loaded into the oil well for each channel. After droplet generation, droplets were pipetted to a 96-well PCR plate gently. The plate was heat-sealed, placed in a thermal cycler for PCR with the following cycling conditions: 95°C× 10min (1 cycle), 40 cycles of 94°C× 30s and 58°C×

1min, and 12°C hold. At last the PCR plate was read on the droplet reader, followed by data analysis with QuantaSoft analysis software (Bio-Rad).

2.4 Results and discussion

2.4.1 High viscosity fluid influence on acoustofluidic separation

The device performance for bead separation in normal PBS is shown in Figure 2-2. Simulation and experimental results demonstrate the acoustofluidic chip's performance is not dramatically decreased in high viscosity conditions. DI water (with viscosity of 0.89 mPas) and 30% sucrose water solution (2.65 mPas at room temperature) represent different viscosity conditions (Telis et al., 2007). Simulation results in Figure 2-2A and B show the first and second stages can separate particles in both with low and high viscosity fluids. Upon SAW activation, the acoustofluidic device can separate 2μm beads to waste outlet in both low viscosity (Figure 2-3D) and high viscosity (Figure 2-3E) compared to no SAW activation (Figure 2-3C). Particles distributions on the vertical direction of the channel were analysis by Image J and demonstrated by fluorescent intensities. Compared to low viscosity conditions, in high viscosity liquid, more particles are closer to exosome outlet, indicating high viscosity impedes particle movement to the waste side. The second stage of removing of 500nm particles was also successful in both low and high viscosity conditions (Figure 2-3F, G, and H). For 500nm particales however, fluorescent intensity distribution differences between low and high viscosity conditions was not as obvious as 2μm particles, indicating weak drag force disruption on small particles discrimination.

For particles smaller than 150nm, SAW fields in the two stages cannot generate enough acoustic radiation force, meains these particles can flow to exosome outlet.

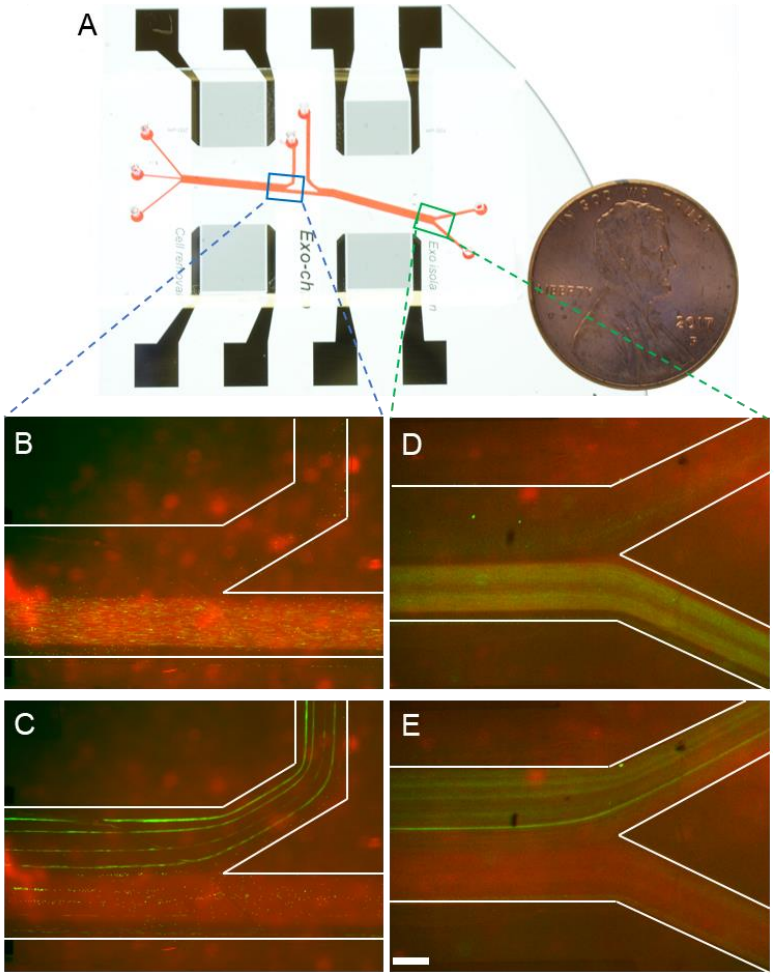

Figure 2-2: Particle isolation using different size polystyrene particles mixture. (A) Photo of the acoustofluidic platform. Squares demonstrate areas for microscopy capturing. (B) Mixture of 2μm (green) and 50nm (red) particles after the first stage without SAW. Both of large and small particles flow to the second stage. (C) Mixture of 2μm (green) and 50nm (red) particles after first stage with SAW field in the channel. 2μm particles are pushed to the waste outlet, while 50nm particles continuous go to the second stage. (D) Mixture of 500nm (green) and 50nm (red) particles after the second stage without SAW. Both of large and small particles flow to the exosome outlet. (E) Mixture of 500nm (green) and 50nm (red) particles after first stage with SAW field in the channel. 500nm particles are pushed to the waste outlet, while 50nm particles continuous go to the exosome outlet. Scale bar 200μm.

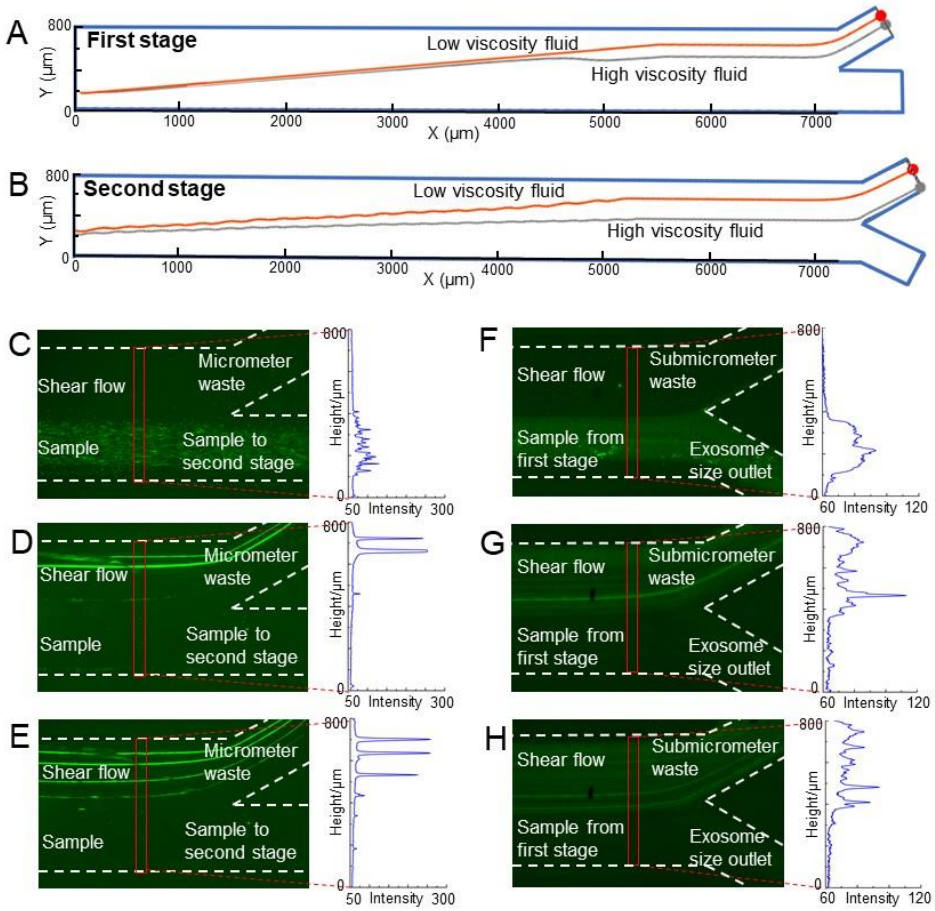

Figure 2-3: Fluid viscosity's influence on particles separation. (A) Simulation of 2μm particles routes in different viscosity conditions with 20 MHz SAW in 0.89 and 2.65 mPas viscosity fluid. (B) Simulation of 500 nm particles routes in different viscosity conditions with 40 MHz SAW in 0.89 and 2.65 mPas viscosity fluid. 2μm particles routes in SAW off (C), SAW on in low viscosity liquid (D), and SAW on in high viscosity liquid (E) conditions. SAW can achieve separation ignoring viscosity, but high viscosity causes more particles closer to exosome outlet. 500nm particles routes in SAW off (C), SAW on in low viscosity liquid (D), and SAW on in high viscosity liquid (E) conditions. SAW can achieve separation ignoring viscosity, and impedance caused by viscosity difference is not obvious. There is no mention of panels F, G, and H in this legend.

2.4.2 Salivary exosome isolation and validation

Following simulation and experimental validation using polystyrene particles, acoustofluidic chip performance for salivary exosome isolation were validated by saliva samples collected by different approaches. Since collection methods can potentially influence saliva samples' compositions, directly collected whole saliva, centrifugation of processed cell free saliva, and saliva collected by the Oasis Diagnostics' collector were compared. Flow rates for each inlet and the driving power on two stage IDTs are consistent with seSAWings used for particle validation. NTA measured particle size distributions of different saliva samples after processing by acoustofluidic chip (Figure 2-4 A, B, and C) contain low concentrations of particles bigger than 200nm. Compared to samples before isolation (Figure 2-4D, E, and F) that contained high ratio of particles larger than 150nm, acoustofluidic chip processed samples demonstrated successful elimination of particles that are not in exosome size range. Size distributions of products from exosome, submicrometer waste, and micrometer waste outlets showed each product contained particles in different size ranges. Further evaluation of isolated exosome morphology was processed by TEM images. Particles with diameters around 100 nm with cup-like concavity, which is consistent with the established morphology of exosomes, are marked by arrows in Figure 2-4G and H, which are isolated and original whole saliva samples. TEM images of isolated exosome samples lacked big fractions and irregular shape components, indicating a high purity isolation. Isolated salivary exosomes present

same morphology as blood exosomes. Exosomal biomarkers CD63, TSG101, and HSP90 are found in the isolated samples but are absent in wastes, and the abundances of targeted proteins are similar with proteins from an equal volume original sample, indicating isolated samples preserved exosomal proteins at a high yield.

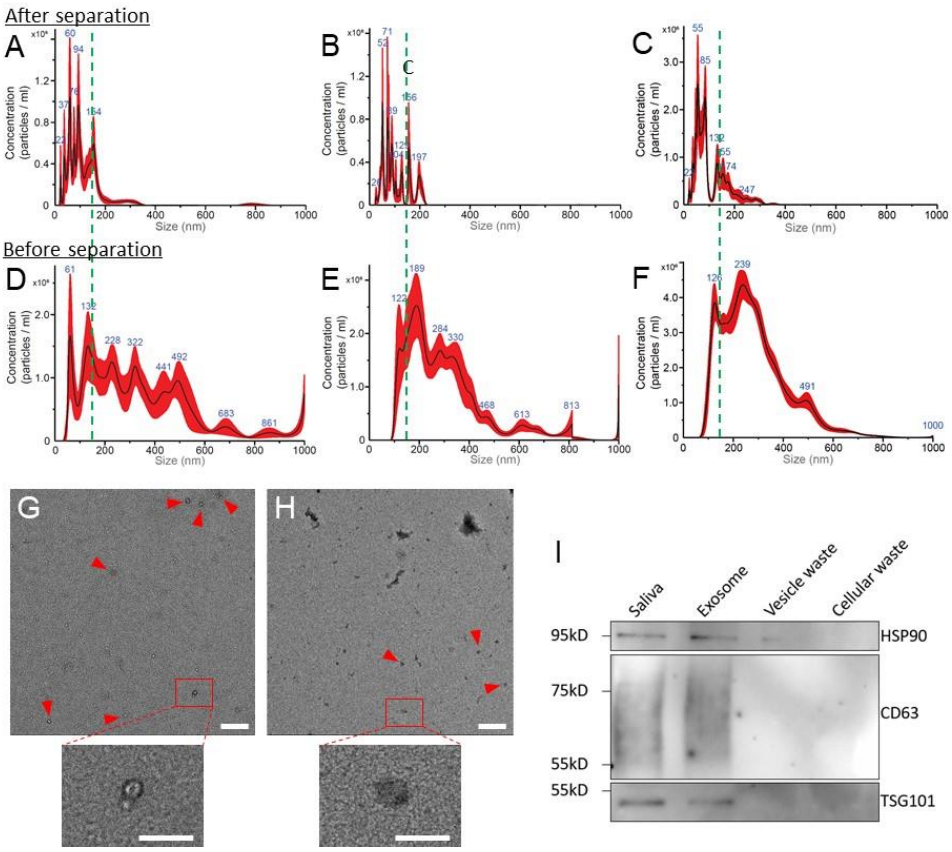

Figure 2-4: Characterization of acoustofluidic chip exosome isolation. Particles size distributions of acoustofluidic isolated cell free saliva (A), Oasis collector collected saliva (B), and whole saliva (C) demonstrate low concentration of particles bigger than 200nm compared original samples of cell free saliva (D), Oasis collector collected saliva (E), and whole saliva (F). TEM image demonstrate isolated whole saliva sample (G) containing less contaminations than original sample (H), particles with exosomal morphology are tagged by red arrow. (I), western blot for exosomal protein biomarker. Only isolated exosome product demonstrates exosomal biomarkers with similar levels of original sample. Scale bar: 500nm for zoom out, 200 nm for zoom in.

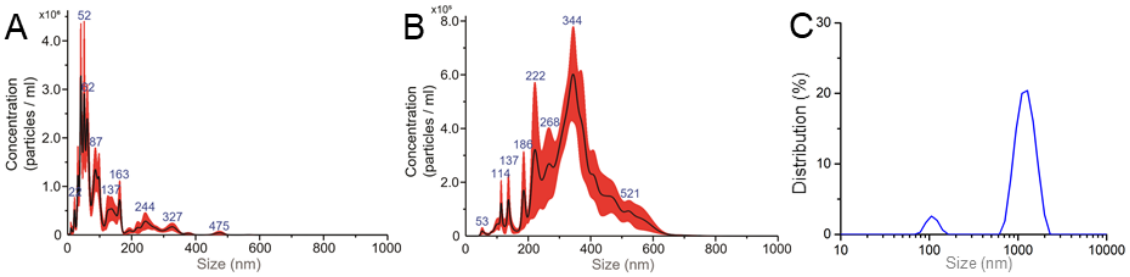

Figure 2-5: Size distribution of saliva isolation products from different outlets. (A) Size distribution of isolated saliva from exosome outlet. Majority of particles are smaller than 200nm. (B) Size distribution of isolated saliva from submicrometer waste outlet. Majority of particles are between 200 and 600nm. (C) Size distribution of isolated saliva from micrometer waste outlet. Majority of particles are around 1μm.

2.4.3 Acoustofluidic salivary exosome isolation yield

We further investigate whether the yield of exosome from acoustofluidic isolation platform compare with referenced method by ultracentrifugation. It has been previously demonstrated that the majority of small RNAs including miR148a and piR014923 were packaged in salivary exosomes.(Bahn et al., 2015) These two small RNAs were used as markers to compare the yields of exosome from different methods with the identical saliva sample. The RNA was extracted from exosomes isolated from ultracentrifugation and different vesicle fractions from acoustofluidic platform. The droplet digital PCR (ddPCR) was performed to compare the copy number of miR148a and piR014923. As shown in Figure 2-6A, both of miR148 and piR014923 are predominantly located in the exosome fraction compared with other factions (microvesicles and apoptotic bodies) from acoustofluidic platform. It is consistent with results that published previously and suggested the acoustofluidc platform can efficiently separate different salivary excellular

vesicles.(Bahn et al., 2015) Based on the measurements of these two small RNAs, the average yield of exosome from acoustofluidic platform is 15.18 fold (9.37-18.94 fold, SD ± 4.48) higher than that from an ultracentrifugation method (Figure 2-6B).

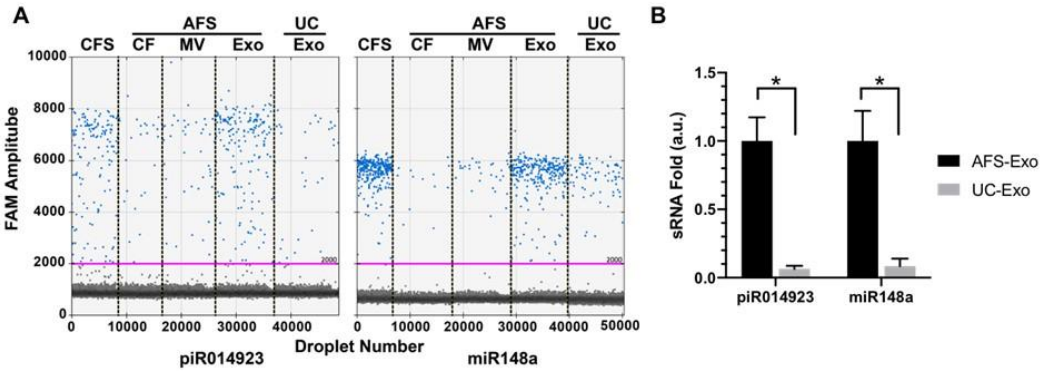

Figure 2-6: Comparison of yields of exosome from acoustofluidic separation technology and ultracentrifugation (UC) method. (A) DNA samples extracted from cell free saliva (CFS), different acoustofluidic isolated fractions (Cell Fraction, CF; Microvesicle, MV; Exosome, Exo) and exosome from ultracentrifugation (UC) were tested with RT-ddPCR assays for piR014923 and miR148a which were reported predominately located in salivary exosomes. (B)The yield (expressed as relative fold difference) of individual small RNA in isolated salivary exosomes with acoustofluidic separation (AFS-Exo) technology and ultracentrifugation (UC-Exo) method. *P < 0.05 (T-test).

2.4.5 Analysis of HPV virus from exosome separated from HPV-OPC patient samples

To validate whether acoustofludic system isolated salivary exosome is effective for HPV-associated OPC screening and subtype analysis, we explored the detection of HPV-16 DNA for early detection/risk assessment of HPV-OPC patients. Wang et al. reported that when analyzing whole saliva from HPV-OPC positive patients with ddPCR, they only detected HPV-16 DNA in 40% of cases. We hypothesize that the HPV-16 DNA sequences in HPV-OPC patients are packaged in salivary exosomes and exosome isolation

will enhance the detection of HPV-16 DNA (Borsetto et al., 2018). To determine the distribution of HPV16 DNA in different EVs (Exo, MV), different vesicles were isolated by acoustofluidic separation from HPV-OPC patients and DNA was extracted from each fraction. A ddPCR assay for detection of HPV16 DNA was designed and tested on DNA extracted from acoustofluidic isolated different vesicles. As shown in Figure 2-7A and B, 92% of total HPV16 signals were concentrated in the exosome fraction which is about 12 folds higher than in microvesicles. HPV16 DNA can be reliably detected in the exosome fractions from HPV-OPC patients. We further tested HPV16 DNA in acoustofluidic isolated saliva exosomes with a 10 HPV-OPC patient cohort. Eight out 10 patients (80%) were tested positive for HPV16 DNA with HPV16 ddPCR assay (Figure 2-7C). These data demonstrated that with the robust acoustofluidic isolation technology and ddPCR assay, the high risk HPV16 for OPC can be detected in 80% of HPV+ OPC patients and the majority of circulating HPV16 DNA are contained in the exosomal fraction. These results demonstrate the existence of virus induced oral cancer pathology related molecules exist in the acoustofluidic exosome separation technology isolated samples. Compared with conventional exosome separation technologies including ultracentrifugation, acoustofluidic technology has higher isolation yield, which enables the detection of low abundance target exosomes that contains the pathology related molecules.

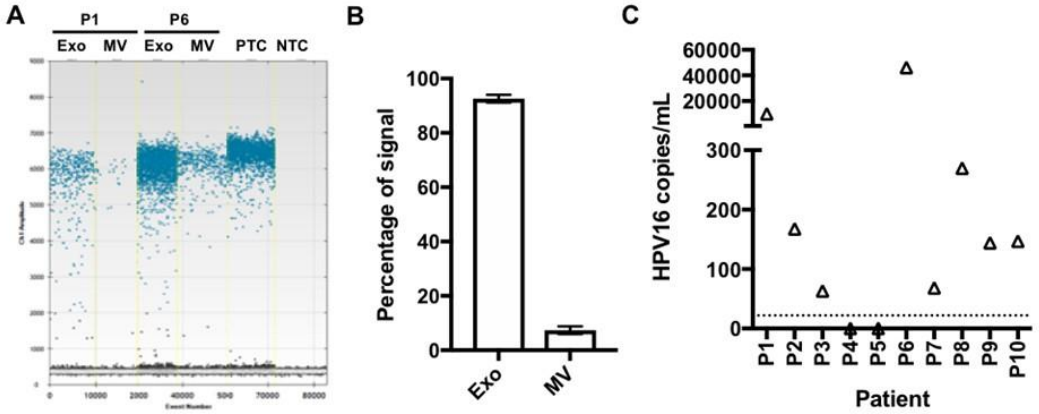

Figure 2-7: Detection of HPV16 DNA in acoustofluidic separated saliva exosome of HPV16 positive OPC patients. (A) Distribution of HPV16 DNA in exosome (Exo) and microvesicles (MV) isolated from saliva of HPV16+ OPC with acoustofluidic technology. Representative results from two HPV16 exosome positive patients. ddPCR HPV16 DNA detection on different vesicle fractions isolated by acoustofluidic device. (B) HPV16 signals in different vesicle fractions. (Exo: exosomes; MV: microvesicles; PTC: positive control with synthetic HPV E7 gene; NTC: negative control). (C) Results of HPC16 ddPCR assay for saliva exosome of HPV-OPC patients. Eight of 10 patients were positive for HPV16 DNA (80%). Dashed line shows a threshold of detection at 21.9 copies/mL saliva.

2.5 Conclusion

The acoustofluidic platform achieved rapid, high purity, and high yield for salivary exosome isolation based on size difference between exosome and other salivary components. Driven by acoustic radiation force and fluid drag force, the isolation process is physical and biocompatible.

The acoustofluidic platform has high tolerance for sample viscosity fluctuations and multiple saliva collection protocols. Different than blood, which has a relatively stable composition, components in saliva show dramatic differences related to health statu.(Dawes, 2008, Epstein et al., 2012) Composition change leads to dramatic viscosity

differences: compared to the viscosity of plasma (1.10-1.30 mPas), saliva viscosity ranges from 1.10 to 2.30 mPas, which can cause unpredictable fluidic drag force interference on acoustofluidic exosome isolation.(Christersson et al., 2000, Késmárky et al., 2008) For OPC patients, physical and mental stress during salivary collection or radiation-induced xerostomia can alter salivary properties and affect viscosity.(Dirix et al., 2006) Successful performance in high viscosity fluid and reproducible isolation on saliva collected by multiple approaches shows the platform's high adaptability, which is important for real-life clinical applications.

The acoustofluidic platform performs biocompatible exosome isolation with high purity and yield. Particles in isolated saliva samples have exosomal size and morphology, indicating isolated samples contain high purity exosomes. Isolated samples containing exosomes' biological features and cargoes, indicates exosome integrity was protected. Through quantitative PCR for miRNAs, we further determined that isolated samples contained equivalent abundance of exosomal miRNA as with the original untreated samples. Abundance of exosomal miRNA in acoustofluidic isolated samples was higher than sample isolated by differential centrifugation isolation, indicating acoustofluidic exosome isolate can achieve higher isolation yield. An explanation is that during differential centrifugation process, remnant exosomes in the supernatant may be inadvertently discarded. Furthermore, when processing small volume samples by differential centrifugation, pellets containing exosomes are difficult to visualize and

difficult for complete recovery. Since exosomes in OPC patients' saliva have complex origins and sample volume is often low, reproducible biocompatible, high purity, and high yield properties of acoustofluidic exosome isolate can significantly benefit the salivary exosome-based liquid biopsy.

OPC related biomarkers were further identified in the acoustofluidic platform isolated sample. We have successfully detected the human papillomavirus-16 (HPV16) DNA in saliva of OPC patients. Salivary HPV DNA biomarkers could evaluate the risk of HPV OPC, which is present in more than 80% of OPC cases.(Herrero et al., 2003, Wong, 2006) Studies have also shown tumor progression is promoted by HPV16 DNA integration that inactivate p53 and retinoblastoma tumor suppressor gene.(Gasco et al., 2003) These evidences indicate acoustofluidic isolated salivary exosomes can used for early detection and screening for the pathogenic subtype of OPC.

Developing salivary exosome isolation for liquid biopsy enables OPC early detection, risk assessment and treatment monitoring. Head and neck cancer (HNC) is the sixth most common cancer worldwide, with an annual incidence of around 600,000 cases; it has a poor outcome with a 5-year mortality rate of around fifty percent. OPC is a subtype of HNC that starts inside the part of the throat directly behind the nose. The most common type of OPC is squamous cell cancer of the oropharynx, which is difficult for clinical detection.(Neville et al., 2002, Brocklehurst et al., 2013) Traditional biopsy can provide histological definition and demonstrate genetic profile of the cancer, which determine the

appropriate therapy and precise prognosis, by single snap-shot of the lesion.(Lingen et al., 2008) But current clinical examination approaches, mostly visual examination and palpation, cannot identify premalignant lesions in oral cavity.(Neville et al., 2002) Considerable tumor heterogeneity further causes the response of cancer to therapy diversified and bring the necessity of continuous monitoring, which is challenging to traditional biopsy approaches that are invasive and bring inherent clinical risk to the patient. Liquid biopsy can screens tumor through genomic and proteomic molecular targets in saliva.(Bardelli et al., 2017)

Multiple studies have revealed salivary exosomes are suitable candidates for liquid biopsy. Since exosomes are released through fusion between endosomal membrane compartments and plasma membrane, both extracellular and intracellular biomarkers that can reveal the type and status of the origin cell are contained. Tumor cells derived exosomes contain specific cargoes that can activate tumor progression and metastasis, and has been investigated in diagnostics and therapeutics.(Kahlert et al., 2013, Hoshino et al., 2015) Previous studies have demonstrated exosome isolation enriches salivary miRNAs and surface biomarker of tumor cells, indicating salivary exosomes' potential for liquid biopsy. However, isolation has become the main limitation for developing salivary exosome for early diagnosis. Since saliva is composed of a complex mixture of secretory products from multiple tissues, salivary components other than exosomes can interfere the detection of exosomal cancer biomarkers.(Michael et al., 2010)

Previous research has demonstrated more miRNAs are detected from purified salivary exosomes than whole saliva, indicating exosome isolation will enhance and advance disease biomarker detection.(Gallo et al., 2012)

Acoustofluidics is an efficient biocompatible platform for sample isolation. With a single device, exosome isolation is automated and avoid multistep protocols that require several instruments and trained technicians. Shortened isolation time and low sample consumption enhance biosafety and allow high throughput screening in large population of patients. High toleration to physical property fluctuation of sample further provide the platform potential for applicable in real conditions. Since isolation derived by low-power-intensity SAW is potentially gentler than long term exposure to high centrifugal force, the platform has potential to isolate structurally intact and biologically active exosomes. Furthermore, high purity and yield properties allow the investigation of rare exosomal miRNAs and proteins' signature in OPC patients' saliva, which can significantly improve the genomic and proteomic profiling efficiency by liquid biopsy. OPC has an approximate incidence of 115,000 cases per year worldwide and is one of the fastest rising cancers in Western countries, due to increasing HPV-related incidence.(Chaturvedi et al., 2011) With the increasing incidence of HPV+ OPC it is paramount that surveillance methods are developed to improve early detection and outcomes. Considering these facts, successful detection of HPV16 from salivary exosomes isolated by the acoustofluidic system supports the system can offer exosome isolation with distinct advantages that can benefit

saliva-exosome-based liquid biopsy detection of HPV16 for early detection, risk assessment and screening for HPV OPC.

3. Acoustofluidic exosome separation for TBI diagnosis

Traumatic brain injury (TBI) is a global cause of morbidity and mortality. Initial management and risk stratification of patients with TBI is made difficult by the relative insensitivity of screening radiographic studies, as well as the absence of a widely available, noninvasive biomarker diagnostic. In particular, a blood-based biomarker assay could provide a quick and minimally invasive process to stratify risk and guide early management strategies in patients with mild TBI (mTBI). Analysis of circulating exosomes allows the potential for rapid and specific identification of tissue injury. By applying acoustofluidic exosome separation—which uses a combination of microfluidics and acoustics to separate bioparticles based on differences in size and acoustic properties—we successfully isolated exosomes from plasma samples obtained from mice after TBI. Exosomal biomarkers for TBI could be detected in the first 24 hours following head trauma, indicating the potential of using circulating exosomes for the rapid diagnosis of TBI. Elevated levels of TBI biomarkers were only detected in the samples separated via acoustofluidics; no changes were observed in the analysis of the raw plasma sample. This demonstrated the necessity of sample purification prior to exosomal biomarker analysis. Since acoustofluidic exosome separation can easily be integrated with downstream analysis methods, it shows great potential for early diagnosis and treatment decisions associated with TBI. Results and discussion in this chapter comes from my published first author paper (Wang et al., 2021).

3.1 Motivation

Traumatic brain injury (TBI) represents a significant public health issue in the United States and internationally.(Faul et al., 2010) Around the globe, more than 50 million individuals are estimated to suffer from TBI annually, resulting in more than 50,000 deaths and 100,000 disabilities.(Hyder et al., 2007) The complicated pathology and multiple forms of TBI result in unpredictable outcomes. Long-term complications from TBI—which include cognitive impairment, post-traumatic epilepsy, chronic traumatic encephalopathy, dementia, and cranial nerve injuries—can lead to lifelong consequences and high medical costs. A main factor contributing to the progression of TBI to more serious conditions is a lack of early diagnostics for TBI. Approximately 40% of TBI patients fail to get proper medical attention because of ineffective initial diagnosis. Imaging modalities, which include computed tomography (CT) and magnetic resonance imaging (MRI), are sensitive to the presence of intracranial hemorrhage and edema. These modalities, however, cannot distinguish TBI cases that do not present significant structural injury.(Bigler et al., 2011, Kim et al., 2011) Furthermore, there is a gap between primary screening based on symptoms and imaging modalities. Many TBI patients with unclear or minor symptoms do not receive imaging-based diagnostics, resulting in inaccurate diagnoses.(Dash et al., 2010, Gardner et al., 2018)

As an adjunctive approach for risk stratification in TBI, cerebrospinal fluid (CSF) is effective; however, the invasiveness of the procedure severely limits its utility. To

reduce high-risk populations from suffering lifelong TBI-related disabilities or even fatal outcomes, it is critical to develop more effective, noninvasive diagnostic methods for the early identification of tissue injuries.(Olson et al., 2011) This identification might facilitate triage and early decision-making in high-risk populations.

The analysis of biomarkers found in circulating exosomes represents a potential approach for low-cost and minimally invasive screening of TBI.(Goetzl et al., 2018) Exosomes are 30–150 nm membranous vesicles released by viable cells, including neurons, into bodily fluids. When cells are in abnormal states—including malignant transformation, cells that have undergone damage, and apoptosis-related changes—their secreted exosomes contain altered protein and molecular signatures. Circulating exosomes found in the blood have been studied as potential targets for the development of blood-based, point-of-care diagnostic platforms for cancer.(Zhao et al., 2016) Because exosomes are released into circulation, they offer the potential to detect remote lesions. A similar strategy can be employed to monitor the status of the brain by analyzing exosomes released from injured CNS tissue into circulation.

Conventional attempts at using blood-based biomarkers for TBI diagnosis are restricted by the complex components of blood and the blood-brain barrier (BBB). These components often limit the ability to detect intrathecal injury markers in peripheral blood.(Blyth et al., 2009) Exosomes, on the other hand, mediate intercellular communication and readily traverse the BBB.(Zhang et al., 2015, Xiong et al., 2017)

Furthermore, the membranous vesicle structure of exosomes can protect disease-related biomarkers from degradation, so the biomarkers can remain in circulation longer. During neuronal injury and dysfunction events, neuron and glial secreted exosomes have been shown to contain biomarkers that can be released into peripheral blood, indicating the potential of circulating exosomes for TBI initial diagnosis. However, current exosome isolation technologies have low yields and can damage exosomes, resulting in a loss of biomarkers. Furthermore, conventional ultracentrifugation and affinity capture take a long time (several hours to several days), which limits their use in point-of-care settings. As a result, with most current exosome isolation technologies, it is not suitable to use exosomes as point-of-care biomarkers for TBI screening and diagnosis.

Acoustofluidic technology is a potential solution for exosome-based TBI diagnosis. The underlying mechanism of acoustofluidics uses acoustic waves to generate acoustic radiation forces on particles in the fluid; the strength of the acoustic radiation force depends on the size and density of the particle. High biocompatibility of acoustofludic devices also benefit downstream analysis by providing samples with complete structures and components. Previously, we have used acoustofluidics to separate bioparticles, including cells, bacteria, and platelets, in a highly biocompatible manner. By generating surface acoustic waves (SAWs) with tilted-angle interdigital transducers (IDTs) pairs, a tilted-angle standing wave field is generated and can separate particles based on differences in size and density.(Wu et al., 2018, Kang et al., 2020) In our previous study,

the acoustofluidic device was used to successfully isolate exosomes from whole blood at a high yield, while maintaining the morphology and molecular content of isolated exosomes .

3.2 Mechanism and system

In this work, we have further investigated whether the advantages of our acoustofluidic device can enable the early diagnosis of TBI based on biomarkers found in circulating exosomes. To simulate the neuropathology of TBI, we collected blood in a well characterized model of rodent closed head injury. Early diagnosis is critical for the treatment of TBI in order to minimize secondary tissue injury and optimize triage and initial care. To evaluate the possibility of early TBI diagnosis based on the analysis of circulating exosomes, we used a murine head injury model to comprehensively simulate pathology changes that occur immediately after TBI. Closed skull impact models (Figure 3-1A) are widely accepted as animal models for TBI as they recapitulate many of the clinical features associated with TBI, and they have been used to screen for molecular signatures of TBI in its early stages. Murine blood samples were collected before TBI treatment to gather baseline measurements of all blood components, and additional samples were collected at times 3 h, 6 h, and 24 h after pneumatic impact to measure levels of potential exosomal biomarkers for TBI.

Before flow cytometry analysis, samples were first processed by acoustofluidic exosome separation chips. When flowing through these devices, particles in the sample

were separated based on differences in size. This separation eliminated larger cells, platelets, and other extracellular vesicles (such as apoptotic bodies and microvesicles), which are larger than exosomes. The driving force behind this size-based isolation was the acoustic radiation force, which was induced by the acoustic fields generated by the IDTs around the channel (Figure 3-1B). The device contained two separation modules to sequentially remove particles larger than exosomes. The IDTs in the first module generated a lower frequency acoustic field, which is optimized for removing cell components and platelets. The second module generated a higher frequency acoustic field for removing apoptotic bodies and microvesicles, which are extracellular vesicles larger than exosomes. Collected samples are then processed by flow cytometer for evaluating the abundance of TBI pathology related exosomes (Figure 3-1C).

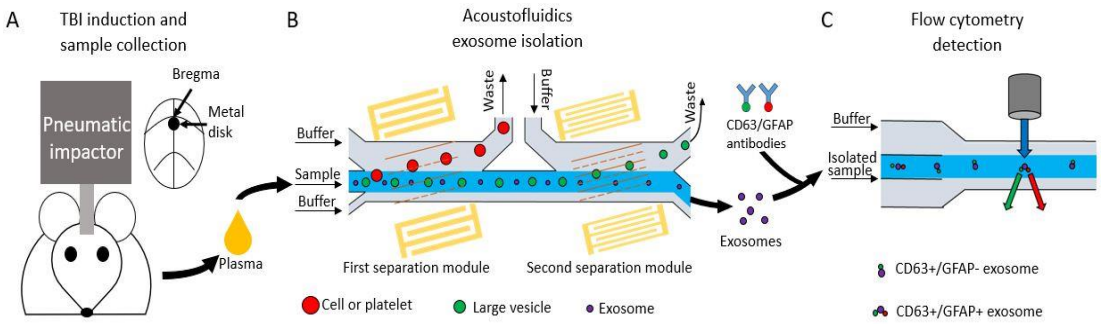

Figure 3-1: Schematics detailing the process of detecting exosomal biomarkers for TBI from the blood of animal models. (A) A pneumatic impactor induced TBI in murine models; the impact was at the bregma, covered by a metal disk. (B) Mice plasma samples were processed through an acoustofluidic chip with two separation modules. Cells and platelets were removed by the first separation module, while large vesicles, including microvesicles and apoptotic bodies, were removed by the second separation module. Exosomes remained in the collected samples. (C) Isolated samples were stained with fluorescence-tagged anti-CD63 and anti-GFAP antibodies and analyzed with a flow cytometer for detecting CD63+/GFAP+ events.

By using acoustofluidics to isolate exosomes from mouse plasma samples and analyzing the abundance of glial fibrillary acidic protein (GFAP), we associated an exosomal biomarker for TBI with reactive astrocytes responding to brain injuries. We found an increase in GFAP-positive exosomes soon after a closed head injury. Neuron intake experiments further show that exosomes isolated from TBI mice have higher intake rates as compared to healthy controls. These rates indicate that the exosomes isolated via acoustofluidics are bioactive and involved in TBI pathology. These results indicate that acoustofluidic exosome separation technology is a powerful method for exosome-based TBI initial diagnosis and research.

3.3 Experiment methods

3.3.1 Acoustofluidic device fabrication

Fabrication of the acoustofluidic device followed our previously published procedures.(Wu et al., 2017) During photolithography and lift-off processes, two pairs of tilted-angle IDTs with frequencies of 20 MHz and 40 MHz were deposited on a Y+128° X-propagation lithium niobate (LiNbO3) substrate. The designs of the IDTs were created by UV exposure combined with SPR3012 photoresist (MicroChem Corp., USA) aligned by a MA/BA6 mask aligner (SUSS MicroTec., Germany). Unwanted photoresist was then removed by CD26 developing solution (MicroChem Corp., USA), and a metal double layer (Cr/Au, 50 Å/500 Å) was deposited by an e-beam evaporator (Semicore Corp., USA) on the substrate. IDTs with electrode widths of 50 and 25 μm were formed through a lift-

off process using PRS3000 resist stripper (VWR, USA). A silicon mold was created by SU-8 photoresist (MicroChem Corp., USA) through soft lithography. A PDMS microchannel of height 100 μm and width 800 μm was solidified by Sylgard 184 Silicone Elastomer Curing Agent and Base (Dow Corning, USA) on the mold. The substrate and microchannel were then treated by oxygen plasma coating and bonded at 65 °C overnight.

3.3.2 TBI animal preparation and plasma collection

The murine closed head injury model used in this study was previously described, and it is associated with reproducible histological and functional deficits.(Laskowitz et al., 2010) As is the case with human TBI, the selective closed-head impact injured vulnerable neurons in the cortex and hippocampus. This impact is associated with vestibulomotor deficits and long-term neurocognitive deficits. Although animals do lose body weight, they rapidly regain spontaneous ventilation, righting reflex, and the ability to ambulate.

Briefly, 12–14 week-old C57Bl/6 J male mice (Jackson Laboratories, USA) were endotracheally intubated after anesthesia induction with 4.6% isoflurane, and the lungs were mechanically ventilated with 1.6% isoflurane in 30% O_2/70% N_2 through tracheal intubation. A rectal probe was used for maintaining each mouse's core body temperature at 37°C. After being secured in a prone position, the mouse's head was shaved for identifying anatomical landmarks. The skull was then adhered with a concave 3 mm metallic disc just caudal to bregma, and a single midline impact was delivered to the center of the disc through a pneumatic impactor (Air-Power Inc., USA). The isoflurane

was reduced to 0%, the ventilation was disconnected, and the trachea was extubated after recovery of spontaneous respiration. Each mouse was then returned to its home cage with free access to food and water. The blood extraction time points were before impact, 3 h, 6 h, and 24 h after impact. For each time point, 200 μL of whole blood was extracted with a heparinized syringe through the thoracentesis and ventricle, then centrifuged at 2000 g for 10 min to eliminate blood cells. Collected plasma samples were stored at -80 °C before acoustofluidic exosome isolation.

3.3.3 Acoustofluidic separation and isolated exosome validation

A syringe pump (neMESYS, CETONI GmbH, Germany) was used to independently control the sample and the PBS (Thermofisher, USA) sheath flow. To avoid excessive heat generation from the IDT, a Peltier cooling system (TEC1-12730, Hebei IT, China) powered by a variable DC power supply (TP1505D, Tekpower, USA) was used for cooling the acoustofluidic chip during the exosome separation. The separation process was monitored with an upright microscope (BX51WI, Olympus, Japan) combined with a CCD camera (CoolSNAP HQ2, Photometrics, USA). A function generator (E4422B, Agilent, USA) and an amplifier (100A250A, Amplifier Research, USA) were used to power the IDTs and generate SAWs. Isolated exosome samples were collected in 1.5 mL centrifugation tubes placed on ice, and the size distributions of particles were measured with a Nanoparticle Tracking Analysis (NTA, Nanosight LM10, Malvern, England) system.

To validate the isolated exosome morphology and biomarkers, immuno-blot and immune-TEM were applied. A mixture of Pierce Cell Lysis Buffer (Thermofisher, USA) and Halt Protease Inhibitor Cocktail (Thermofisher, USA) mixture was used to lyse exosome samples. Samples were then processed by electrophoresis and transferred to a polyvinylidene fluoride membrane (Bio-Rad, USA). Mouse anti-CD63 (sc-5275, 1 μg/mL, Santa Cruz, USA), mouse anti-HSP90 (ab13492, 1 μg/mL, Abcam, USA), and rabbit anti-TSG101 (ab30871, 1 μg/mL, Abcam, USA) were used as primary antibodies for incubating the membrane at 4°C overnight. Goat anti-mouse IgG (ab97040, 0.05 μg/mL, Abcam, USA) and goat anti-rabbit IgG (ab97080, 0.05 μg/mL, Abcam, USA) were used as secondary antibodies. Protein abundances were analyzed with a ChemiDoc XRS+ system (Bio-Rad, USA). For antibody-conjugated gold staining, 10 μL of isolated exosome sample was covered by a 300-mesh copper grid support film (Electron Microscopy Sciences, USA) for 20 min of absorption. The grids then incubated a 100 μL drop of 50 mM glycine PBS solution for 10 min, followed by PBS washing. 1% BSA PBS solution was then used for blocking grids. Primary antibodies—mouse anti-CD63 (NBP2-32829, Novus Bio., USA) and rabbit anti-GFAP (NB300-141, Novus Bio., USA)—were independently used for 30 min staining of the grids, followed by PBS washing. 10 nm gold-conjugated, goat-anti-rabbit IgG (Electron Microscopy Sciences, USA) and 15 nm gold-conjugated goat-anti-mouse IgG (Electron Microscopy Sciences, USA) were used for 30 min secondary antibody staining followed by PBS washing. The grids were then incubated with uranyl–acetate

solution for 10 min followed by water washing for complete negative staining. An electron microscope (FEI Company, USA) was used to image the grids.

3.3.4 TBI pathology related exosome detection

For validating whether acoustofluidic isolated exosomes participate TBI pathology, isolated cells intake by astrocyte was evaluated. C8-D1A astrocytes, which is an astrocyte cell line generated from cerebral cortices of neonatal C57BL/6 mouse, were cultured in Dulbecco's Modified Eagle's Medium (Gibco, Maryland) supplied with 10% exosome-depleted fetal bovine serum (Gibco, Maryland). Isolated blood exosomes from a same mouse before pneumatic impactor TBI treatment and 24 h after TBI treatment were labeled by fluorescent tracking dye (Invitrogen, California) and were separately added to C8-D1A culture medium. C8-D1A cells were observed by ZOE Fluorescent Cell Imager (Bio-Rad, California) at 2 h, 4 h, and 6 h after adding isolated exosomes for evaluating exosomes intake rates by fluorescent strength.

The TBI pathology related exosome abundances were evaluated by flow cytometer. To label the general exosomal CD63 and TBI exosomal GFAP, 5 μl of PE rat anti-mouse CD63 (BD Bioscience, California) and 2 μl of Alexa Fluor 647 Mouse anti-GFAP (BD Bioscience, California) were added into 50 μl acoustofluidic isolated exosome samples and original plasma. After incubation, the samples were diluted by 250 μl PBS and fixed by 4% paraformaldehyde (Santa Cruz Biotechnology, California). A BD LSR II flow cytometer (BD Bioscience, California) from Duke Human Vaccine Institute was used

for examining the stained samples. For setting threshold for eliminating noise signals, no staining, only CD63 staining, and only GFAP staining samples were also be examined. Analysis was performed using BD FACS Diva software and FlowJo V10.2.

3.4 Results and discussion

3.4.1 Isolated exosomes validation

To identify the existence of normal exosomes and TBI pathology related exosomes in the isolated sample, particle size distribution, exosome general protein biomarkers, and immuno-TEM morphology analysis were used for sample validation. Compared with the plasma sample, particles' size distribution is similar with exosomes size distribution ranges as Figure 3-2A shows, indicates the successful removal of blood components larger than exosomes. Isolated samples were then processed by western-blot (Figure 3-2B), the existence of CD63, TSG101, and HSP90, which are general exosomal protein biomarkers, demonstrates isolated samples containing exosome components. To further validate the morphology and existences of CD63 and TBI pathology related biomarker GFAP on the surface of isolated exosomes, isolated samples were stained by anti-CD63 or anti-GFAP primary antibodies, followed by gold conjugated secondary antibodies. As Figure 3-2C shows, TEM images shows vesicle structures with gold nanoparticle black dots attached. These results demonstrate isolated samples containing exosome structure vesicles with CD63 or GFAP.

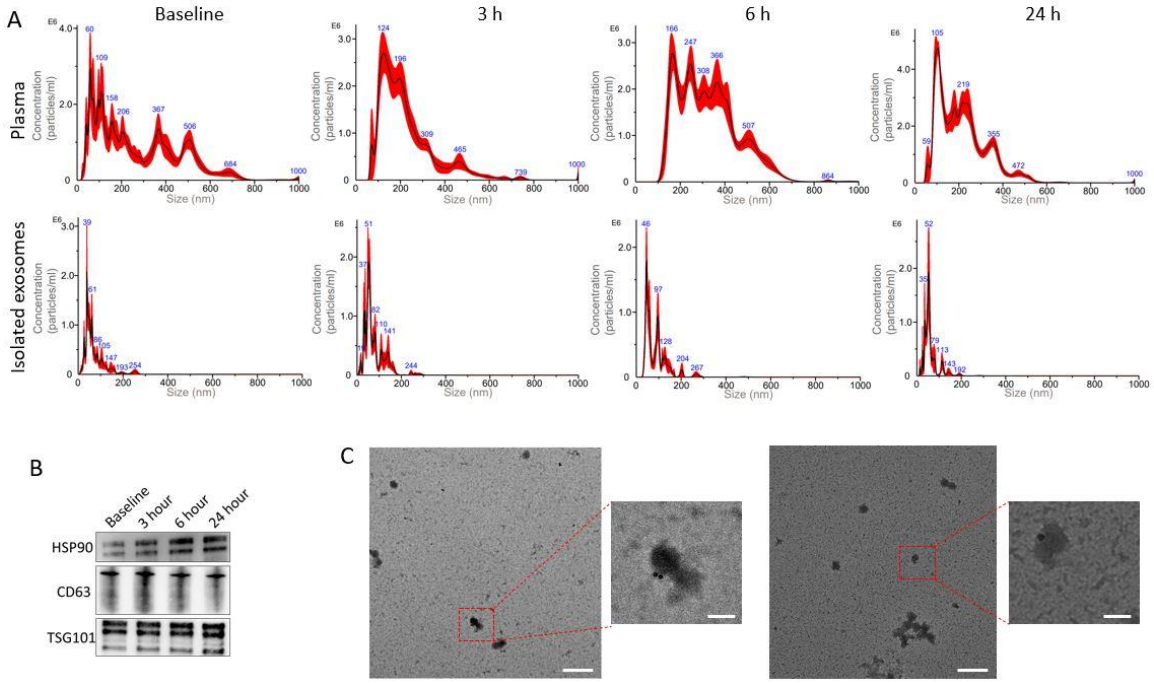

Figure 3-2: Isolated samples validation. (A) Size distributions of plasma without acoustofluidic separation and isolated exosome samples from the plasma collected before TBI, 3 h, 6 h, and 24 h after TBI treatment, isolated samples only containing particles in exosomes' size range, (B) Western-blot analysis of exosome biomarker proteins CD63, TSG101, and HSP90, exosomal biomarkers exist in all isolated samples from plasma collected at different timepoint, (C) Immuno-transmission electron microscopy of isolated exosome samples, exosomes are attached by gold conjugated antibodies, indicate the existence of CD63 and GFAP proteins in exosomes, scale bars: 500 nm, 100 nm.

3.4.2 Astrocytes TBI exosome intake

To evaluated whether the detected CD63+/GFAP+ exosomes participated TBI pathology, isolated samples before TBI and 24 h after TBI were tagged by DIO fluorescent dyes and added for C8-D1A astrocytes culture. As Figure 3-3 shows, during the 6 h intake period, C8-D1A added with exosomes isolated from 24 h after TBI shows higher strength of intracellular fluorescence than the before TBI sample. This result indicates in 24 h after

TBI samples, there are more exosome populations that are easily be intake by astrocytes. Since exosome derive intercellular communication and transport pathology molecules among neurons in neurodegeneration diseases, high intake of 24 h after TBI samples indicate TBI derived exosomes are released to blood and preserve pathological functions.

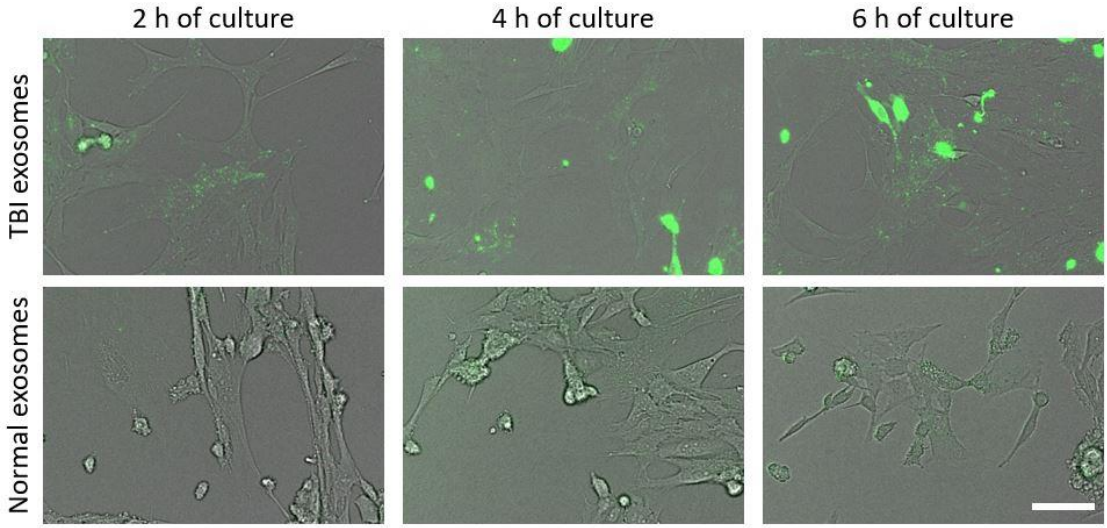

Figure 3-3: C8-D1A astrocytes cultured with isolated exosomes from mice plasma, compared with normal exosomes isolated from mice plasma before TBI treatment, exosomes isolated from plasma collected 24 h after TBI treatment have a higher intake rate by astrocytes demonstrated by fluorescence strength, indicate existence of exosomes that participate neuronal activities.

3.4.3 Validate the feasibility of TBI exosome detection using flow cytometer

Currently using flow cytometer for exosome detection is challenging and lack of standard procedures because of exosomes' small size. To increase the flow cytometer's ability for detecting exosomes, fluorescent GFAP antibody and CD63 antibody were used for tagging TBI pathology related exosomes and normal exosomes. To determine the detection thresholds for distinguishing CD63-/CD63+ particles and GFAP-/GFAP+

particles, isolated blood exosomes from mice models after TBI treatment for 24 h were separated to three same volume samples and stained by fluorescent GFAP antibody and CD63 antibody separately. The rest sample was not stained for getting the baselines of fluorescence strength. According to Figure 3-4A and B, compared with no fluorescent tagged exosomes and PE-CD63 tagged exosomes show a rapid increasing of PE fluorescent signal, demonstrated by most of the events in the no fluorescent tagged sample are concentrated at CD63-/GFAP- area, while for PE-CD63 tagged samples, part of the events migrated to the CD63+/GFAP- area. This signal difference indicate fluorescent antibody can staining CD63+ exosomes and the exosomal CD63 fluorescent signals could be detected by flow cytometer. The event distribution comparison between no fluorescent tagged exosomes and Alexa fluor 647-GFAP tagged exosomes do not show very significant difference, since compared with GFAP- normal exosomes, TBI pathology related GFAP+ exosomes have lower population that cannot demonstrate obvious event migration. However, the particle size (FSC) and granularity (SSC) information shows the particles in the GFAP+ area of no fluorescence tagged samples containing events from large size and granularity particles as the red circle demonstrates in Figure 3-4D. While in Figure 3-4F, which is GFAP+ area of Alexa fluor 647-GFAP tagged samples, majority of the events are from particles with lower size and granularity. This size and granularity distribution difference indicate the GFAP+ events in no fluorescence tagged samples are noise, while the majority of GFAP+ events in Alexa fluor 647-GFAP tagged samples are

from exosomes containing GFAP. Figure 3-4A and C also show Alexa fluor 647-GFAP tagged samples have more event of GFAP+ signals (13.8%) than no fluorescence tagged samples (7.34%), indicate GFAP exosomes could be stained and detected. The GFAP+ events in PE-CD63 tagged samples show similar FSC and SSC distribution with no fluorescence tagged samples as red circle in Figure 3-4E shows, indicate these events also caused by noise.

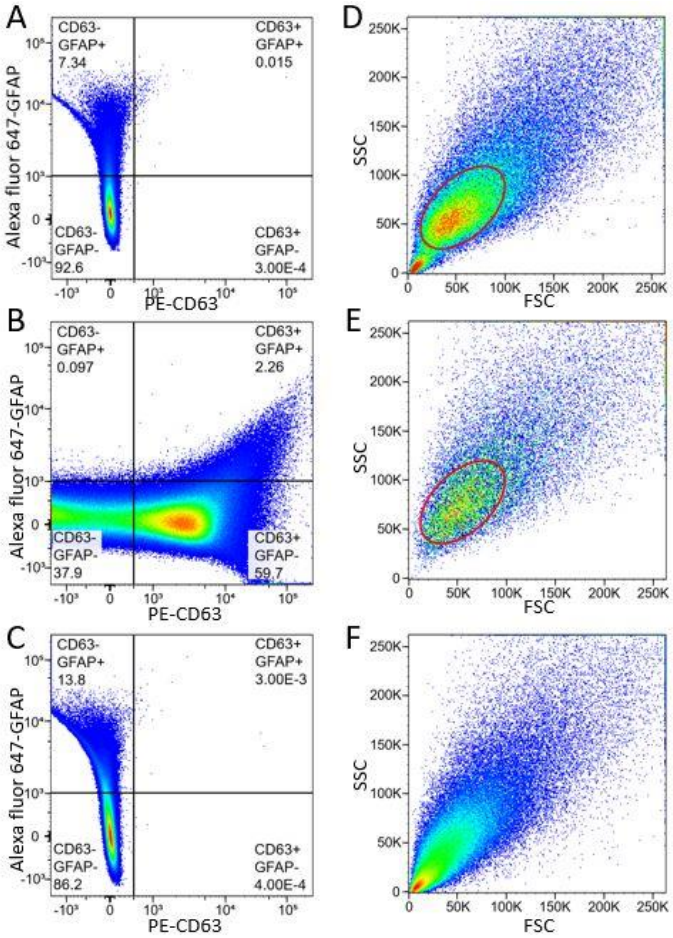

Figure 3-4: Single staining of exosomes isolated from plasma collected 24 h after TBI treatment. (A) Exosomes without fluorescence tagged antibody staining, most of the events concentrate in CD63-/GFAP- area, (B) Exosomes only stained by

PE-CD63, events migrate to CD63+/GFAP- area represent existence of normal exosome containing CD63 protein, (C) Exosomes only stained by Alexa fluor-647-GFAP, events at CD63-/GFAP+ area show percentage increase compared with Fig. 17A, indicate existence of TBI exosomes containing GFAP protein, (D) FSC and SSC of CD63-/GFAP+ area of Fig. 17A, indicate events are induced by noise from large particles as the red circle shows, (E) FSC and SSC of CD63+/GFAP+ area of Fig. 17B, indicates most of events are induced by noise from large particles, (F) FSC and SSC of CD63-/GFAP+ area of Fig. 17C, indicates majority of events are from small size particles including exosomes.

3.4.4 TBI related exosomes population change after TBI

Based on the threshold for distinguish CD63+/- and GFAP+/- events, blood samples from three TBI mice were proceed AFS isolation and flow cytometer. Samples were were collected before TBI treatment, and 3, 6, 24 hours after the treatment, and the CD63+/GFAP+ events show an increase trend on percentage following time increase, as Figure 18A shows. The CD63+/GFAP+ events increase from 2.08% of baseline to 2.65%, 5.24%, and 7.03% at 3 h, 6 h, and 24 h after TBI, indicates CD63+/GFAP+ exosomes' abundance increases in blood. To evaluate the percentage of noise signals in the CD63+/GFAP+ events, FSC and SSC data of these events were demonstrated as Figure 18B shows. Particle size and granularity of CD63+/GFAP+ events for the sample collected before TBI are significantly larger than exosomes, indicate these events are induced by noise from large particles. For the sample collected after 3 h of TBI treatment, a population of CD63+/GFAP+ events induced by low FSC/SSC signals occurs, and continuous increase at 6 h and 24 h. This CD63+/GFAP+ population size change indicate before TBI, the CD63+/GFAP+ signals are noise and TBI induced exosomes are released to blood after TBI treatment. This increase trend of CD63+/GFAP+ exosomes after TBI could only be

identified in AFS processed samples, the flow cytometry results of plasma samples cannot show CD63+/GFAP+ events increase and exosomes size FSC/SSC as Figure 18C shows. FSC and SSC results in Figure 18D show CD63+/GFAP+ events in plasma are majorly induced by large particles, indicate the necessary of using acoustofludic separation for analyzing TBI related exosomes in blood. Acoustofluidics isolated exosomes for the other two mice show similar CD63+/GFAP+ event increasing after TBI treatment, and failure of detecting similar trend using plasma samples as Figure 3-6 and 3-7 shows, and plasma flow cytometry result still cannot distinguish CD63+/GFAP+ event increasing. The average of CD63+/GFAP+ events detected by acoustofluidics separated samples and plasma samples is shown in Figure 3-8, only acoustofluidics separated samples can show the TBI related exosomes abundance increasing after TBI, indicate the technology have positive effect for downstream analysis.

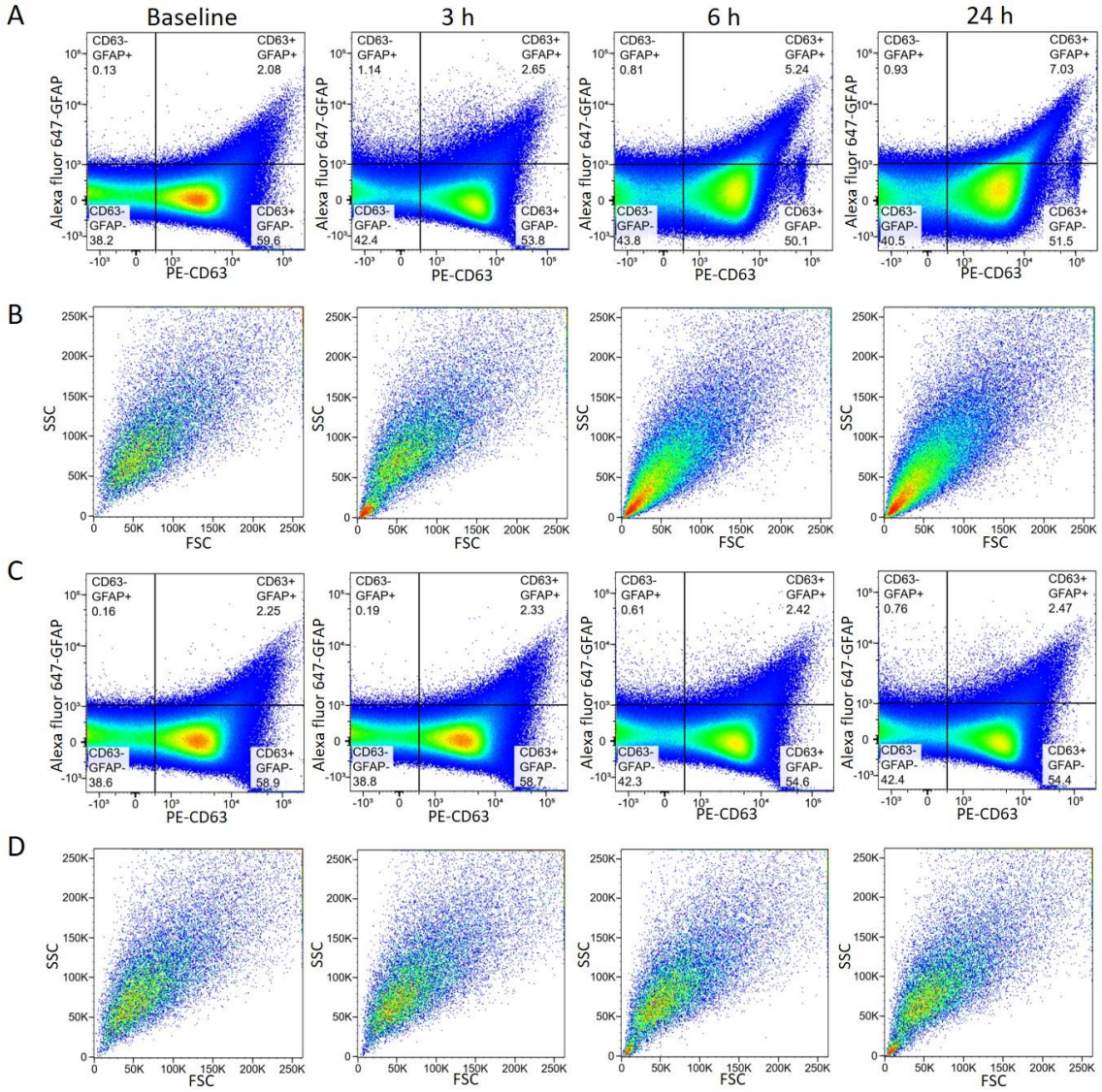

Figure 3-5: CD63+/GFAP- exosomes population change after TBI treatment. (A) Acoustofluidic isolated exosomes stained by both PE-CD63 and Alexa fluor-647-GFAP, samples collected at different timepoints shows CD63+/GFAP+ events increasing after TBI, indicate TBI related exosomes abundance increasing in blood, (B) FSC and SSC of CD63+/GFAP+ area for exosomes at each timepoint, indicate the CD63+/GFAP+ events initially induced by noise from large particles, but then induced by exosome signals after TBI, (C) direct flow cytometry analysis using plasma samples can not demonstrates CD63+/GFAP+ events increasing after TBI, (D) FSC and SSC of CD63+/GFAP+ area of plasma collected each timepoint, majority of the signals are noise from large particles.

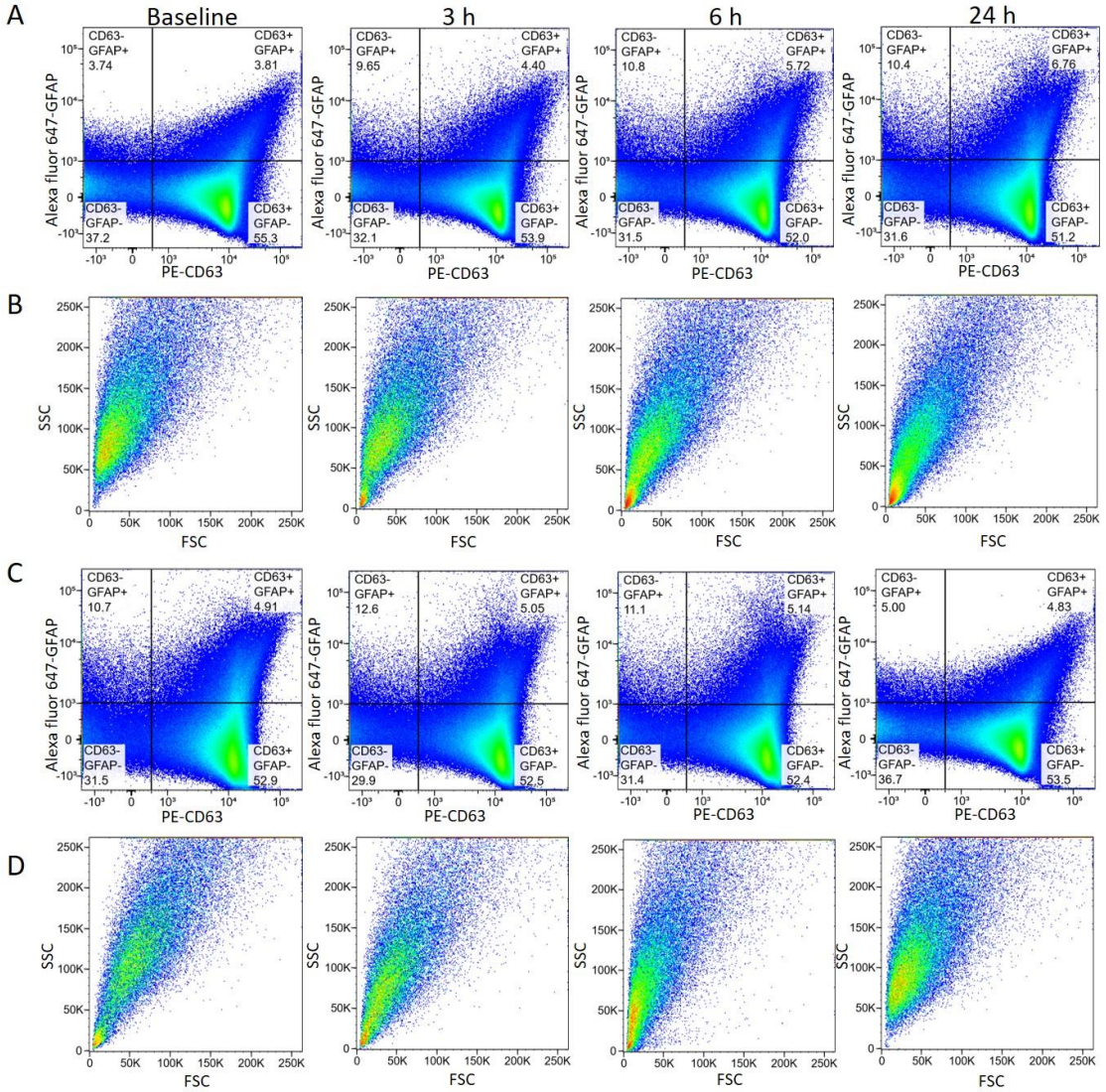

Figure 3-6: CD63+/GFAP- exosomes population change after TBI treatment of mouse 2. (A) Acoustofluidic isolated exosomes stained by both PE-CD63 and Alexa fluor-647-GFAP, samples collected at different timepoints shows CD63+/GFAP+ events increasing after TBI, indicate TBI related exosomes abundance increasing in blood, (B) FSC and SSC of CD63+/GFAP+ area for exosomes at each timepoint, indicate the CD63+/GFAP+ events initially induced by noise from large particles, but then induced by exosome signals after TBI, (C) direct flow cytometry analysis using plasma samples can not demonstrates CD63+/GFAP+ events increasing after TBI, (D) FSC and SSC of CD63+/GFAP+ area of plasma collected each timepoint, majority of the signals are noise from large particles.

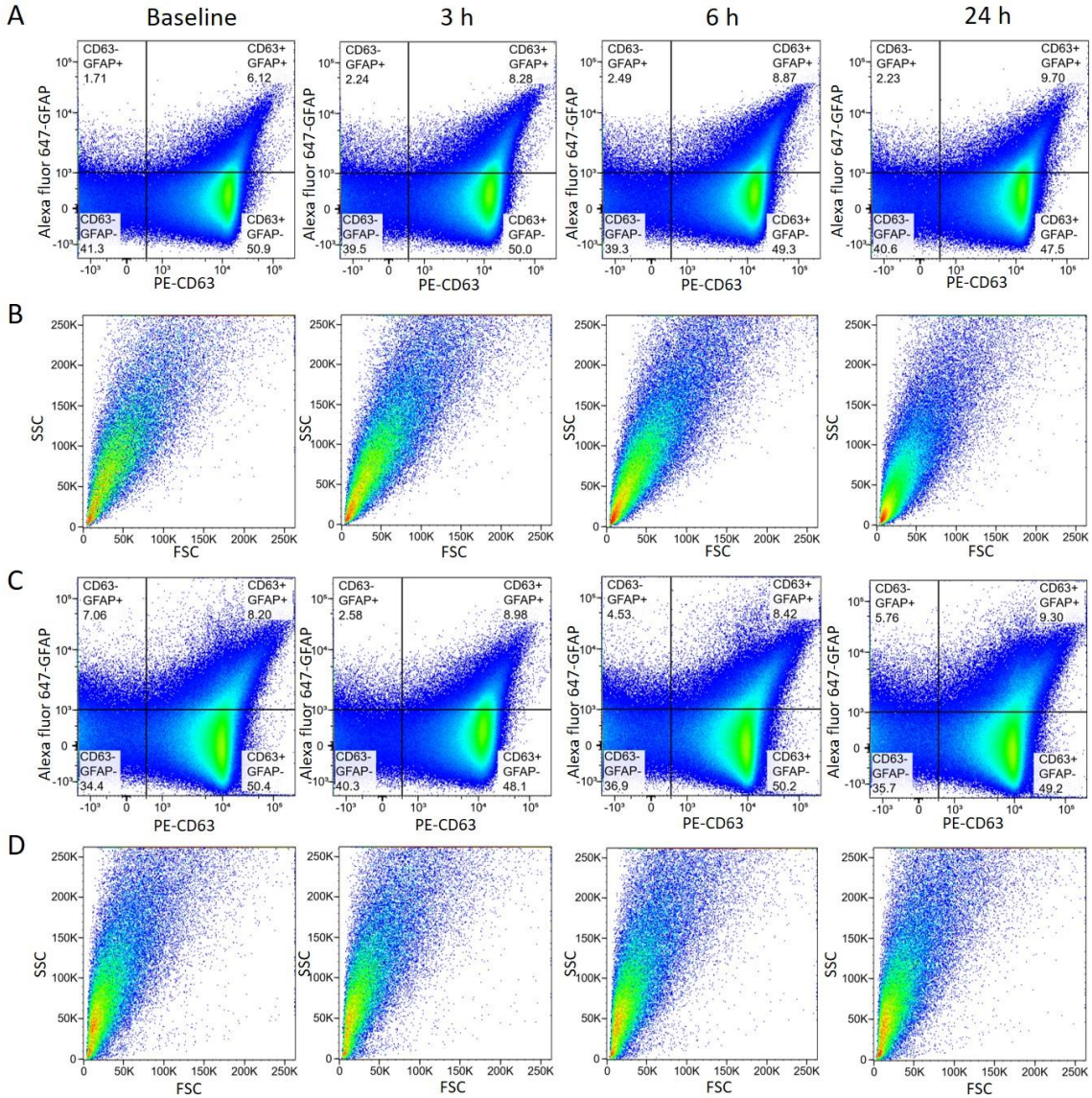

Figure 3-7: CD63+/GFAP- exosomes population change after TBI treatment of mouse 3. a) Acoustofluidic isolated exosomes stained by both PE-CD63 and Alexa fluor-647-GFAP, samples collected at different timepoints shows CD63+/GFAP+ events increasing after TBI, indicate TBI related exosomes abundance increasing in blood, b) FSC and SSC of CD63+/GFAP+ area for exosomes at each timepoint, indicate the CD63+/GFAP+ events initially induced by noise from large particles, but then induced by exosome signals after TBI, c) direct flow cytometry analysis using plasma samples can not demonstrates CD63+/GFAP+ events increasing after TBI, d) FSC and SSC of CD63+/GFAP+ area of plasma collected each timepoint, majority of the signals are noise from large particles.

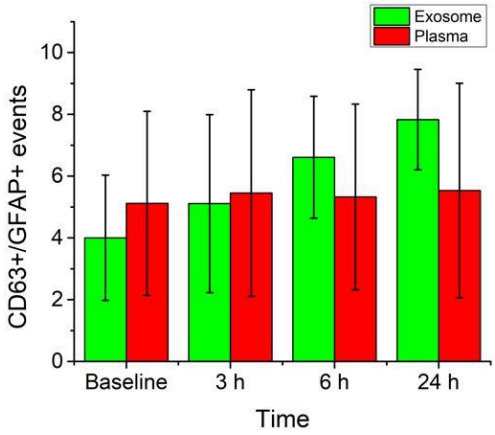

Figure 3-8: Comparison of CD63+/GFAP+ events of acoustofluidics isolated exosomes and plasma samples, CD63+/GFAP+ events of isolated exosomes showing increasing trends while plasma samples have no change with time after TBI, indicate acoustofluidics separation has potential for revealing the TBI related blood exosome population change.

3.5 Conclusion

By applying acoustofluidic exosome separation we successfully use flow cytometer to detect TBI related exosomes in blood. Animal experiments indicate after TBI treatment abundance of GFAP+/CD63+ exosomes in blood is increasing, which has potential as a biomarker for early screening of TBI. According to comparative test using plasma without processed by acoustofluidic separation, the increasing of GFAP+/CD63+ exosomes in blood could not be detected, indicates acoustofluidic separation is an important sample processing procedure. One potential explaining for the necessary of using acoustofludic separation prior for flow cytometry exosome analysis is it can eliminate large particles that can induce noise and interference exosome detection. Because of exosomes' small size (30-150 nm), using flow cytometer for exosome detection is always challenging. Small vesicle structures may not generate strong enough forward-

scattered light (FSC) and side-scattered light (SSC) signals, which demonstrate particle's size and internal complexity. Small size also indicates low abundance of biomarkers and low strength of fluorescent signals from antibodies that specifically labeled exosomes. Although increasing laser strength and decreasing detection threshold can make it possible for detecting exosomes' FSC, SSC, and fluorescent signals, it also brings strong noises from background and other blood large particles, including macrovesicles, apoptosis bodies, and platelets. Acoustofluidic separation decreases interferences from large size blood components, which enable the successful monitoring of TBI related exosomes' abundance in blood.

Traumatic Brain Injury is a brain dysfunction, caused by a blow or penetrating injury to the head. TBI can lead to acute symptoms including chronic traumatic encephalopathy, cognitive impairment, dementia, movement disorders and motor neuron dysfunctions.(Taylor et al., 2014) TBI affects at least 5.3 million people in the United States and annual healthcare costs associated with the disease are in excess of $60 billion.(Lange et al., 2011, Control et al., 2013) Although much progress has been made in identifying risk factors associated with TBI,(Gavett et al., 2010) diagnosing the injury, especially in its more mild forms, remains a challenge. There are currently no sensitive, objective diagnostic tests or validated biomarkers for diagnosing TBI. The accurate diagnosis of a TBI relies on a neurological evaluation and interpretation of a patient's signs and symptoms. In cases of severe TBI, which involve a loss of consciousness, a diagnosis

can be fairly straightforward; however, mild TBIs (mTBIs), which are the most common type of TBI, are much more difficult to diagnose. It is estimated that 50-90% of patients with mild TBI (mTBI) go unidentified or undiagnosed in hospital emergency departments.

Recent advances in neural imaging have led to the development of technologies that can be used to more accurately diagnose TBI. A computed tomography (CT) scan is the most common tool used to diagnose TBI; however, CT scans are expensive (~$1,100 per scan), expose the patient to ionizing radiation, and are typically unable to detect mTBI (sensitivity of 3-10%).(Yuh et al., 2013) As a result, more advanced imaging techniques, including magnetic resonance imaging (MRI), functional MRI (fMRI), susceptibility-weighted imaging (SWI), and diffusion-weighted imaging (DWI), have been implemented for their enhanced sensitivity and ability to detect functional and structural changes associated with mTBI. However, these techniques all suffer from requirements for expensive equipment and highly trained personnel, and as a result, they are not widely used in diagnostic applications. In an attempt to overcome these limitations, researchers have recently begun to explore the diagnostic potential of exosomes (30-150 nm extracellular vesicles)(Sokolova et al., 2011) and their molecular cargo as a biomarker for TBI.(Hamlett et al., 2017) Exosomes are found in high abundance in both plasma and cerebrospinal fluid, allowing for continuous, non-invasive sample collection and disease monitoring. In addition, exosomes are very durable and capable of preserving their

molecular cargo through multiple freeze and thaw cycles. Exosomes play an important role in neuron-to-neuron communications, and recent studies have shown that they may play a role in the progression of TBI to more long-term neurodegenerative coditions. By analyzing the molecular cargo proteins carried by circulating exosomes, researchers found that exosomal levels of αII-Spectrin breakdown products (SBDPs), total-tau (t-tau), and CD63 are elevated in the mTBI group 6 hours after injury, indicating the potential use of plasma exosomes in diagnosing mTBI at its earliest stages.

Although in this research plasma samples were used, this two modules acoustofluidic device can achieves whole blood exosomes separation in a continuous manner, which is could be highly integrated with flow cytometer like detection devices. A combination of acoustofludic separation unit and flow light detection unit has high potential for an easy handle, biocompatible, and rapid TBI early diagnosis system. The significance of fast diagnosis for TBI is it can help to prevent secondary brain injury, which includes both mechanical and molecular damages. TBI induced cerebral vasodilatation and increased cerebral blood flow can cause intracranial pressure increasing and brain swelling, which can induce mechanical secondary damage to brain tissues. The inflammation related cytokines secretion and molecules released by damaged neurons also induce the expending of damage areas. Acoustofluidic based exosome counting has potential for bring a rapid diagnosis method can bring opportune and proper treatment and reduce secondary damage, which can reduce the risk of TBI developing to long term

disease and causing complications. Compared with conventional exosome isolation method including ultracentrifugation and antibody capture, acoustofludic separation is rapid, biocompatible, low-cost, and its' microfluidic platform is easier for handling and integrating with downstream analysis. These advantages can benefit TBI early diagnosis and laboratory studies for exosomes' roles in TBI pathology, which has potential for investigating new mechanisms of TBI development and related complications.

4. Acoustofluidic live virus separation

Virus study is an important branch that has both biological and biomedical significance. The outbreak of COVID-19 since 2020 is one representative example of processing virus related diagnostic and pathological studies. However, despite the rapid development of diagnostic studies, which could be achieved by reverse transcription, high efficiency sequencing, and sensitive quantitative PCR, the pathology study of virus study is still facing multiple obstacles. Among these obstacles including difficulties for identifying protein structures and functions, on of the most critical limitation is virus separation technologies. Conventional virus separation methods include ultracentrifugation and density gradient centrifugation, which all time cost and bring potential damage to virus structures. Since virus is environment and time sensitive, which cause virus particles quickly lost viability in unsuitable environment because of protein denaturation and membrane disruption, these unbiased separation methods only collect sequence data that could be used for detection, but not proteomic date that can reveal mechanism of infection. Here we developed an acoustofluidic based virus separation technology that can rapidly extract virus particles from original samples. By deriving high frequency acoustic wave by dummy finger IDTs, the acoustic radiation force is strong enough for pushing virus out from original samples. By using cultured M-MLV virus, the acoustofluidic platform not only processed high yield and purity virus separation, but also keeps virus viability, which can be validated by infection experiments using isolated

samples. This acoustofluidic virus separation method is reagent free and biocompatible, and have potential for separating live virus for pathological and infection mechanism studies.

4.1 Motivation

Virus is a type of organism that do not containing cellular structures and relies other eukaryotic or prokaryotic cells for completing proliferation processes. Although some type of virus can symbiosis with host cells for long-term, even integrate their genome into host cells genome, the parasitic feature still causes the end of the virus proliferation term could be the lysis of the host cell for releasing progeny virus. Virus could be powerful tools in biological and biomedical fields, including using bacteriophage for therapeutic purpose and using reverse transcription virus, which is a virus population that use RNA as genome and insert their genome to host cell genome during infection, for transfection and generating stable gene editing cell lines (Cheung et al., 2007). However, virus that can infect human cells can serious diseases and still difficult for developing reliable treatment. After entering the 20th century, several years there is an outbreak of pandemic because of virus and bring economic severity, including severe acute respiratory syndrome (SARS) in 2003 induced by coronavirus, H1N1 pandemic in 2009 caused by Influenza A virus, and pandemic caused by COVID19 virus starting from 2020 (He et al., 2020). Because of their strong infection rate and fatality rate, each outbreak of these virus causes economic stagnation or recession in global scale. Except these globally

spreading virus, regional or periodic outbreak virus also continuously bring negative influence on local economy. Only in America, for preventing the flu pandemic each year there is more than billions of vaccines are required and cost more than 10 billions budgets for direct medical cost reported by Centers for Disease Control and Prevention (CDC) (Ortiz et al., 2011). With the development of global economy, it is even harder for control virus since the frequency people and commodity exchanges among countries increase the chance of virus spreading.

Although virus has cost serious threaten on economy and the stable of society, there still less efficient therapeutic approaches for treating virus induced disease. Different with bacteria, which could be controlled by large types of antibiotics, there still lack of drug that can inhibit the proliferation and spreading of virus in human body. Since virus dose not have cell structures and derive proliferation processes using host cells' protein and nuclei acid synthesis system, it is difficult for find the target for inhibiting virus proliferation (Boyer et al., 2001). Currently the most efficient and widely used tool for defending virus infections is still the natural method, which is the immune system. For preventing infection, the mechanism of vaccine is introducing virus' specific antigens into human body in advance by approaches including inactivated virus, attenuated virus, artificially synthesis antigen, or mRNA that can inducing body cell expressing antigen. After immune system recognized virus antigens, specific antibodies will be secreted, and Memory T cells population will be developed for reaction during next infection. These

immune defenses can prevent virus infections, but cannot react to virus that has not been recognized. The therapeutic methods for virus infection induced disease also rely on immune response. Although drugs include reverse transcription inhibitors could inhibit virus proliferation, hormone therapy, which use combination of hormones including estradiol, is still the most commonly used methods. However, hormone therapy cannot directly influence virus proliferation and can only activate or regulate the immune system for increasing response speed or inhibit over response events including inflammatory storm caused by over expression of immune response related cytokines ((Smith et al., 2000)). These therapeutic methods can only adjust body status and providing the immune system more time and chance for generating specific immunity but cannot eliminate virus. Furthermore, since virus proliferation relies on the host cells' protein and nuclei acid synthesis system, it also means that the treatments targeting on directly inhibiting virus proliferation also inhibit host cells normal metabolic events. Since targeted drug delivery is still under research and cannot delivery acute delivery, therapeutic methods that directly inhibit virus proliferation can bring potential negative influence on health cells and can cause long-term or serious side effects.

Except the lack of therapeutic method, the instability of virus further increases the difficulty for virus infection preventing and treatment. Based on genome molecule types, virus could be separated to DNA virus and RNA virus. Unlike DNA that has double strand structure and the specific paring between nucleobases bring a repair mechanism

for preventing mutation, RNA molecules only have single strand without nucleobases paring, which cause RNA virus has rapid mutation rate (Grubaugh et al., 2020). The mutations cause antigen structure change and cause antibodies and immune cells that can recognize original antigens failed for identifying mutated virus, indicating less efficient immune response. To preventing mutation induced immune failure, for wide spreading RNA virus including flu virus, each year new vaccine needs to be designed and synthesized based on the predicting the virus mutations. The frequent updates of vaccines not only increase cost, there is chance of prediction failure and can cause ineffective vaccines. Furthermore, frequent mutation increases the interspecies transmission of virus. In different species there are symbiotic virus that cannot cause serious disease, but after transmission to other species these viruses could be deadly including swine flu, avian influenza, and SARS virus from bat (Guan et al., 2003). The high mutation rate of virus cause difficulty for constructing stable defense and therapeutic methods.

Since virus can cause severe influence and difficult for preventing and therapy, it is an important target for biological and biomedical research. However, different with the rapid development of diagnostic methods, which rely on robust genome sequencing and PCR technologies, the mechanism of virus infection is still a difficult topic. The target cell of virus infection is depending on the protein recognition and affinity, which is depending on the study of protein dynamics and bioinformatics research. And the intercellular events after virus infection also need comprehensive research that covers reverse

transcription, gene editing, protein expression, virus particle assembly, and secretion processes. Different with sequencing and PCR based diagnosis that can use dead or incomplete virus, purified live virus samples are ideal materials for these studies related with virus infection events. However, currently there still lack for efficient method for live virus isolation. Conventional virus separation methods include physical approaches and chemical approaches. Physical virus separation methods including ultracentrifugation and density gradient centrifugation. However, these methods are time costing and can cause potential damage to virus structures by pressure and shear stress during high gravity centrifugation and resuspension, and osmotic pressure interference induced by gradient density solution. Previous reported ultracentrifugation isolated viruses demonstrate morphological changes including fusion and membrane degradation, which potentially cause important proteins that participate virus invasion lost. Chemical virus isolation uses antibody-antigen affinity for specific capturing virus. However, the antibody-antigen capture only works on identified virus but cannot separate new virus and mutated virus. The washing steps that release the virus from the antibody can further cause structure damage and protein lost of the virus. Since the fast mutation rate of virus and continuous emerging of new virus, a biocompatible method that can rapidly isolate live virus can significantly benefit the biological and biomedical study of virus.

To develop a fast virus separation way, we utilize acoustofludic technology for virus separation. Acoustofluidic technology has been demonstrated as a biocompatible

approach for nanosized particle separation. It provides an exosome isolation method with high yield and purity, keeps exosome specific biomarkers during the isolation. Since the size of exosomes is 50-200 nm and the virus size range is 80-200 nm, which have overlap, and acoustofluidic separation technology is a separation based on size difference between particles, it is possible for using acoustofluidic technology for achieving biocompatible isolation of live virus.

4.2 Mechanism and system

To achieve acoustolfluidic virus separation, the major challenge is the small size of the virus. Our previous acoustofluidic device derive exosome separation by eliminate particles that are larger than exosomes. However, the target exosomes are still existing in the original sample fluid, indicating solvable proteins and other small molecules remaining in the sample. To achieve virus separation that can benefit downstream research including virus infection mechanism study and protein dynamic study during infection, it is necessary for isolating virus out from the original sample for eliminating solvable protein and nuclei acid contaminations. This requirement induces the virus acoustofluidic technology having a lower threshold for pushing nanoparticle for enabling pushing virus out from the original sample flow.

To manipulate smaller particles, one solution is increasing frequency of acoustic wave in the acoustofluidic system. The acoustofluidic separation system derive separation based on acoustic radiation force. From Equation 1 and 2 in Chapter 1, we can find particle

volume demonstrate a positive relation with strength of acoustic radiation force on that particle. To manipulate virus particles that share same size with exosomes, our current acoustofluidic exosome separation device's working frequencies, which are 20 MHz and 40MHz, are not sufficient for generating strong enough acoustic radiation force on the virus particles. To increase the acoustic radiation force, one solution is increasing frequency of the acoustic field, since from Equation 1 and 2, the frequency is also positive related with strength of acoustic radiation force. Since the mechanism of generating surface acoustic wave on piezoelectric substrate is generating vibration by IDTs that introducing altering electric currency, and the wavelength of the generated acoustic wave is four times of the distance between neighboring electrodes, to increasing the acoustic wave frequency the simplest approach is designing IDTs that have less width electrode and less distance between electrodes. Because of stable propagation speed of surface acoustic wave on the piezoelectric substrate, decreasing the wavelength of acoustic wave can increase the frequency.

However, decreasing electrodes width and distance bring a problem that is the uneven acoustic strength. As Figure 4-1A shows, the acoustic field generated by normal IDTs has strong areas distributed in the edge area of the device, while in the center area of the device the acoustic wave strength is not strong for manipulating particles. This tendency become more obvious when the working frequency of IDT increase. At 20 MHz working frequency normal IDTs can generated uniform strength acoustic field, at 40 MHz

low frequency area could be observed. However, at 60 MHz or higher working frequencies cause the strength of acoustic field in the center areas not strong for particle separation. A potential reason of this phenomenon is the uneven distribution of electric voltage on the electrodes. When width of electrodes decreases, increasing of the resistance cause electric voltage attenuation on the electrode and cause enter areas of the IDTs cannot generating enough voltage of activating the vibration of the piezoelectric substrate. Decreasing the width of the channel further increase fabrication difficulty since small defects occurring lithography process can break the structure of the electrodes.

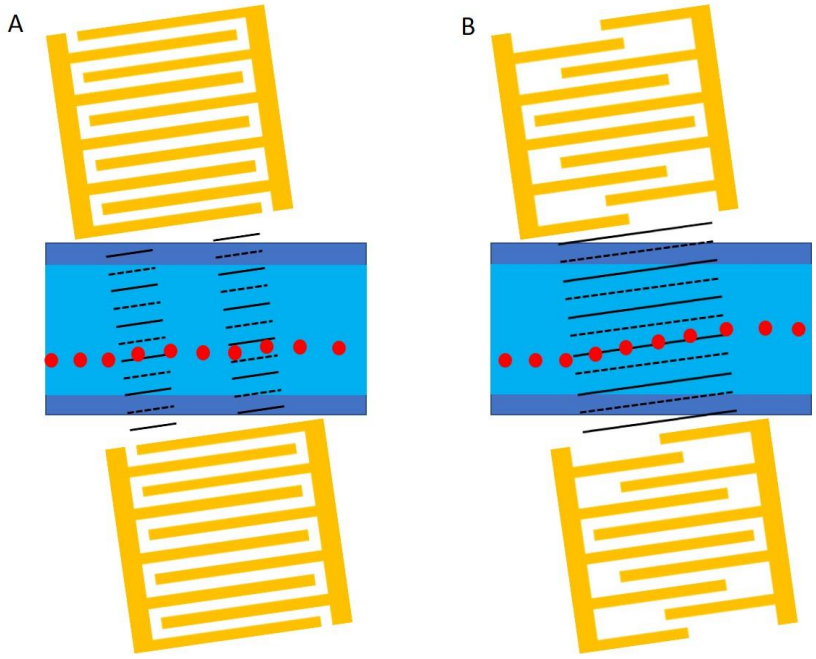

Figure 4-1: Schematics of normal IDTs and dummy finger IDTs difference when deriving acoustofluidic separation. (A) The normal IDTs generate strong acoustic field in two edge areas but weak acoustic field in the center area, cause particle cannot be manipulated in the center area. (B) The dummy finger IDTs generate uniform strength acoustic field, enable particles being manipulated in the whole area and push particles to a longer distance than normal IDT, indicate a better isolation outcome.

A potential solution of uneven acoustic field distribution is a special design called dummy finger IDT. It cuts the length of electrodes in the edge areas as Figure 4-1B shown. Previous research demonstrates in same working frequency, dummy finger IDT demonstrate a more uniform acoustic wave distribution than normal IDT, indicate it could be used for improving performance of high frequency IDTs for virus separation.

4.3 Experiment methods

4.3.1 Acoustofluidic device fabrication

For validate dummy finger design's influence on device performance, we design three types of IDTs, including normal IDTs, dummy finger IDT with less edge cuts, and dummy finger IDTs with edge cuts. All three IDTs share same working frequency of 60 MHz. The photolithography and lift-off processes were achieved by depositing SPR3012 photoresist (MicroChem Corp., USA) on the Y+128° X-propagation lithium niobate (LiNbO3) substrate aligned by a MA/BA6 mask aligner (SUSS MicroTec., Germany). CD26 developing solution (MicroChem Corp., USA) was then used for removing unwanted photoresist. An e-beam evaporator (Semicore Corp., USA) was used for depositing a metal double layer (Cr/Au, 50 Å/500 Å) on the substrate for a lift-off process using PRS3000 resist stripper (VWR, USA) to form the IDTs.

The PDMS channel model is created by SU-8 photoresist (MicroChem Corp., USA) through soft lithography. PDMS was solidified by Sylgard 184 Silicone Elastomer Curing Agent and Base (Dow Corning, USA) on the mold. A glass layer was placed on the mold

for creating glass cover in the channel. After incubating in 65 °C for one hour, PDMS channel and the substrate were coated by oxygen plasma and bounded.

4.3.2 Live virus culture

Since the hazard biosafety level limitation and a considering for benefiting downstream for virus viability analysis, we did not use wide type live virus but using cultured virus for transfection experiment as the sample for acoustofluidic isolation. The virus we use comes from M-MLV, which is a reverse transcription virus. To culture the virus, RV101 cells (Cell Biolabs, USA) were firstly cultured in DMEM culture medium (Gibco, USA) containing 10% FBS (Gibco, USA) with the protection of Penicillin-Streptomycin (Gibco, USA) at 37 °C with 5% concentration of CO_2. After the cell density reached to 80% of the cell culture plate, virus vectors pMXs-GFP (Cell Biolabs, USA) that are plasmid containing M-MLV genome integrated with GFP gene were transfected into the cells by liposome transfection reagent (FuGENE, USA) following the instruction of the reagent. Transfected cells were then cultured by 10% FBS DMEM culture medium in 37 °C with 5% CO_2 for 48 hours. After 48 hours culture, culture medium containing virus particles were collected for acoustofluidic virus isolation.

4.3.3 Virus separation and downstream validation

To injecting the virus samples to the acoustofluidic device, a syringe pump (CETONI GmbH, Germany) was used to independently control the sample and the sheath flow, which is PBS (Thermofisher, USA). To protect the virus from excessive temperature,

a cooling system containing Peltier cooling plate (Hebei IT, China) powered by a variable DC power supply (Tekpower, USA) was used for cooling the acoustofluidic chip. To generate acoustic wave, IDTs on the acoustofluidic device were connected with a function generator (Agilent, USA) and an amplifier (Amplifier Research, USA). The virus separation processes were monitored by an upright microscope (Olympus, Japan) and a CCD camera (Photometrics, USA).

To validate the purity and morphology of the isolated virus, the size distributions of collected particles were measured by Nanoparticle Tracking Analysis (Malvern, England) system and negative staining TEM. Negative staining of the virus sample was processed by uranyl–acetate negative staining. To validate the infection ability of the isolated virus, same volume of isolate virus and original culture medium that containing virus particles were added to NIH/3T3 cells cultured by 10% FBS DMEM culture medium in 37 °C with 5% CO_2. After 48 hours culture, NIH/3T3 cells were validated by fluorescent microscope and flow cytometer for evaluating GFP expression level. Since the virus genome is integrated with GFP gene, expression green fluorescence indicates the virus successfully infecting the cells.

4.4 Results and discussion

4.4.1 Distribution of acoustic field in the channel

To validate whether the dummy finger design can improve the acoustic field distribution for high frequency IDTs, we processed simulation by COMSOL using there

60 MHz IDT designs. As Figure 4-2A shows, the normal design IDT generated acoustic wave that demonstrates highest amplitude at tow edge areas indicating in the acoustofluidic device there is not continuous acoustic field in the channel. Figure 4-2B demonstrate the acoustic field strength distribution in an IDT that is a combination of dummy finger IDT and normal IDT, it shows the introduction of IDT significantly uniform the acoustic field distribution. Figure 4-2C is the acoustic field distribution in a dummy finger IDT, the generated acoustic field strength shows peak in the center area of the device.

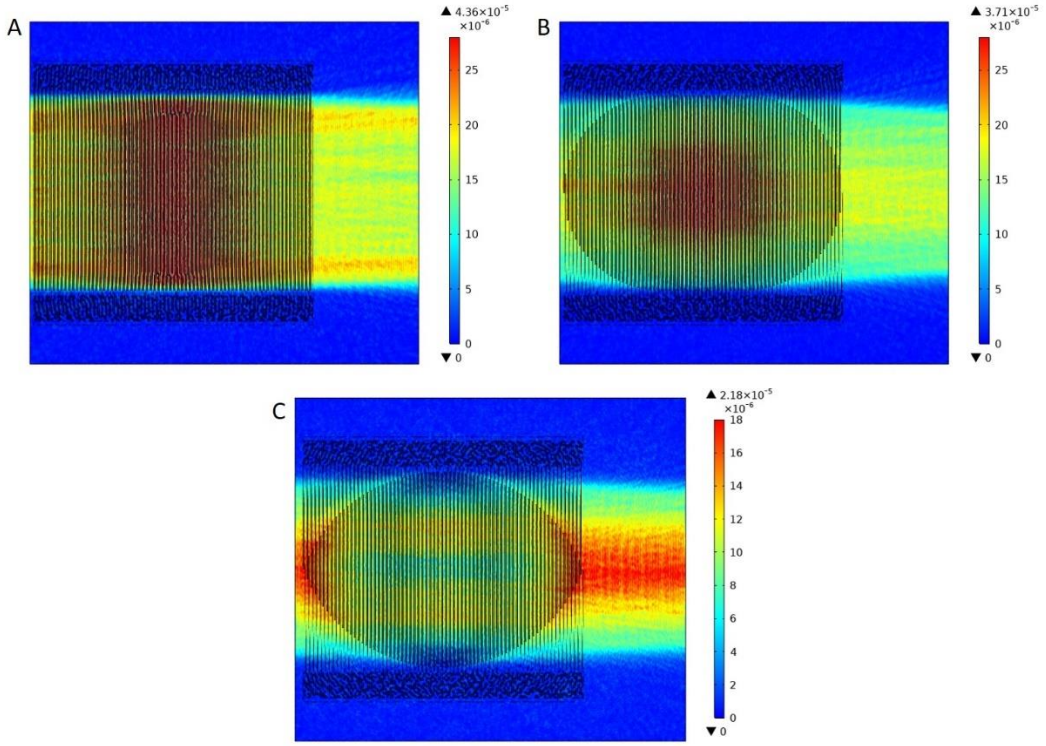

Figure 4-2: Simulation of acoustic field generated by different IDT designs. (A) Acoustic field generated by normal IDT. (B) Acoustic field generated by an IDT combined by the normal IDT and dummy finger IDT. (C) Acoustic field generated by dummy finger IDT.

To evaluate the experimental performance of different design of IDTs, we derived acoustofluidic separation using 100 nm polystyrene nanoparticles. As Figure 4-3A demonstrated, 100 nm polystyrene beads cannot be manipulated by the acoustic field generated by normal IDT, while the bead could be pushed by acoustic field generated by the dummy finger IDT as Figure 4-3B shows. There is no significant fluorescent line in the channel using normal IDTs, indicating less nanoparticles are manipulated by the acoustic radiation force and migrated to the pressure node areas in the channel. On the other hand, in the acoustofluidic device using dummy finger IDTs, in the center area of the channel beads show significant concentration in the pressure node areas, indicating the dummy finger IDT can derive strong enough acoustic field for pushing 100 nm nanoparticles from on side of the channel to the other side. Although the hybrid IDT that combined the normal IDT and dummy finger IDT demonstrate a uniform acoustic field distribution in simulation, in experiment it has same performance with normal IDT, indicating only dummy finger IDT can perform uniform acoustic field in high frequency. Since the energy in surface acoustic wave can been transformed to vibration induced heat in materials attached on the piezoelectric substrate, we used a heat sensitive film that can demonstrate color change when temperature increasing for visually demonstrating the acoustic distribution in the channel. Figure 4-3C demonstrates in the device using normal IDTs, high temperature areas focus on edge, while dummy finger IDTs device has a uniform temperature distribution.

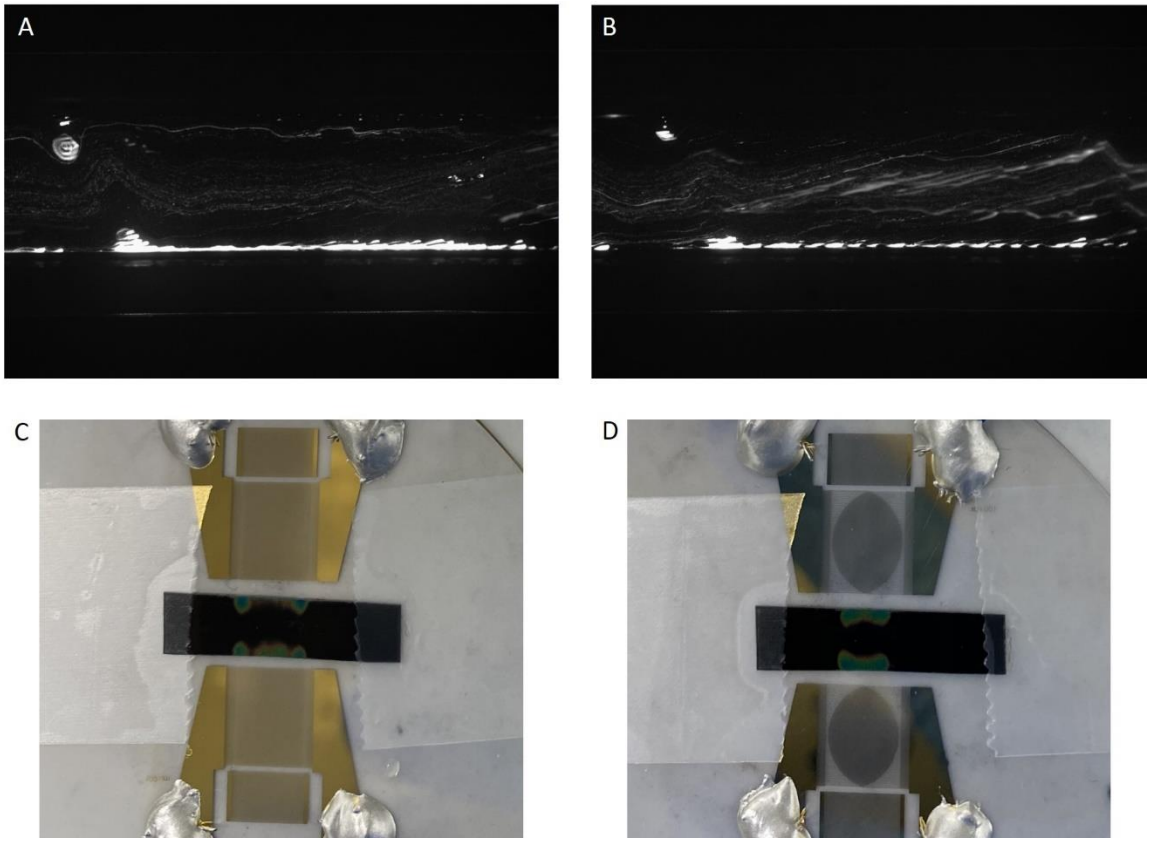

Figure 4-3: Experimental validation of acoustic field distribution in the acoustofluidic devices. (A) 100 nm beads cannot pushed by 60 MHz normal IDTs and concentrate at pressure nodes. (B) 100 nm beads in acoustofluidic separation device using 60 MHz dummy finger IDTs could be concentrated at pressure nodes and be separated. (C) Heat distribution in normal IDTs demonstrates high pressure areas are in the edge of the IDT. (D) Heat distribution in dummy finer IDTs demonstrate uniform distribution, indicating the acoustic field is uniform.

4.4.2 Virus separation validation

Based on the simulation and experimental results using beads, we used design 3, which is the 60 MHz dummy finger IDT device for virus separation. The virus samples are processed by the acoustofluidic device with a flow rate of 6 μL/min, and the voltage on the IDT is 65 V. Two outlets, which are isolated virus outlets and waste outlets

containing remained culture medium were collected and the original sample, which is culture medium contain M-MLV virus, was used as control. To validate the sample purity, NTA that can analysis particles size distribution in the sample was applied. To get visualized information of collected particles, negative staining, which is the widely used staining method for virus TEM microscopy, was applied for the samples. The isolated virus sample's NTA analysis result was shown in Figure 4-4A. In the isolated virus samples the particles' sizes are ranged from 100 nm to 500 nm and show highest concentration at 100 nm to 200 nm. This result is consistent with previous research about M-MLV size, which is among 100 nm to 150 nm. The TEM image of the isolated virus is also consistent with the NTA, since no particle less than 100 nm could be found in the TEM images. Furthermore, the morphology of the isolated virus by the TEM image is consistent with M-MLV virus observed by TEM in previous research, which is bright in the center and circuited by a darker layer which is the protein capsid and membrane complex. The isolation yield of the acoustofluidic technology is also high, which could be found in the NTA results analyzed from the sample collected from waste outlet as Figure 4-4B shows. Since the size distribution of the sample from the waste outlet is among 20 nm to 101 nm, most of the virus particle are separated out from the original culture medium. TEM image also shows no particles larger than 100 nm in the sample from the waste outlet. NTA and TEM results of the original culture medium are shown in Figure 4-4C, indicate before isolation the virus and waste both exist in original sample.

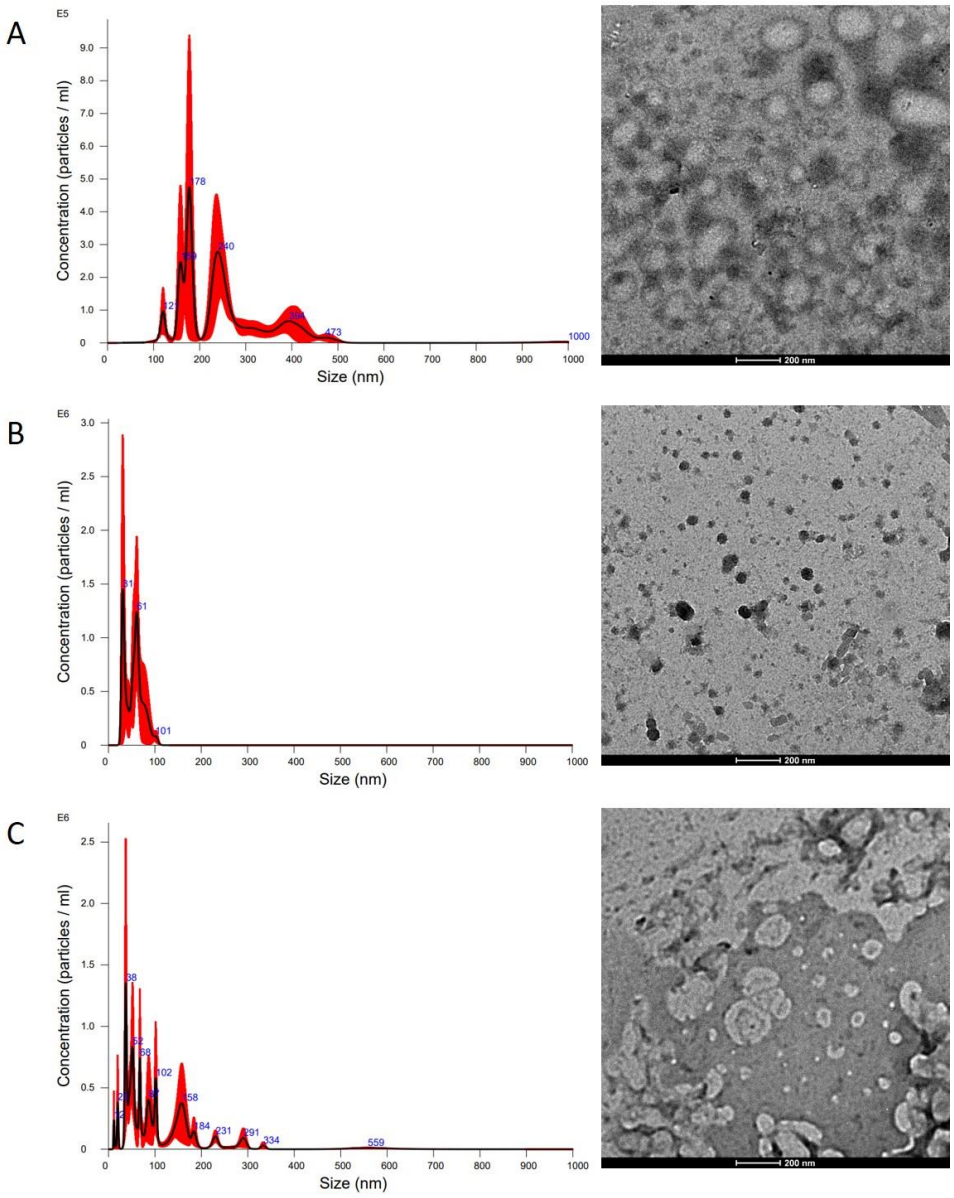

Figure 4-4: Validation of acoustofluidic virus isolation by NTA and TEM. (A) NTA and TEM results of isolated virus, most of the particles are larger than 100 nm and shows virus morphology. (B) NTA and TEM results of the sample collected from waste outlet, most of the particles are smaller than 100 nm, which is not belong to M-MLV's size range. (C) NTA and TEM results of original sample, which show a combination of the isolated virus and waste.

4.4.3 Virus infection analysis

To validate isolated virus viability, we use the virus for transfection experiments. Since the M-MLV genome has been inserted with GFP gene, successful infection of virus can induce cells having green fluorescence. As Figure 4-5A shows, transfection using isolated virus cause most of the cells showing green fluorescence under microscope, and the flow cytometer result indicates 86.8% of the cells having fluorescence. Since Figure 4-5B which is transfection using sample collected from waste shows zero transfection rate and Figure 4-5C which is transfection using original sample shows a transfection rate of 88.3%, acoustofluidic separation do not influence virus' viability.

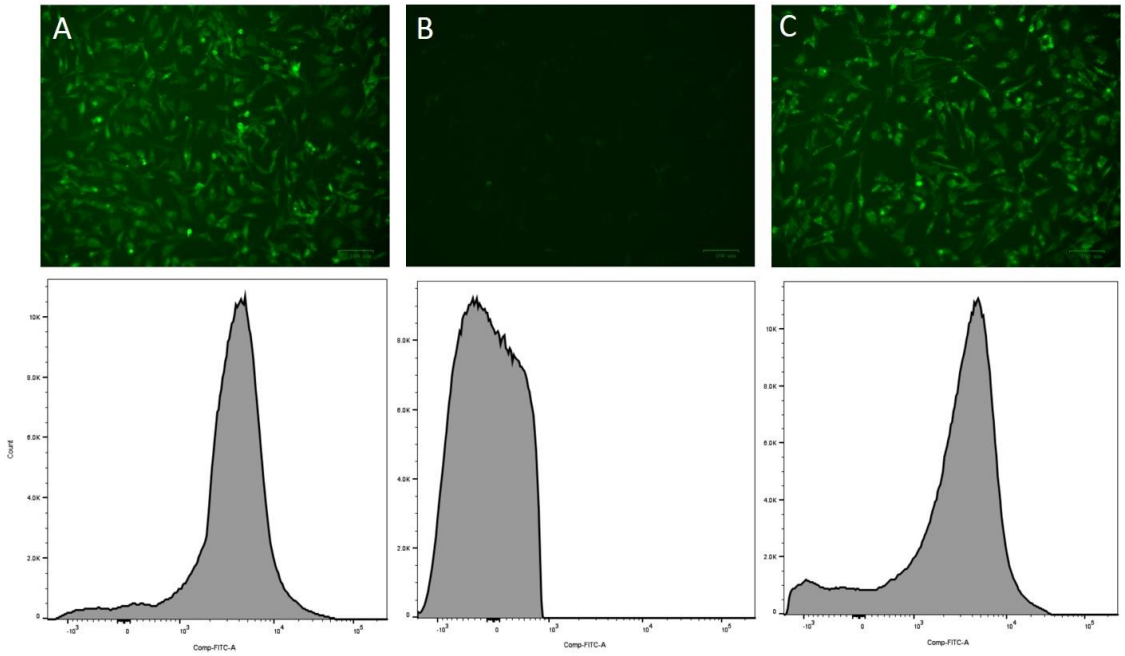

Figure 4-5: Virus viability validation. (A) Fluorescent microscopy and flow cytometer results of isolated virus, indicate high infection ability. (B) Fluorescent microscopy and flow cytometer results of sample collected from waste outlet, no cell is infected. (C) Fluorescent microscopy and flow cytometer results of original sample, showing similar infection rate with isolated virus.

4.5 Conclusion

By introducing the dummy finger design, we developed a frequency IDT that can generate uniform strength acoustic wave. The working frequency increasement improve the surface acoustic wave generated acoustic radiation force on smaller nanoparticles and enable the manipulation of particles larger than 100 nm. Compared with our previous acoustofluidic separation device, the dummy finger high frequency acoustofluidic device has lower separation threshold and enable the isolation and purification of smaller bioparticles. Utilizing this new design, we successfully demonstrated M-MLV, which is a reverse transcription virus with size ranges from 100 nm to 160 nm, could be isolated in a high yield and high purity way. The isolated virus demonstrates complete virus structure and same level transfection rate with virus in the original samples, indicating the acoustofluidic separation process is biocompatible and keeps the virus viability.

Studying the infection mechanism of virus can provide clues for investigating therapy and diagnosis methods. Since the high mutation rate and emerging of new virus, unbiased live virus separation can significantly improve the identification of mutated and new virus. Separated live virus could not only be used for diagnostic study, but also could be used for investigating infection mechanism and antigen structure. In this project we used M-MLV virus, which has a representative virus structure containing capsid and membrane, for representing virus. M-MLV also has size range that overlap with most of virus that can cause disease. Furthermore, in previous research M-MLV has been used as

comparison with coronavirus, indicate this virus is eligible for using as an example for virus study. By successful separating live M-MLV, the acoustofluidic technology demonstrates a reagent free, unbiased, and high biocompatible live virus separation method, which has potential for improving the virus study on both diagnostic and therapeutic aspects.

5. Acoustofluidic homogenizator for cell lysis

Detection of intracellular biomarkers provides a wealth of information related with fundamental research, disease diagnosis and monitoring. Continuous physical cell lysis methods can significantly simplify experiments and increase detection efficiency. Here we demonstrate a cell homogenizator that utilizes acoustic microstreaming-generated shear stress to lyse cells. The homogenizator has a trapping effect on integral cells, yielding an outlet product containing only the lysed sample. Microstreaming is generated by acoustic vibration-derived sharp-edge structures, which is the effecting unit of the device and can be added at a low cost to achieve higher lysis throughput. The homogenizator is reagent-free and the lysed sample can be directly used for downstream analysis. Results and discussion in this chapter comes from my published first author paper (Wang et al., 2019).

5.1 Motivation

Molecular detection based on biomarkers including nucleic acids, proteins, and small molecules can provide important information for disease diagnosis and monitoring.(Niemz et al., 2011) In purpose of continuously monitoring disease progression, point-of-care has become an important concept for medical development.(Rusling et al., 2010) However, achieving point-of-care requires frequent molecular detections aiming at monitoring changes of disease-related biomarkers. To achieve frequent detection, fast and continuous sample preparation methods that can

simply combine with downstream analysis is required. Microfluidics has been demonstrated with great potential on point-of-care applications. Since sample preparation and analysis can be integrated into an automated system that can quickly process a small amount of sample, developing microfluidics-based cell lysis technology can improve the sample preparation process for point-of-care applications.(Jung et al., 2015, Sharma et al., 2015)

Lysis, or permeabilization of the cell membrane, is the typical approach used to release biomarkers from cells.(Kim et al., 2009) Microfluidic cell lysis can be achieved by chemical and physical strategies. Chemical strategies are the most common method for cell lysis. Since cellular membranes are lipid bilayers sustained by polar and nonpolar balances, surfactants that can interfere with these balances and cause membrane solubilization are frequently used for chemical cell lysis.(Brown et al., 2008) However, the introduction of surfactants can cause protein denaturation and inhibit reactions including polymerase chain reaction, which is essential for genetic analysis.(Meacle et al., 2004) To eliminate surfactants' influences, multiple washing and protein refolding steps are required and increase sample preparation duration. Compared with chemical cell lysis, physical methods can achieve reagent-free and continuous cell lysis.(Salonen et al., 2010) The main limitation of these methods is the throughput since physical methods' lysis efficiencies are limited by the distribution of effecting units in the devices.(Lam et al., 2011) For example, for optical and electrical methods, the effecting units are laser effecting

ranges and electrode distributed positions. Cells can only be lysed in these areas because, although these methods can achieve uniform cell lysis, their throughputs are limited by the quantity of effecting units. However, for optical and electrical methods, increasing effecting units indicate adding light systems or electrodes, which increase the cost of the system. Among physical cell lysis methods, acoustic approaches' effecting units are the contact region of the sample and transducer, which provide benefits for increasing lysis efficiency at a low-cost.(Zhang et al., 2007) However, heat generated by acoustic energy can damage intracellular macromolecules.(González-Fernández et al., 2012) A reagent-free homogenization method that can continuously process small volume of sample, and its lysis efficiency can be increased in simple and low-cost way can significantly benefit the sample preparation for point-of-care application.

Here we describe a sharp-edge system that can achieve cell lysis through shear stress generated by the acoustic streaming. The system can process surfactant free cell lysis in a continuous pattern using small volume samples. Previous studies have demonstrated that sharp-edge generated acoustic microstreaming can achieve in-channel micro-mixing, gradient flow-induced chemical signal generation, and high viscosity sample liquefaction. In this study, sharp-edge derived acoustic microstreaming is demonstrated to achieve high-efficient cell lysis. Cells in the sharp-edge channel are exposed under two main effects: the shear stress generated by sharp-edge induced acoustic microstreaming, and the particle trapping effect caused by acoustic radiation

force and circulating microstreaming.(Nama et al., 2014) When exposed under acoustic fields that have suitable frequencies, tips of sharp-edge structures can intensely vibrate and generate microstreaming that has extreme higher flow rate than streaming flowing through the channel.(Nama et al., 2016) Since the tip of sharp-edge structures have smaller size than integral cells and can generated strong microstreaming in small areas, flouting cells in these areas will exposed under microstreaming fields that have ununiform flow rate distribution. The great flow rate difference occurred in a scale that is lower than size of cells creates strong shear stress on cellular membrane, and the shear stress can break cellular structures and drive homogenization. The trapping effect is determined by the drag force from streaming and radiation force from acoustic field, which are dependent on particles size when other physical factors, including contrast factor, frequency, and fluidic property, are held constant.(Wu, 2007, Collis et al., 2010) If integral cells and cellular debris share the same physical factors except their sizes, by Yosioka and Kawasima's works,(Yosioka et al., 1955) integral cells that have a larger size are captured more easily by the acoustic field.(Masudo et al., 2006) Furthermore, the acoustic microstreaming between two sharp-edges can from a circulating microstreaming, which can capture integral cells into the circulation since streaming provide high drag force on particles with large sizes. The radiation force and drag force provide a stronger trapping effect on large particles and cause integral cells staying longer in the channel and having more chance flow through areas with high shear stress than cell debris. By combining the

acoustic trapping and microstreaming shear stress, the sharp-edge system can achieve high efficient and uniform cell homogenization. Unlike previous acoustic methods that directly break the membrane through high power acoustic forces, the sharp-edge system lyses cells through sharp-edge generated microstreaming when there is acoustic vibration. Acoustic energy is converted to shear stress in microstreaming, achieving homogenization at a lower power and avoiding generating heat that can denature biomolecules. Furthermore, the throughput of the sharp-edge cell lysis device can be increased by adding more effecting units, which are PDMS sharp-edge structures, in the channel wall. Compared with optical and electrical methods, increasing effecting units for the sharp-edge device is easier and cheaper. Western-blot and PCR, which are commonly used for downstream analysis, have been processed directly on the homogenized production of the sharp-edge device. HeLa, Jurkat, and malaria Plasmodium falciparum strain 3D7 infected red blood cells have been processed by the sharp-edge device and cell lysis. In downstream analysis that directly use lysis products, cell lysis and internal components releasing have been confirmed on morphological, protein, and genome level. Successful detection of target proteins and DNA fragments indicate that the homogenizator can lysis sample without surfactants' participation, which significantly simplify the lysis processes. Furthermore, since the acoustic streaming sharp-edge homogenizator can process small volume of samples in a continulus way and achieve reagent-free cell lysis, the

homogenizator could be directly integrated with on-chip analysis, which can provide a simple and efficient method for point-of-care application.

5.2 Mechanism and design

The device concept is depicted in Figure 5-1A. PDMS sharp-edge structures with 0.5mm length are placed on the channel wall of the device with intervals of 1.0mm on two side of channel walls. The acoustic transducer is not in direct contact with the sharp-edge channel, but the acoustic wave spread on the glass substrate can cause the vibration of the sharp-edge structure, which can cause microstreaming and streaming-induced shear stress in the channel. The homogenizator lyses cells in a continuous flow pattern since multiple sharp-edge structures are uniformly distributed in the channel. Integral cells are injected into the channel and continuously endure shear stress. The physical force causes the lysis of cells to debris and releases intracellular components to the downstream of the channel. The schematic of the in-channel microstreaming in shown in Figure 5-1A. The microstreaming is generated by the vibration of the sharp-edge. Multiple sharp-edges placed on two sides of channel wall can increase the chance that cell flow through sharp-edge tips area. The chance is increased because of the increasing of function unit number and the formation of circulating microflow between neighboring sharp-edges. For single sharp-edge, the direction of the microstreaming is parallel to the direction of the sharp-edge, which is vertical to the channel. A pair of sharp-edges can form circulating microstreaming. Since the circulating microstreaming has higher flow rate than macro-

streaming flow to downstream of the channel, it provides higher drag force and captures integral cells. Cells in this circulation will flow through sharp-edge tips multiple times and have higher chance to be lysed. Lysed debris have smaller sizes that are not large enough to be captured by the acoustic radiation force or circulating streaming and can be released to the downstream of the channel.

To maximally utilize the trapping effect caused by acoustic radiational force and circulating microstreaming, the homogenizator consists of multiple sharp-edge structures as the Fig. 1B shows. The large cross-sectional area allows the flow rate in-channel to be much lower than acoustic microstreaming, which can provide more stable circulating streaming among sharp-edges. Large quantities of sharp-edges provide a higher chance for cells to be captured by the trapping effect in-channel and allow for uniform lysis. In-channel images are shown in Figure 5-1C, D, and E, and their positions in the channel are in squares on Figure 5-1B. Figure 5-1C demonstrates the fluorescent image of Calcein-AM stained cells, which are green dots in the channel. The left side channel of Figure 5-1C is the upstream channel of the device and the right side is the nearby downstream channel. Compared with the upstream, the downstream channel contains a lower number of fluorescent dots, which indicates that cells are being lysed in the channel. Figure 5-1D and E are bright field images at two corners in the device. Figure 5-1D is the corner close to the upstream and Figure 5-1E is close to the downstream. Large gray particles in Figure 5-1D are cells that have not been lysed, and small particles in Figure 5-1D and E are lysed

debris. The trapping effect is demonstrated in the red circle in Figure 5-1D, which is cells concentrating around the tip of a sharp-edge. Compared with Figure 5-1D, Figure 5-1E has less cellular size particles but more smaller debris. The debris cannot be captured around the sharp-edge because of lower drag force and acoustic radiation force, indicating that the lysed product can flow to the outlet of the channel and be collected for downstream analysis. The device contains large number of sharp-edges, majority of cells have been lysed at a middle position in the channel, indicate sharp-edges in downstream excess the need for homogenization. Recruiting excessing number of sharp-edges can increase throughput. Large flow rate provides a high drag force that can resist trapping effect from circulating microstreaming and acoustic radiation force. Cells will be mandatorily dragged to downstream without circulating enough times through sharp-edges areas, and this problem could be solved by increasing amount of sharp-edges. Furthermore, when the density of cells entering the channel excesses the lysis efficiency of one sharp-edge, limited number of cells will occupy the limited space in the channel and mandatorily push other cell without lysis to the downstream of the channel. Increasing number of sharp-edges can capture higher numbers of cells, and more sharp-edges can increase the overall lysis efficiency of the device, which allows the device reaching a balance with higher density of injected cells.

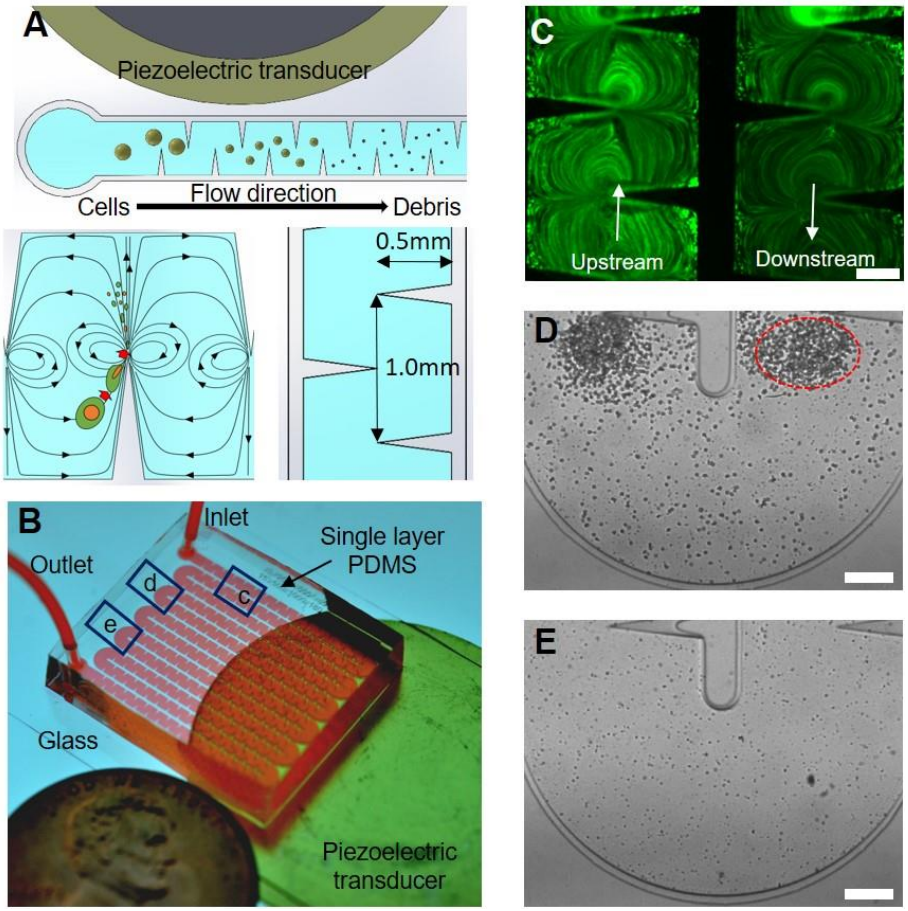

Figure 5-1: Overview of the homogenizator structure and working pattern. (A) Schematic of the homogenizator structure and cell lysis pattern. (B) Real device structure. (C) Comparison of upstream and downstream channel. (D) Upstream sharp-edge trapping effect on cells. (E) Downstream lack of cellular structure. Scale bars for C, D, and E, 250 μm

5.3 Experiment methods

5.3.1 Acoustofluidic sharp-edge homogenizator fabrication

2-D structures of the sharp-edge channels were designed by AutoCAD (AUTODESK®). A channel with 360 sharp-edge structures was designed as homogenizator and a channel without sharp-edge structures was designed as control.

Deep ion etching (DRIE) followed the patterns of CAD files was recruited for manufacturing masks for photolithography. We used standard photolithography followed by anisotropically etched on single-side polished silicon wafer to create silicon master molds with 100◎m height channels. After 20min coating with silane vapor using 1H,1H,2H,2H-perfluorooctyl-trichlorosilane (Sigma-Aldrich, USA), silicon master molds were covered by a mixture consisted by PDMS-Sylgard 184 silicone elastomer base and Sylgard 184 curing agent (Dow Corning, USA) in a ratio of 10:1. The mixture and models are placed under vacuum for air bubble elimination, followed by incubation at 65°C for 1 hour to solidify the channel structures. Solidified PDMS channels and glass slides were then treated by oxygen plasma (Electro-Technic Products, USA) and bonded together. An incubation at 65°C for 24 hours was recruited for stabilization of the bonding. PDMS and glass complex was then bonded with an acoustic transducer (RadioShack, USA) under the glass slide using epoxy (Permatex, USA).

5.3.2 Acoustofluidic cell lysis and staining

HeLa cells (ATCC, USA) and Jurkat cells (ATCC, USA) that can represent attached cells and suspension cells respectively were the main cell lines for homogenizator performance validation. HeLa and Jurkat were respectively grown in DMEM (Gibco, USA) and RPMI 1640 (Gibco, USA) culture medium, both added with 10% Fetal Bovine Serum (Gibco, USA) and Penicillin Streptomycin (Gibco, USA). Cells are cultured in

incubator (NuAire, USA) at 37 °C and 5% CO_2 condition. HeLa cells are harvest when grown to 90% confluency and Jurkat cells are harvest at a density of 8×10^5 cell/mL.

HeLa cells were detached by trypsin–EDTA (Gibco, USA) and responded in DMEM. Jurkat cells were directly centrifuged and responded in RPMI 1640. For staining cytoplasm, Calcein-AM (Invitrogen, USA) was added to a final concentration of 5 μg/mL. After 15 minutes staining with Calcein-AM, cells were centrifuged and culture medium containing Calcein-AM was discarded. Cells were washed and resuspended in phosphate buffered saline (Gibco, USA) in a final density range from 105 to 106 cell/mL. Resuspended cells were then injected to the homogenizator by a pump system combined with 1 mL syringes (BD Bioscience, USA) and automated syringe pump (neMESYS, Germany) in settled flow rate. The acoustic transducer in the homogenizator was driven by a power system consists of a function generator (Tektronix, USA) and an amplifier (Amplifier Research, USA) in a working frequency of 5.5 kHz and settled voltage. Collected samples were stained with 1 μM SYTOX Orange (Invitrogen, USA) in purpose of recognizing cells that have plasma membrane damage but keep cellular structures.

5.3.3 Lysis efficiency analysis

Since the densities of cells are different in different experiments, to calculating lysis efficiency, control groups were collected respectively for each experiment. To avoid cross contamination between control and experiment groups, control groups were firstly collected when the acoustic transducer was off. The channel was then washed by PBS and

after washing experiment groups was collected when the transducer was on. In each experiment, control groups and experiment groups were using same batch of samples with similar cell density. Lysis rates for one experiment were calculated by the number of cells of control and experiment groups using same samples.

To validate whether the main reason causes homogenization is the shear stress caused by share-edge induced acoustic microstreaming, not the heat and acoustic pressure produced by the acoustic transducer, a control channel without sharp-edge structure was recruited. Both the non-sharp-edge channel and sharp edge channel were working with acoustic transducer power of 50 V sine wave and sample flow rate of 5 μL min^{-1}. Homogenization efficiencies of the non-sharp-edge channel and sharp-edge channel were compared.

To study the voltages' influence on homogenization efficiency, 0, 10, 20, 30, 40, and 50 V sine waves were applied on the acoustic transducer. Sample flow rates were stable at 5 μL min^{-1} for different voltages. Homogenization efficiencies of different voltages were demonstrated by the percentage of remaining cell number in a specific voltage compared with the cell number in 0 V. Experiments were repeated for three times and for each time every voltages experiments used same batch of sample with same cell densities. Homogenization efficiency for a specific voltage was calculated by the average of the three repeats.

To study the flow rate influence on homogenization efficiency, samples were injected with 5, 7.5, 10, 15 μL/min flow rate with the acoustic transducer working with 50 V sine wave. Homogenization efficiencies of different voltages were demonstrated by the percentage of remaining cell number in a specific flow rate compared with the cell number in the 0 V and 15 μL/min condition. Experiments were repeated for three times and for each time every flow rate experiment used same batch of sample with same cell densities. Homogenization efficiency for a specific flow rate was calculated by the average of the three repeats.

5.3.4 Lysis product validation

Homogenized samples were collected with the acoustic transducer working in 50 Vpp and 5 μL/min flow rate. To avoid the positive signals from un-lysed cells, collected samples were centrifuged with 800 rpm for 10 minutes. For western-blot analysis, after centrifugation the supernatant was collected. 5 μL supernatant was mixed with 10 μL Tricine Sample Buffer (Bio-Rad Laboratories, USA) and heated to 95 °C for 5 minutes. Samples were processed by sodium dodecyl sulfate polyacrylamide gel electrophoresis (Bio-Rad Laboratories, USA) and transferred to PVDF membrane (Bio-Rad Laboratories, USA) through Trans-Blot Turbo Transfer System (Bio-Rad Laboratories, USA). PVDF membranes were incubated with mouse anti-human beta-actin (Abcam, USA) at 4 °C for 12 hours, followed incubated with Goat anti-mouse HRP antibody (Abcam, USA). Bands of target protein were imaged by ChemiDoc Imaging System (Bio-Rad Laboratories, USA).

PCR reactions was processed using AmpliTaq Gold 360 Master Mix (Applied Biosystems, USA) with 26 PCR reaction circles. Primers are shown in Table 3. The amplicons were stained by SYBR green (Invitrogen, USA) and image were captured by ChemiDoc Imaging System (Bio-Rad Laboratories, USA).

RBCs infected by malaria parasite were provide by Taylor's malaria Lab (Duke University). Generally infected RBCs were cultured in RPMI1640 culture medium with a concentration of 106 cell/mL and 5% of RBCs have been infected with 3D7 parasite. Samples was injected into the homogenizator with a flow rate of 5 μL/min, and the lysis group was collected when the transducer was working under 50 V sine wave. Control group was collected with same flow rate with transducer turned off. Cell slide of collected samples were prepared following the instruction of Doublesytoslide system (Thermofisher, USA), and the slide staining was following the instruction of Diff-Quik staining kit (Thermofisher, USA). For PCR analysis, collected samples were centrifugated under 3000g for 5 minutes and the supernatant was collected for templet. Primers were found in a reference and are shown in Table 3.

Table 3 Primers for PCR validation

		Sequence
Cell PCR primer	Forward	ACCTGGGTCTTCAGTGAACC
	Reverse	CAGTCAGATCCTAGCGTCGAG
Malaria PCR primer	Forward	TTAAACTGGTTTGGGAAAACCAAATATATT
	Reverse	ACACAATGAACTCAATCATGACTACCCGTC

5.4 Results and discussion

5.4.1 Acoustic microstreaming and shear stress distribution

The main lysis effect of the homogenizator is the shear stress generated by the sharp-edge. Figure 5-2A and B, which are flow field and shear stress simulation in different acoustic transducer power, demonstrate high shear stress is generated by high acoustic fields and the relationship between microstreaming flow rate and shear stress. Lines in Figure 5-2A demonstrate the direction of flow in channel, and color distribution indicates the flow rate strength. Compared with flow field when transducer is off, high acoustic field significantly increase the microstreaming flow rate around sharp edge. Shear stress simulation result in Figure 5-2B shows high shear stress areas are similar with high flow rate distribution. Since the sharp-edge vibrations that generate microstreaming and shear stress are induced by the acoustic force, the high working power of the acoustic transducer can induce a stronger flow rate and shear stress. Figure 5-2C are the cell moving pattern in-channel influenced by micro-streaming, which is demonstrated by Calcein-AM stained fluorescent cells. Compared with simulated streaming lines in Figure 5-2A, the streaming lines in Figure 5-2B lack some vortex circulations. The reason for this difference is the ununiform distribution of acoustic field on the device, and the physical properties difference, including density and size, between flow and particles like cells.

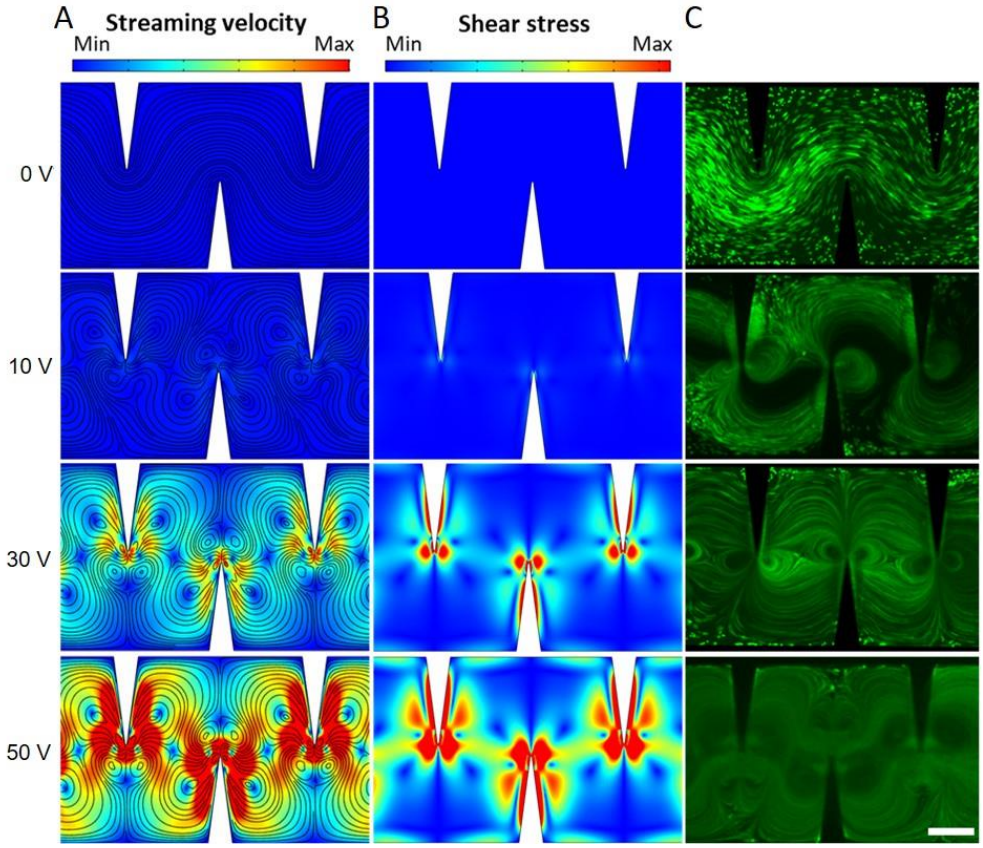

Figure 5-2: In-channel microstreaming and shear stress distribution. (A) simulation of in-channel microstreaming. (B) simulation of shear stress. (C) cell flowing pattern when acoustic transducer is working at 0, 10, 30, 50V. Scale bars for C, 250 μm.

5.4.2 Validate role of sharp-edge in homogenization

Since the heat generated by transducer can potentially cause cell lysis, we analyzed the temperature of the transducer after the device have worked for 20 minutes and reached the highest temperature. The highest temperature of the transducer is around 29 to 30 °C, which cannot cause cell lysis. Infrared images of the device before work and worked for 20 minutes are shown in Figure 5-3A. To further validate the sharp-edge is the main reason causes cell lysis, we designed a control device without sharp-edge structures

to validate whether acoustic microstreaming generated by sharp-edges is the main cause for lysis. The control device has a non-sharp-edge channel that shares a similar width and length with the homogenizator and has the same bounding as the acoustic transducer. The comparison of the lysis results of the homogenizator and control are shown in Figure 5-3. Figure 5-3B is the lysis result of HeLa and 29C is the result of Jurkat. The Calcein-AM channel is the fluorescence of cytoplasm, so only cells debris that have complete membrane structures have the green fluorescence. The SYTOX-orange channel indicates the cells that have experienced membrane damage or debris from the nucleus, since SYTOX-orange cannot permeate through the cell membrane and only has red fluorescence when combined with DNA molecules. Since the no-sharp-edge device and sharp-edge device use same cell density samples and products are diluted with a constant ratio, the lysis efficiency can be compared by directly calculating quantities of cells in microscope images. As shown in Figure 5-3, the no-sharp-edge device has similar cell quantities when the acoustic transducer is on and off, indicating that the acoustic pressure and heat generated by the acoustic transducer cannot lyse cells. Compared with the no-sharp-edge device, when the acoustic transducer is on, the sharp-edge device' sample has fewer quantities of cells in the view and has small debris in both Calcein-AM and SYTOX-orange channels. Furthermore, the Calcein-AM channels of the lysed sample have a strong green background, which indicates that intracellular dyes have been released from cells. These

results indicate that sharp-edge induced microstreaming under acoustic vibration is the main reason for cell homogenization.

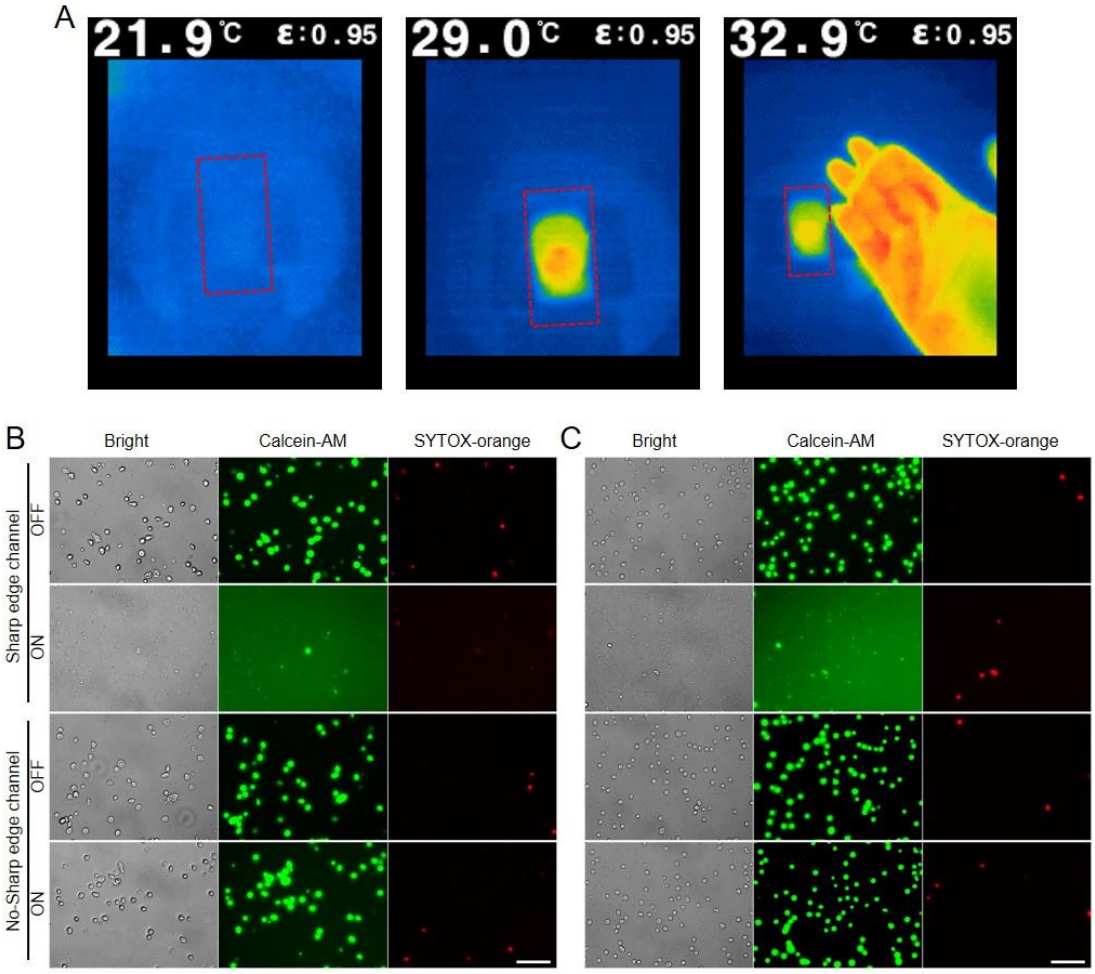

Figure 5-3: Temperature during device working and comparison between no-sharp-edge device and sharp-edge device when acoustic transducer is on and off. (A) Temperature monitoring over a time interval of 20 minutes. The red-dashed rectangles mark the perimeter of the device (B) Comparison using HeLa cells. (C) Comparison using Jurkat cells, the order of groups is same with a. Scale bars for A and B, 100 μm.

5.4.3 Lysis efficiency influenced by device power

To evaluate the influence of the acoustic transducer's power on the homogenization result, lysis samples with the transducer working at different power levels were analyzed. Transducer power is evaluated by the voltage, and six power types, which are 0, 10, 20, 30, 40 and 50 V were used for both HeLa and Jurkat cells. Fluorescent microscope images of lysed HeLa and Jurkat cells with voltages of 0, 10, 30, and 50 V are shown in Figure 5-4A and B. All voltage conditions use one batch of harvested cells that have a similar cell density, and the lysed samples are diluted with the same ratio. When the power of the acoustic transducer increases, total cell number in the transducer decreases, and the background Calcein-AM fluorescence increases, which indicates that the lysis efficiency of the transducer becomes higher. Figure 5-4C and D demonstrate analytical results of the influence of power on cell lysis efficiency. Total cell percentage for the 0 V condition is 100%, because at 0 V the transducer is off and no microstreaming generating in channel. In other power conditions, cell numbers in views with same area sizes were calculate, and the percentage of cells in Figure 5-4B and C are proportion of remaining cells compared with 0 V situation. The error bars demonstrate standard deviations generated from three repeats of the experiment and indicate the trend that integral cell number is decreased when power increase is correct. Transducer power influence cell lysis rate by strength of microstreaming. The flow rate of sharp-edge induced microstreaming determines the strength of shear stress, which break membrane

structure, and drag force of circulating microstreaming, which increase the chance cell flow through high shear stress area. When transducer is in low power, the shear stress is not enough for break cell membrane and circulating microstreaming cannot provide enough drag force to capture cells. Since the microstreaming is generated by vibrating sharp-edges, the power of acoustic transducer that influence vibration strength can influence lysis efficiency.

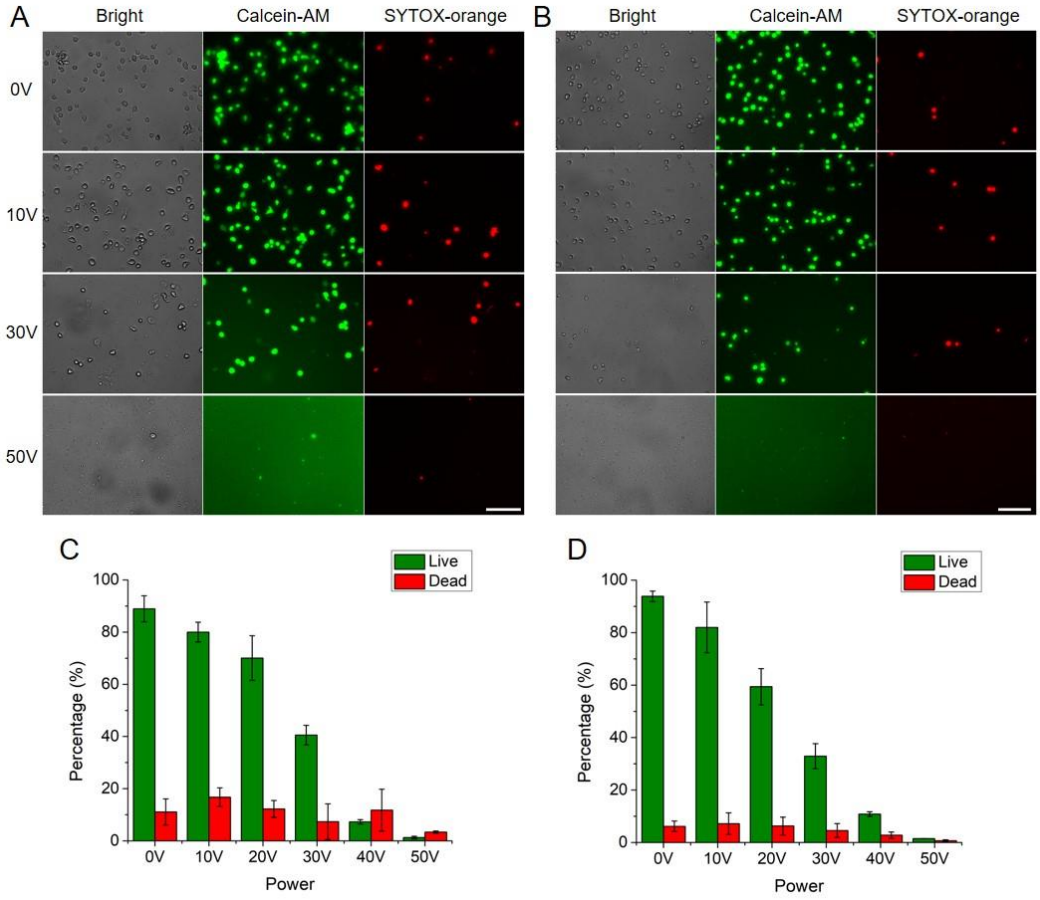

Figure 5-4: Acoustic transducer power influence on lysis efficiency. (A) Fluorescent images of lysed products of HeLa cells by 0, 10, 30, and 50 Vpp voltages. (B) Fluorescent images of lysed products of Jukat cells by 0 , 10 , 30 , and 50 Vpp voltages. (C) Percentage of remaining HeLa cells after lysis by different power. (D)

Percentage of remaining Jurkat cells after lysis by different power. Scale bars for A and B, 100 μm.

5.4.4 Flow rate influence on lysis efficiency

To investigate different flow rates' influence on homogenization efficiency, we used 5, 7.5, 10, and 15 μL/min sample inject flow rates. 5, 10, and 15 μL/min sample inject flow rates' influence on homogenization efficiency of HeLa are Jurkat cells are shown in Figure 5-5A and B, indicating that the homogenizator can achieve higher lysis efficiency when the flow rate is lower. Figure 5-5C and D demonstrate analytical results of the influence of power on cell lysis efficiency. Lysis rate statistical results indicate that when flow rate is lower than 7.5 μL/min, the sharp-edge device can achieve a high lysis rate. Different with acoustic transducers' power, which both determine shear stress and trapping effect, flow rate only against the trapping effect. When flow rate is low, drag force generated by circulating flow and acoustic radiation force have mean effect and cause cells circulating between neighboring sharp edges. However, high flow rate of macro-streaming in channel provide a drag force against trapping effect and force cells flow to the downstream. Since cells cannot circulating around sharp-edges for enough time, although the shear stress is enough for breaking cell membrane, some cells cannot flow through the high shear stress areas and cannot be lysed.

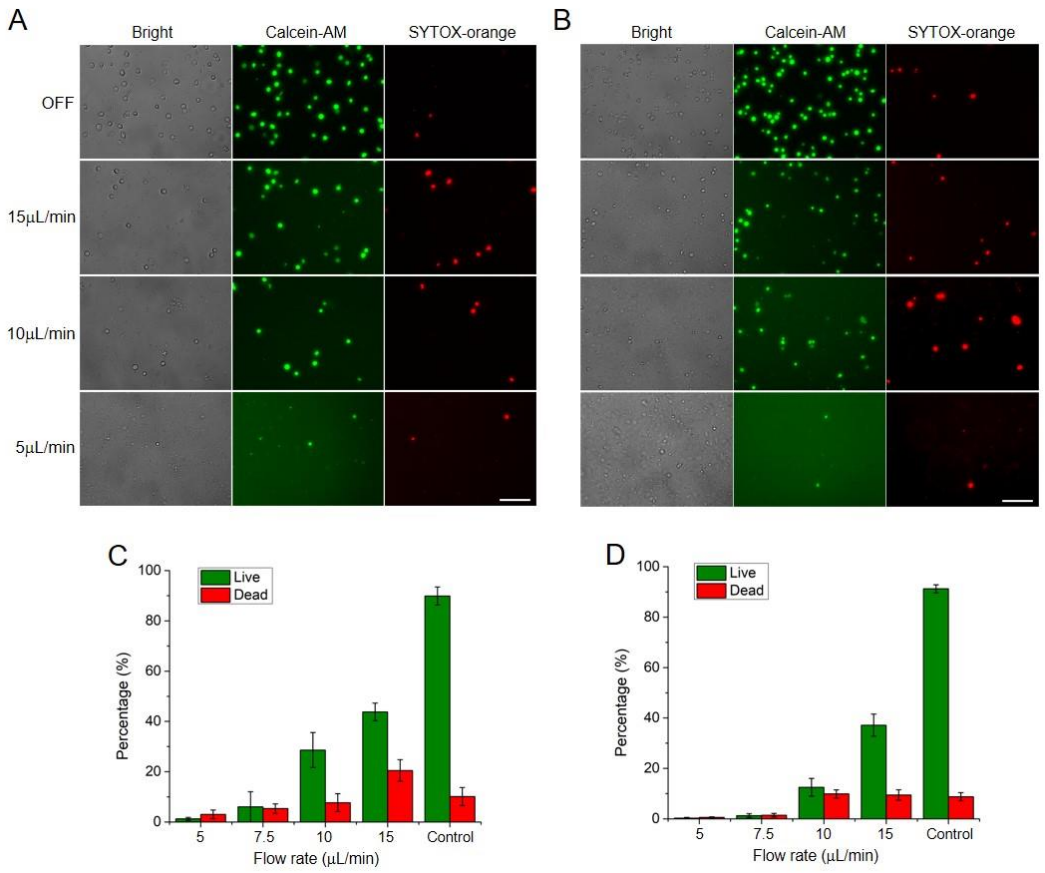

Figure 5-5: Flow rate influence on lysis efficiency. (A) Fluorescent images of lysed products of HeLa cells 5, 10, and 15 μL min^{-1} sample inject flow rates. (B) Fluorescent images of lysed products of Jurkat cells 5, 10, and 15 μL min^{-1} sample inject flow rates. (C) Percentage of remaining HeLa cells after lysis in different flow rate. (D) Percentage of remaining Jurkat cells after lysis in different flow rate. Scale bars for a and b, 100 μm.

5.4.5 Downstream lysis product analysis

Downstream analysis results of western blot and PCR are shown in Figure 5-6A and B. We choose beta-actin, which is widely used as an internal reference. 5 μL samples collected at different transducer power levels were used, and the band of beta-actin could be observed at and above 20 V. For both HeLa and Jurkat lysis products, PCR amplicon

of a 300 bp fragment on exon regions of P53 gene gets positive band using 26 reaction circle as Figure 5-6B indicates, demonstrating that genome DNA of the lysed cells have not degraded during homogenization.

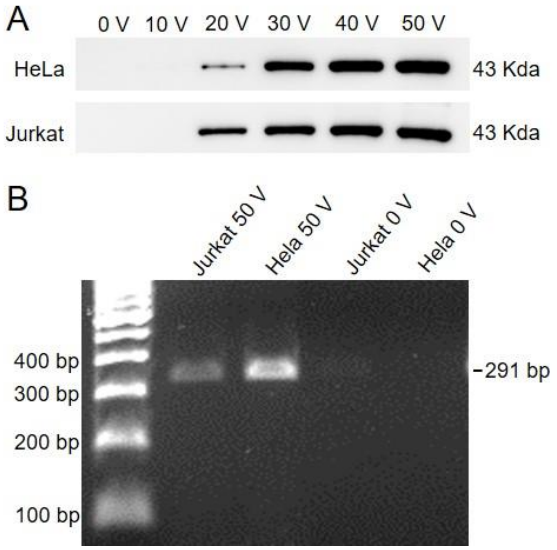

Figure 5-6: Downstream lysis product analysis results. (A) Western-blot result of beta-actin in different voltages. (B) PCR result of a 285bp fragment on one exon of P53 gene.

5.4.6 Malaria infected RBCs lysis and analysis

To validate the sharp-edge homogenizator can process disease sample, RBCs infected with 3D7 malarial parasite were used for monitoring real blood samples. RBCs were suspend in RPMI1640 culture medium with 5% of cells infected with 3D7 parasite. Sample was processed by the homogenizator with a concentration of 106 cells/mL. Figure 5-7A demonstrates the morphology differences between malaria parasites when homogenizator was turn off and turn on. When the sharp-edge not generate microstreaming, parasites are contained by infected RBCs, and are shown in purple by

Diff-Quik staining. When the homogenizator start working, the microstreaming in channel can break RBCs and parasites, cause parasite debris show as black dots. Furthermore, in microscope image of lysed samples, transparent membrane structures can be observed. These structures are RBCs with membrane structure broken can cause the releasing of internal hemoglobin. Figure 5-7B, which demonstrates lysis sample has less precipitation after centrifugation and supernatant containing obvious red color, also indicate the releasing of hemoglobin from RBCs to culture medium. The PCR results in Figure 5-7C demonstrate the 205 bp amplicon on SSUrRNA gene using designed primers can be detected using lysis product as templet, while product flow through the channel without microstreaming lysis failed for getting target band. These results demonstrate the sharp-edge homogenizator is eligible for lysis malaria parasite in RBCs and indicate its potential for lysis and detection of bloodborne pathogens.

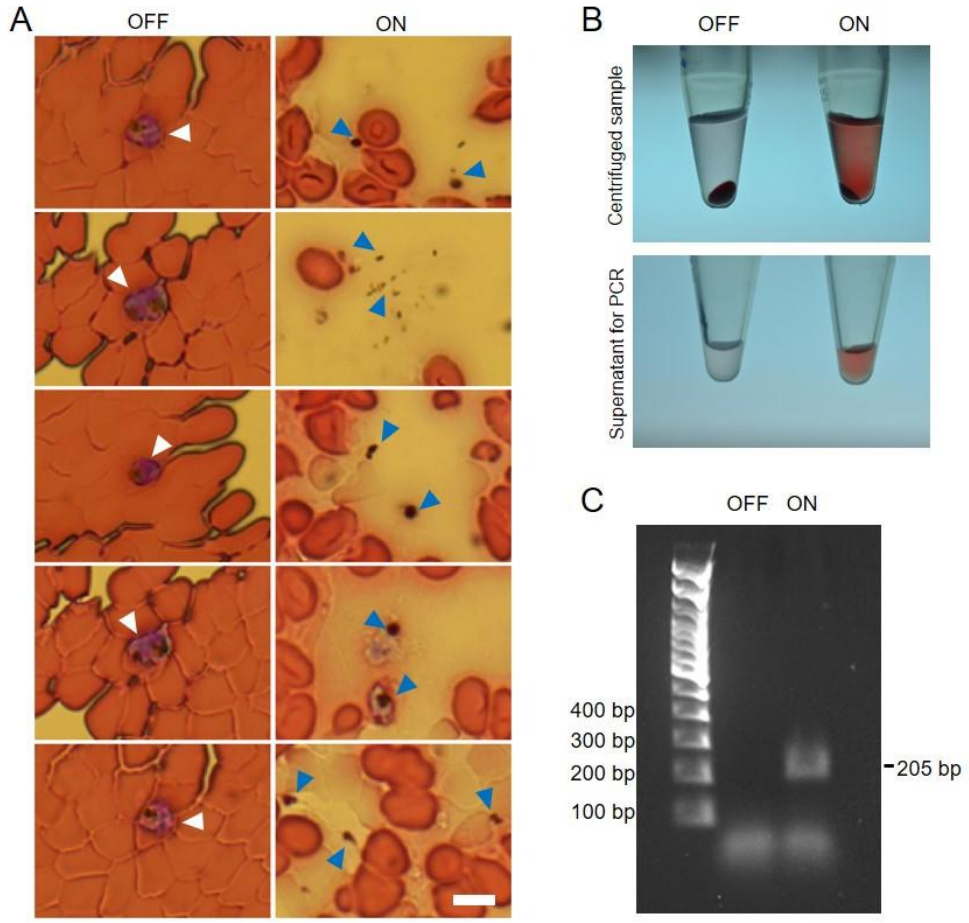

Figure 5-7: Characterization of malaria infected cell lysis product. (A) morphological validation for products when sharp-edge device is off and on. (B) photo comparison between unlysed and lysed products. (C) PCR result using unlysed and lysed products.

5.5 Conclusion

We have described an acoustic microstreaming based sharp-edge homogenizator. By utilizing shear stress generated by microstreaming, the homogenizator can achieve continuous cell lysis. Furthermore, the circulating microstreaming generated by sharp-edges and the acoustic radiation force generated by the transducer introduces trapping effects on complete cells but not debris. The trapping effect can increase the chance of cells

flowing through high shear stress area, which helps to increase the lysis efficiency and achieve uniform lysis. The effect unit of the homogenizator is PDMS sharp-edges, by increasing the number of the effect unit the homogenizator has potential to achieve higher throughput and efficiency. Since the PDMS sharp-edges can be increased without adding related power source and electrode, the lysis efficiency and throughput could be further increased in simple and low-cost method. Lysis product can be directly used for downstream protein and DNA analysis, indicating the homogenizator's potential for integration with on-chip analysis and building a faster sample processing and analysis system.

Improving cell lysis technology is always an important direction for microfluidics, since with the progress of downstream analysis methods and different applications, optimized cell lysis approaches that can satisfy these new requirements are still needed to be developed. Although currently there are decreasing number of publications discuss 'fundamental cell lysis', which are devices focusing on achieving single function of cell lysis, works that try to integrate new functions to cell lysis microfluidic devices have emerged and demonstrated strong impact. Among those emerging works, single cell lysis microfluidic systems and multi-function cell lysis microfluidic systems have become two mainstreams of cell lysis technology development. Single cell lysis studies is motivated by the robust development of single cell analysis technology and bring high impact publications.(Klein et al., 2015, Kim et al., 2018) And multi-function cell lysis devices

usually integrated separation function,(Huang et al., 2016, Ramachandraiah et al., 2017) which allows the devices to process huge number of cells. The acoustofluidic sharp-edges cell lysis system we developed has integrated both lysis and separation functions by deeply investigating and applying the complex acoustofluidic physical phenomenon. While cell membranes are lysed via shear stress induced by strong acoustofluidic microstreaming, complete cells are also trapped in the system by comprehensive trapping effect generated by microstreaming vortex and acoustic radiation force. This trapping effect provides our device separation function and makes the system become multi-function cell lysis system that can separate cells and lysis debris. Furthermore, our group has deeply studied the acoustofluidic sharp-edge physics and flexible used physical properties for multiple applications, including pumping,(Huang et al., 2014) mixing,(Nama et al., 2016) and cell stimulation.(Huang et al., 2015) Application on cell lysis is an new branches of this high impact sharp-edge microfluidics. Works reported in our cell lysis paper not only improve physics and application studies of sharp-edge microfluidics, but also indicate sharp-edge cell lysis device's potential for easily integration with devices with other functions. By integrating with sharp-edge pump and mixer, the sharp-edge cell lysis device reported in this paper can become a highly automatic system for achieve both cell lysis and downstream analysis, while external pumping system are not required. Since the sharp-edge cell lysis system itself is a multi-function system that achieves both lysis and separation, and shows high integration

potential with other sharp-edge devices for achieving highly automatic running for comprehensive processes, it has strong scientific and application value.

Multiple mechanical cell lysis methods have already been developed and showed portable and zero-power consumption advantages. These advantages, especially zero-power consumption, indeed challenging the application significance of our acoustofludic sharp-edge cell lysis system. However, external power derived sharp-edge vibration makes our device lyse cells in a non-contact way and provide related benefits. The biggest difference between non-contact and contact cell lysis is the complexity of devices' structures. Our sharp-edge device achieves cell lysis by complex acoustofludic microstreaming, but the structure of the sharp-edge device is very sample. This simple structure makes the device low cost, easy for fabrication, and easy for increasing lysis efficiency by adding sharp edges' numbers in the channel. Compared with this simple fabrication of our sharp-edge system, nanoscale structures cutting lysis need complex fabrication steps, including deep reactive ion etching or photoelectrochemical etching,(Di Carlo et al., 2003, So et al., 2014) which increase fabrication cost. Furthermore, direct contact cell lysis devices with complex solid structures usually bring clogging problems induced by debris attached on nanostructures. This clogging problem may reduce lysis efficiency and inhibit the release of lysis product. By applying non-contact lysis, our sharp-edge device lysis can stable keep high efficiency lysis without clogging problems. Furthermore, we agree with the referee that external power supply can influence portable

properties, but this problem could be solved by optimizing power supply and the channel. Our group has achieved acoustofludic sharp-edge device derived by cell phone,(Bachman et al., 2018) indicating portable and power supply could be solved in the future.

Comparing lysis efficiency of our sharp-edge device and other conventional methods is very constructive. Currently cell lysis efficiency of our device is higher than 90% and can achieve 98% in some test. Compared with efficiency of 86% for chemical microfluidic cell lysis,(Mun et al., 2010) electrical cell lysis, which is 74% in early stage(Lu et al., 2005) and can 99%,(Mernier et al., 2010) 78% and 80% of optical microfluidic cell lysis,(Huang et al., 2016) 90% of thermal lysis,(Privorotskaya et al., 2010) and multiple mechanical lysis methods that can achieve 65%(Kim et al., 2004) to 99%,(Di Carlo et al., 2003) lysis efficiency achieved by our sharp-edge device is comparable. Also, by comprehensively evaluating, each method has its drawback. Chemical lysis needs extra reagent, electrical cell lysis needs small scale electrodes(Lu et al., 2005) or conductivity adjusted buffer,(Mernier et al., 2010) throughput limitation of optical lysis, protein denaturation induced by thermal lysis, and fabrication, cost, and continuance of mechanical lysis. Compared with these methods, acoustofludic sharp-edge cell lysis is reagent free, easy for fabrication, can continuous run without clogging issues, less heat generation that is less harmful for lysis products, and can achieve comparable lysis efficacy. Considering these properties, acoustofludic sharp-edge lysis is a moderate but wide-compatible lysis approaches, which expand its unique value for application. Our

device applies comprehensive physic, including acoustic and fluidic, phenomenon to achieve a multifunction device that can both lysis cells by microstreaming generated shear stress and cell/debris separation by vortex and acoustic radiation force. Thanks to the referee's comments we realized the discretion of separation function is not enough and added related discussion in result section and provide data related with separation effect at Fig. 1S. These modifications can strength the multifunction properties of the device. For the application values, our sharp-edge device has high integration ability, comparable lysis efficiency and less harm for lysis products.

6. Acoustofluidic drug loading

To further investigate wither the membrane lysis function of acoustofluidic technology could be applied not only on cells, but also on nanosized bioparticles including exosomes, we developed an acoustofluidic droplet rotation device that can synchronously derive drug loading and vesicle encapsulation, since it can derive both nanoparticle concentration and acoustic streaming shear stress.

Nanocarrier and vesicle encapsulation have been found significantly promoting drug delivery efficiency and achieving targeted delivery. However, problems including early drug releasing and complex procedures for drug loading and vesicle encapsulation limit the development of vesicle encapsulated nanocarrier. Here we developed an acoustofluidic device that synchronously achieves drug loading and exosome encapsulation. By recruiting acoustic radiation force, microstreaming, and shear stress derived in an acoustic droplet rotation system, exosomes, doxorubicin (DOX), and porous silicon nanoparticles are co-concentrated and encapsulated by exosome membrane. This acoustic system achieved high drug loading and encapsulation rate, and the derived nanocarriers promote intracellular intake of DOX. Since the acoustofluidic approach is a short physical process, it provides a high potential method for constructing drug delivery system. Results and discussion in this chapter comes from my first author paper under review.

6.1 Motivation

Nanoscale drug delivery systems have gained noticeable promise for therapeutic applications in the past decade.(Hui et al., 2019) By encapsulating drug molecules with nanoscale carriers, controllable and active targeted release can be achieved.(Blanco et al., 2015) Compared to small drug molecules in suspension, nanoparticles demonstrate enhanced permeation and retention, which induce higher drug accumulation within the target cells.(Singh et al., 2009) Porous silicon nanoparticles are one commonly used nanocarrier and exhibit strong potential for therapeutic applications.(Rizvi et al., 2018) The unique mechanical and electrical properties of silicon particles derive favorable biocompatibility and enable a high intracellular intake rate.(Anglin et al., 2008) Porous silicon particles also demonstrate advantageous features such as biodegradability, low toxicity, and safe renal clearance availability.(Salonen et al., 2008) Furthermore, porous structure-based drug loading relies on the physical effects between the carrier and drug molecules and do not require comprehensive chemical modifications. This high acceptance nature allows silicon nanocarriers to successfully load multiple types of drugs, including doxorubicin (DOX), dexamethasone, and ibuprofen. However, there are limitations with the use and clinical application of silicon nanocarriers, including early drug release, clearance by the immune system, and it is difficult to achieve drug delivery to the target of interest.(Jeelani et al., 2020)

Exosomes are 30-200 nm vesicles secreted by cells and has shown promising potential for improving silicon nanoparticles' efficiency for drug delivery.(Kooijmans et al., 2012) With a phospholipid bilayer structure, like liposomes, exosomes can encapsulate silicon particles and prohibit the release and degradation of loaded drugs. Furthermore, compared with artificial vesicle liposomes, exosomes are naturally produced by cells and have higher biocompatibility and avoid clearance by the immune system.(Smyth et al., 2015) Another advantage for recruiting exosomes in drug delivery is its targeted delivery potential. Since exosomes derive intercellular communication by exocytosis and endocytosis pathways, these vesicles are natural carriers to deliver proteins and nucleic acids among cells.(Milane et al., 2015) Depending on the secretion cells' type, exosomes have been shown to intake into specific cell populations. By this mechanism, exosomes participate in multiple critical bioactivities including the expansion of neuron degeneration, proliferation and invasion of tumor cells, immune system activation, and tissue regeneration.(Bobrie et al., 2011, Hessvik et al., 2018) Previous studies have demonstrated that exosome encapsulated silicon nanoparticles show low immune clearance and have improved targeted delivery abilities.(Illes et al., 2017) However, the major limitation of exosome encapsulation is the low loading rate of the nanoparticles.

Here we developed an acoustofluidic based drug loading technology that simultaneously enables the fast loading of drug into silicon nanoparticles with exosome encapsulation. These functions are derived from our previously developed acoustofluidic

technology for nano-sized particle manipulation and screening. The acoustofluidic technology is an interdisciplinary combination of acoustics and fluidics, which recruits acoustic wave generated radiation forces and microstreaming for size-based particle separation. Our previous investigations have shown that acoustofluidics is eligible for exosomal separation and macromolecule concentration, indicating that the technology can achieve manipulation on small vesicles. A further development of this technology is a droplet acoustofluidic platform that can concentrate exosomes and macromolecules in the center of the droplet.(Gu et al., 2021) This technology enables co-concentration of drug molecules, exosomes, and silicon particles and achieves one step drug loading and exosome encapsulation. The final products are porous silicon nanoparticles containing drug molecules and are enveloped by an exosomal membrane, which is ideal for targeted drug deliver. Since acoustofluidic droplet drug loading technology is fast, reagent free, and shows higher loading rates than conventional methods, including placing and sonication, this platform demonstrates great potential for constructing a drug delivery system for a variety of drugs, nanocarriers, and vesicles. Considering the complex combination of drugs and carriers with different chemical properties used within pharmaceutical development, this physical drug loading and nanocarrier encapsulation system provides a simple, universal platform for both researchers and manufacturers.

6.2 Mechanism and system

Since the small size of nanosized vesicles, different with the cell lysis device that can use bulk wave for generating acoustic radiation force and acoustic streaming, the drug loading device utilize surface acoustic wave, which can achieving high enough frequency for manipulating nanoparticles. The synchronous drug loading and exosome encapsulating is achieved by strong rotating microstreaming induced by the acoustofluidic device. Two surface acoustic waves generated by the interdigital transducers are spreading in opposite directions and induce opposite microstreaming in two edges of the droplet (Figure 6-1A). As a result, high flowrate vortex microstreaming is generated and cause the droplet rotation. During this process, acoustic radiation force and microstreaming comprehensively derive a trapping effect on particles in the droplet, including DOX, exosomes, and silicon nanoparticles. These particles are concentrated in the center area of the droplet with increased frequency of contact, which can result drug loading. Furthermore, strong acoustic microstreaming in the droplet derives shear stress on particles in the fluid field. Since the mobility of the lipid membrane, exosomes' membrane is disrupted by the shear stress. This acoustic microstreaming derived lipid membrane disruption bring a same effect as ultrasonic disruption and can enhance the exosome encapsulating silicon nanoparticles. Since the droplet rotation can derive both concentration and membrane disruption effects, the acoustic platform can achieve one step drug loading and exosome encapsulation (Figure 6-1B).

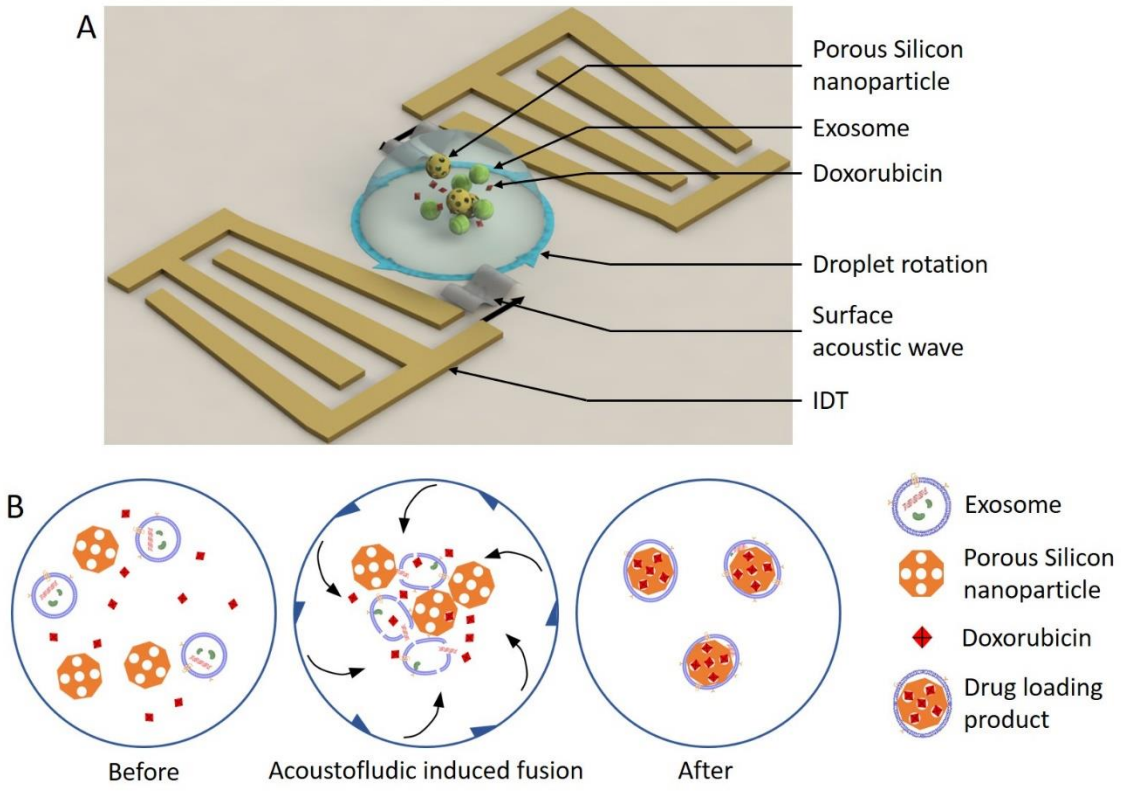

Figure 6-1: Schematics of the acoustofluidic droplet rotation drug loading device. (A) The IDT generated surface acoustic waves induce droplet rotation, induce porous silicon nanoparticles, exosomes, and DOX in the droplet concentrate and fused. (B) Mechanism of acoustic droplet rotation induced drug loading, before device being activated silicon nanoparticles, exosomes, and DOX are uniformly distributed in the droplet, during rotating these particles are concentrated in the center of the droplet, and the high concentration and shear stress induce DOX loaded in silicon nanoparticles and exosomes encapsulate silicon particles.

6.3 Experiment methods

6.3.1 Device fabrication

The acoustic droplet rotation device fabrication followed our previously published procedures. One pair of IDTs was designed by AutoCAD (Autodesk, USA) and a Y+128° X-propagation lithium niobate ($LiNbO_3$) substrate was used for IDT deposition. The

deposition was achieved by photolithography procedures. Generally, the substrate and the mask were aligned by a MA/BA6 mask aligner (SUSS MicroTec., Germany) and SPR3012 photoresist (MicroChem Corp., USA) was exposed under UV light. After CD26 developing solution (MicroChem Corp., USA) for removing unwanted photoresist, an e-beam evaporator (Semicore Corp., USA) deposited a metal double layer (Cr/Au, 50 Å/500 Å) on the substrate, followed by a lift-off process through PRS3000 resist stripper (VWR, USA) for forming the electrodes. A 3 mm diameter PDMS ring made by Sylgard 184 Silicone Elastomer Curing Agent and Base (Dow Corning, USA) were bounded on the substrate for holding the droplet.

6.3.2 *Silicon nanoparticle synthesis*

To synthesize 50, 100 nm porous spheroid silicon and 200 nm porous silicon rod, 1.1, 2.1, and 3.6 g/mL cetyltrimethylammonium bromide (CTAB, Sigma-Aldrich, USA) water suspensions were created by 15 min sonication in 35 °C incubation. Respectively, 0.75, 0.9, and 1.2 mL NH_3H_2O (Sigma-Aldrich, USA) were added to each CTAB suspension, followed by 10 min mixing. Tetraethyl orthosilicate (TEOS, Sigma-Aldrich, USA) was then added by drop with total volumes of 0.45, 0.6, and 0.72 mL, followed by adding 45, 60, and 72 μL of (3-Aminopropyl)triethoxysilane (APS, Sigma-Aldrich, USA), respectively. The silicon nanoparticles tagged with green fluorescence were created by adding APS solution containing with fluorescein isothiocyanate (FITC). After mixing in room temperature for 12 h, synthesized nanoparticles were collected by 13000 g

centrifugation, followed by ethanol washing for 48 h. Porous silicon nanoparticles were then collected by centrifugation and washed by water for 3 times.

6.3.3 Acoustic droplet rotation encapsulation and drug loading

The power system of the acoustic droplet rotation device contains a function generator (Agilent, USA) and an amplifier (Amplifier Research, USA). The substrate was attached on a Peltier cooling system (Hebei IT, China) powered by a variable DC power supply (Tekpower, USA) for avoiding IDT generated heat break the device. Droplet rotation was monitored with an upright microscope (Olympus, Japan) combined with a CCD camera (Photometrics, USA). For exosome encapsulation analysis, the 10 μL droplet contained 1×10^7 particles/mL human plasma exosomes (BioVision, USA), and 400 μg/mL of porous silicon nanoparticles. The products were analyzed by Nanoparticle Tracking Analysis (Malvern, England) system for evaluating the size of the encapsulated nanoparticles. Drug loading efficiency analysis recruit 10 μL droplets containing 400 μg/mL of silicon nanoparticles and DOX with 50, 100, 200, 400, 600 μg/mL, or 400 μg/mL of DOX and silicon nanoparticles with concentrations of 50, 100, 200, 400, 600 μg/mL. DOX concentration were analyzed by the solution's absorption at 480 nm by a microplate reader (BioTek, USA). The synchronous exosome encapsulation and drug loading experiment used 10 μL droplet containing 1×10^7 particles/mL human plasma exosomes, 400 μg/mL of silicon nanoparticles, and 400 μg/mL of DOX, which are the optimized

concentrations. All encapsulation and drug loading procedures were achieved by a 30 V input voltage with 23 MHz frequency, the process lasted with 2 min.

6.3.4 Vesicle encapsulation evaluation

To validate the encapsulated nanoparticle's morphology and whether exosome encapsulation can provide nanoparticle exosome specific biomarkers, TEM microscopy and immuno-blot were utilized.

For TEM microscopy, 10 μL of exosome encapsulation product was covered by a 300-mesh copper grid support film (Electron Microscopy Sciences, USA) for 20 min of absorption. After 3 min water wash for three times, uranyl–acetate solution was used for incubating the grids for 10 min. Girds were then washed by water for three times for completing the negative staining. An electron microscope (FEI Company, USA) was used to image the grids.

For immune-blot, to avoid interference from free exosomes that are not attached with nanoparticles, 10000 g centrifugation was applied for separating nanoparticles. Isolated nanoparticles were then processed by electrophoresis and transferred to a polyvinylidene fluoride membrane (Bio-Rad, USA). Mouse anti-CD63 (Santa Cruz, USA) and mouse anti-CD (ab13492, 1 μg/mL, Abcam, USA) were used as primary antibodies for incubating the membrane at 4°C overnight. Goat anti-mouse IgG (ab97040, 0.05 μg/mL, Abcam, USA) was used as secondary antibodies. Protein abundances were analyzed with a ChemiDoc XRS+ system (Bio-Rad, USA).

6.3.5 Cell intake experiment

Since the aim of developing drug carriers is achieving successful cell intake of the carriers and derive drug functioning. To evaluate the technology's potential in treatment, DOX, exosome, and 50, 100, 200 nm porous silicon nanoparticles were processed by the acoustic droplet rotation and the products were used for culture HeLa and MCF-7 tumor cells.

HeLa cells (ATCC, USA) and MCF-7 cells (ATCC, USA) were grown in DMEM (Gibco, Life Technologies, MA, USA) culture media added with 10% Fetal Bovine Serum (Gibco, USA) and Penicillin Streptomycin (Gibco, USA). Cells were cultured in a Nu-4750 incubator (NuAire, USA) at 37 °C with a CO_2 level of 5%. The concentrations of silicon nanoparticles or exosome encapsulated silicon nanoparticles for HeLa cell intake experiments were 10 μg/mL in culture medium for 6 h. After changing culture medium for discarding free nanoparticles, a fluorescent cell imager (Bio-rad, USA) was used for capturing silicon. For DOX drug deliver experiments, exosome encapsulated silicon nanoparticles loaded with DOX and free DOX are added to the culture medium for a final concentration of 2.5 μg/mL for DOX, MMT test (Thermofisher, USA) and fluorescent microscope were used for analyzing viability of HeLa and MCF-7 and intracellular DOX fluorescence in 3, 6, 12 and 24 h after culturing. A Confocal microscope (Zeiss, German) was used for record DOX and silicon nanoparticle's fluorescence distribution in 6 h after culture.

6.4 Results and discussion

6.4.1 Acoustic streaming and shear stress distribution in the device

The acoustic streaming derived shear stress is the main mechanism for achieving exosome membrane disruption that enables nanoparticle encapsulated by exosomes. To evaluate the concentration effect of the acoustic droplet rotation device, we derived both simulation and experimental validation for analyzing the flow pattern and concentration effects. The microstreaming pattern in the rotating droplet is shown in Figure 6-2, which demonstrated a vortex for trapping the particles in the center area of the droplet. However, since the concentration effect is resulted from acoustic radiation force and microstreaming derived drug force, which are depended on the physical properties of the particles, concentration effects of these particles were analyzed under fluorescent microscope respectively. Compared with uniform fluorescent distribution when the acoustic droplet rotation device is inactivated, during device running all groups show high intensity fluorescence in the center of the droplet. Although the high fluorescent areas are different among 50 nm silicon nanoparticles, exosomes, and DOX, indicate the device's abilities for concentration are different depends on particles, the overlap of concentration area indicates the device can increase contacting chance among particles and increase loading rate. Simulation of shear stress disruption in the rotating droplet is also processed and indicate the device can generate high shear stress through microstreaming for exosome membrane disruption.

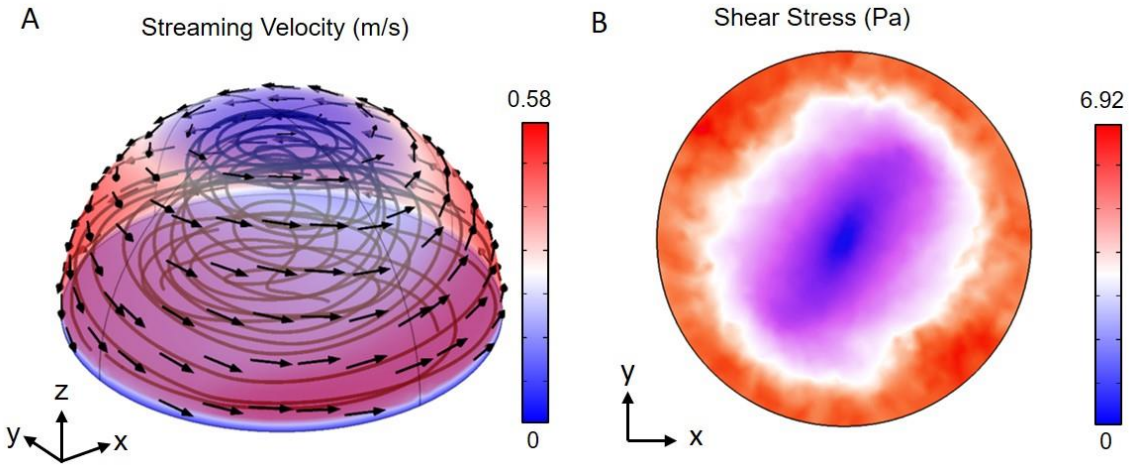

Figure 6-2: Microstreaming in the droplet induce shear stress. (A)The simulation result of microstreaming strength and direction during device working, the flow direction is directed to the center or the droplet. (B) B) Shear stress distribution in the droplet, during particles concentrating to the droplet center, these particles need to cross high shear stress regions.

6.4.2 Acoustofluidics induced concentration effect

Since the concentration effect is resulted from acoustic radiation force and microstreaming derived drug force, which are depended on the physical properties of the particles, concentration effects of these particles were analyzed under fluorescent microscope respectively. Compared with uniform fluorescent distribution when the acoustic droplet rotation device is inactivated, during device running all groups show high intensity fluorescence in the center of the droplet. Although the high fluorescent areas are different among 50 nm silicon nanoparticles, exosomes, and DOX, indicate the device's abilities for concentration are different depends on particles, the overlap of concentration area indicates the device can increase contacting chance among particles and increase loading rate. Simulation of shear stress disruption in the rotating droplet is

also processed (Figure 6-3) and indicate the device can generate high shear stress through microstreaming for exosome membrane disruption.

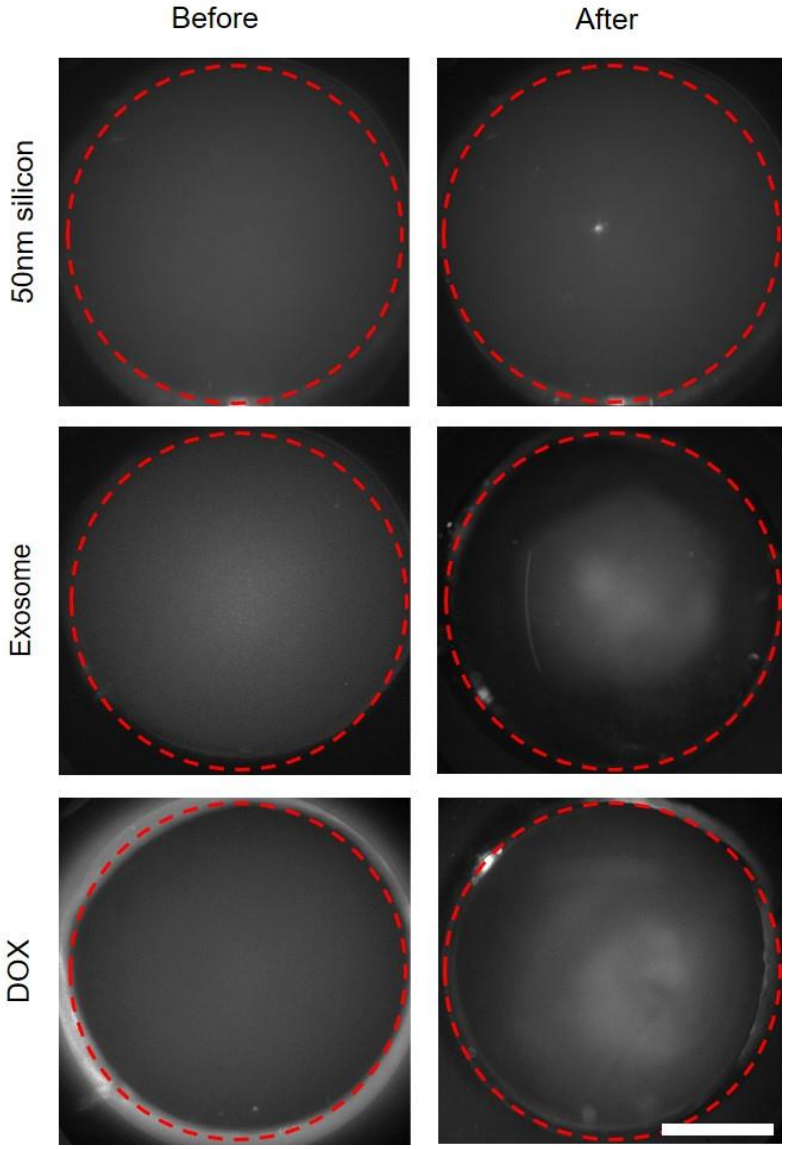

Figure 6-3: Microstreaming in the droplet induce concentration. Fluorescence of silicon nanoparticles, exosomes, and DOX show different degree of concentration during droplet rotation.

6.4.3 Acoustic rotation increases drug loading rate

The acoustofluidic droplet rotation system can achieve both drug loading and vesicle encapsulation. To evaluate its efficiency, these two functions and analyzed separately. Since the drug loading rate of the porous silicon particles depends on concentrations of the drug and nanoparticles, both concentration of DOX and silicon particles have been settled as variable while other side is stable. DOX concentration was analyzed by absorbance of DOX solution at 480 nm, and the loading rate was evaluated by the concentration difference before and after the acoustic droplet rotation. To avoid interference from silicon particles, DOX and nanoparticle mixtures were centrifuged for collecting supernatant for DOX concentration analysis. As control groups, DOX and silicon particle concentrations were same with acoustic rotation groups, but drug and particles were only mixed and incubated for 30 min. The DOX loading rate of 50 nm porous silicon nanoparticles are demonstrated in Figure 6-4A. For the DOX concentration variable and silicon particles keep 400 μg/mL groups, acoustic droplet rotation processed samples show higher loading rate compared with control groups in all DOX concentrations. Although the loading rate shows decrease after DOX concentration reach to 400 μg/mL, the main cause is the saturation of silicon particles loading capability. The comparison between DOX concentration stable groups also shows acoustic rotation can achieve higher loading rates. Same tends also exist in 100 nm spherical and 200 nm rod

silicon nanoparticles (Figure 6-4B and C), indicate acoustic rotation derived drug loading promotion has a wide feasibility for nanoparticles' size and shape.

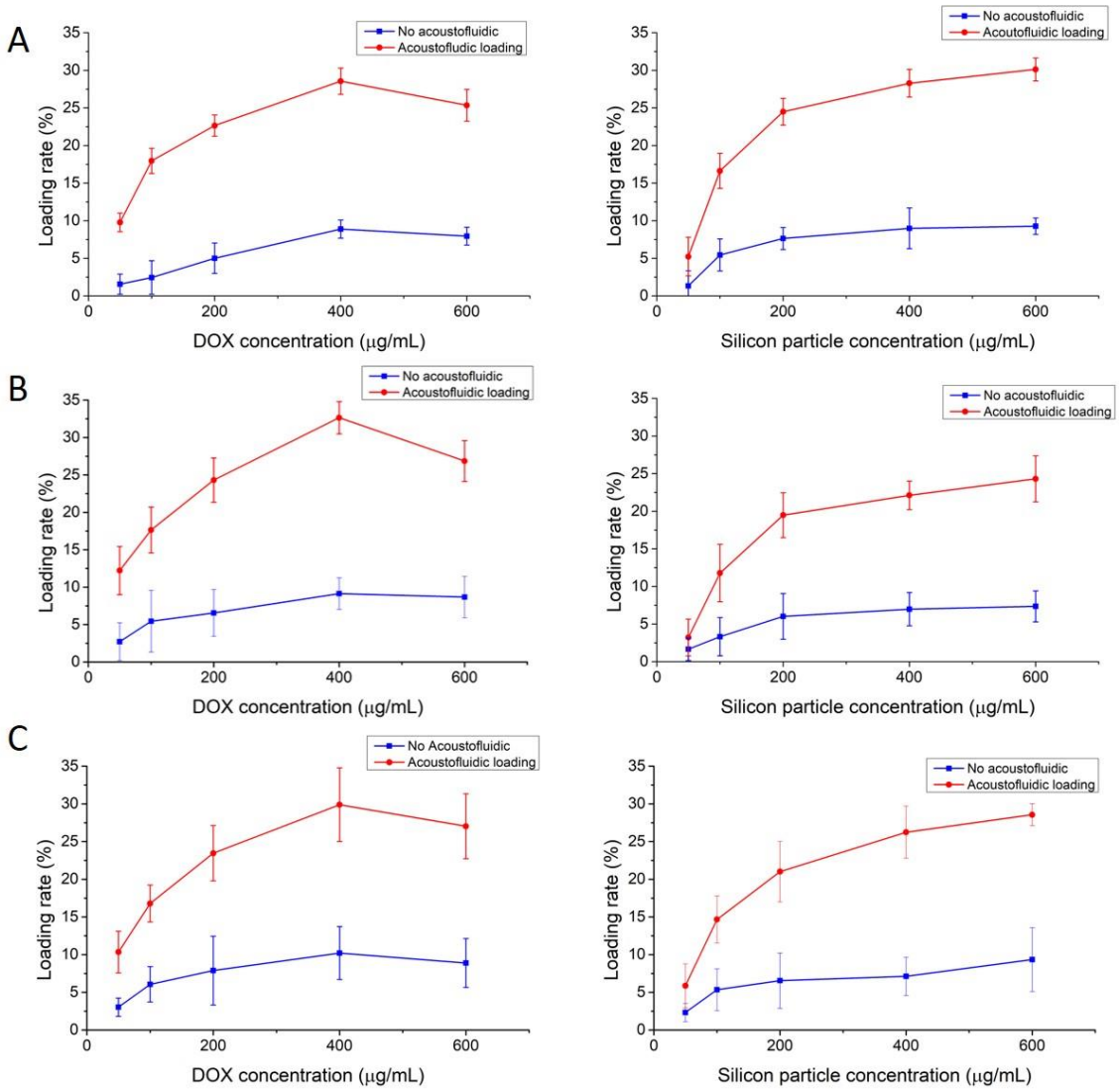

Figure 6-4: Acoustic droplet rotation enhances DOX loading rate to porous silicon nanoparticles. (A) 50 nm spheric silicon nanoparticle demonstrated higher DOX loading rates with different DOX and silicon nanoparticle concentration after acoustic droplet rotation. (B) 100 nm spheric silicon nanoparticle DOX loading rate is enhanced by droplet rotation. (C) 200 nm rod silicon nanoparticle DOX loading rate is enhanced by droplet rotation.

6.4.4 Acoustic rotation derived vesicle encapsulation

Successful vesicle encapsulation can make nanoparticles covered by the vesicle membrane that contain vesicle specific biomarkers. Vesicles that derive intercellular communication contains biomarkers for enhancing target cell intake rate. Since the acoustic droplet rotation device derived nanoparticle encapsulation is a physical process achieved by concentration and membrane disruption, it brings a potential advantage that the device can drive capsulation for nanoparticles with large range of sizes and shapes. To validate whether the device can ignore nanoparticles' shapes, we used 50 and 100 nm spherical, and 200 nm stick silicon nanoparticles for exosome encapsulation. To avoid concentration influence on encapsulation rate, three nanoparticles were kept a same concentration of 400 μg/mL and exosome concentration was 1×10^7 particles/mL during the encapsulation process. Particle size distributions of simply mixing groups and acoustic droplet device processed groups were evaluated by nanoparticle tracking analysis (NTA). As Figure 6-5 shows, all mixing groups demonstrate the peaks of silicon nanoparticle are covered by peaks from exosomes, which contains multiple peaks distributed in a larger size range. However, the acoustic droplet rotation groups demonstrate clear silicon nanoparticles peaks, which are at 50, 100, and 120 nm, respectively. The exosomes' size peaks are lower than mixing groups, indicate acoustic droplet rotation attach exosomes to the silicon nanoparticles' surface. Since the NTA records scattering laser and silicon

nanoparticles' signals are stronger than exosomes, the encapsuled nanoparticles are recognized as silicon nanoparticles' peaks by the NTA.

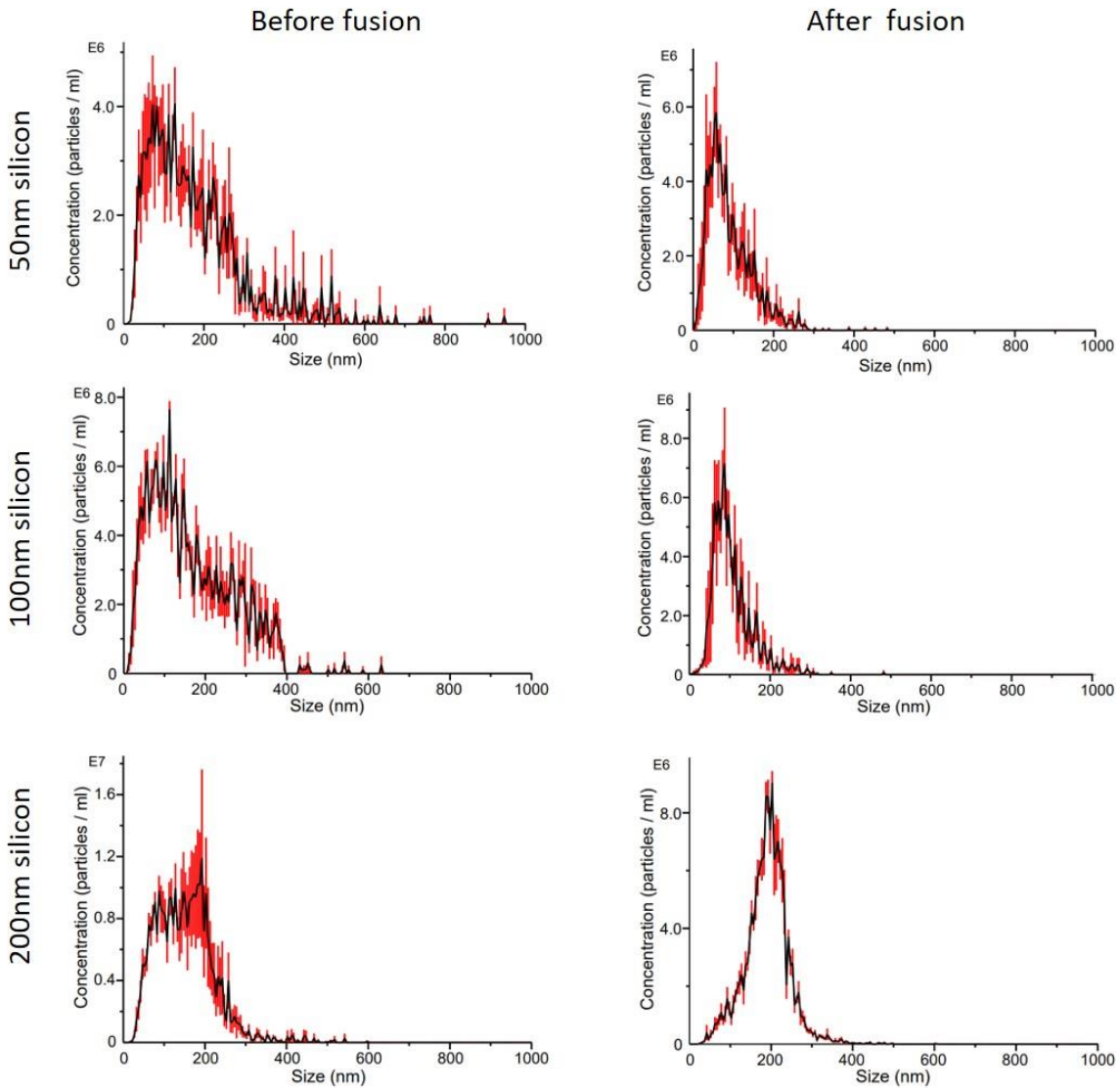

Figure 6-5: Exosomes encapsulate different sizes and shapes silicon nanoparticles after acoustic droplet rotation. Size distribution of exosomes and silicon nanoparticles mixtures, after droplet rotation procedure compared multiple peaks before fusion new peaks are narrower and closer to silicon nanoparticles' sizes, indicate exosomes attached to nanoparticles.

To evaluate the morphology of the nanoparticle after acoustofluidic droplet rotation derived vesicle encapsulation and verify the existence of exosome protein biomarkers on the nanoparticles, we use transmission electric microscope imaging and immuno-blot for evaluating the silicon nanoparticles collected from the acoustofluidic platform after droplet rotation process. Transmission electric microscope imaging was further applied for morphology analysis of the encapsulated nanoparticles. Compared with control groups, nanoparticles processed by acoustic droplet rotation demonstrated a fuzzy layer on the surface. This structure indicates exosome membrane covering the silicon nanoparticles. Since exosomes' membrane proteins derive the endocytosis and can decide target cells, immunoblot technology was recruited for evaluating the existence of exosomal proteins on nanoparticles. To avoid contaminations from free exosomes that are failed for encapsulation, acoustic droplet rotation processed products were separated by 10,000 g centrifugation. The western blot results show rotation processed nanoparticles containing higher level of exosome biomarker CD9 and CD63 than nanoparticles only mixed with exosomes. These results indicate the acoustic droplet rotation can encapsulate silicon particle with exosomes and keep exosome specific proteins. Furthermore, since 50, 100, and 200 nm silicon nanoparticles all demonstrate membrane structure on the surfaces and contain exosome specific biomarkers in the immuno-blot results, the acoustofluidic droplet rotation derived encapsulation is not influenced by nanoparticles' sizes and shapes.

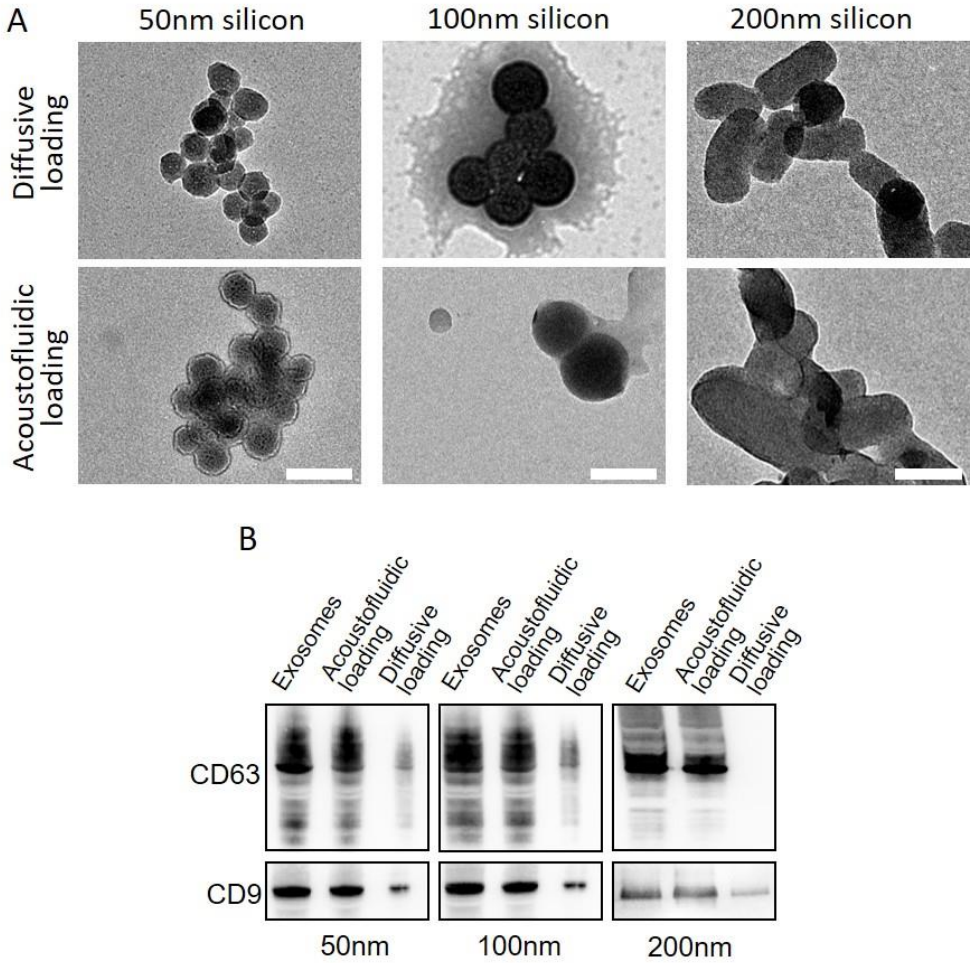

Figure 6-6: Exosome encapsulation morphological and protein validation. (A) TEM images show before rotation the boundary among silicon nanoparticles is clear, while after rotation the boundary is blurred and shows an extra layer, indicate exosome attachment. (B) Western-blot result shows compared with silicon nanoparticles that only mixed with exosomes, droplet rotation treated nanoparticles shows higher level of exosomal surface biomarkers, indicates acoustic treatment cause silicon nanoparticles containing exosome membrane components.

6.4.5 Acoustofluidic exosome encapsulation enhances endocytosis

Exosome membrane coating has been proved promoting cell intake of nanoparticles. To validate whether acoustic droplet rotation derived encapsulation can

derive similar effect, green fluorescence tagged silicon nanoparticles and red fluorescence tagged exosomes were processed by the acoustic device and used for culturing HeLa cells. Compared with mixed nanoparticles and exosomes, green, fluorescence in significantly stronger in acoustic encapsulated samples (Figure 6-7). Furthermore, in encapsulated samples exosomes' fluorescence and nanoparticles' fluorescence show high spatial overlap, indicate exosomes and nanoparticle are intake as an integrated particle. Acoustic derived encapsulation promotes endocytosis of silicon nanoparticles with different size and shapes (Figure 6-8 and Figure 6-9), indicates the device can enhance endocytosis of multiple nanoparticles.

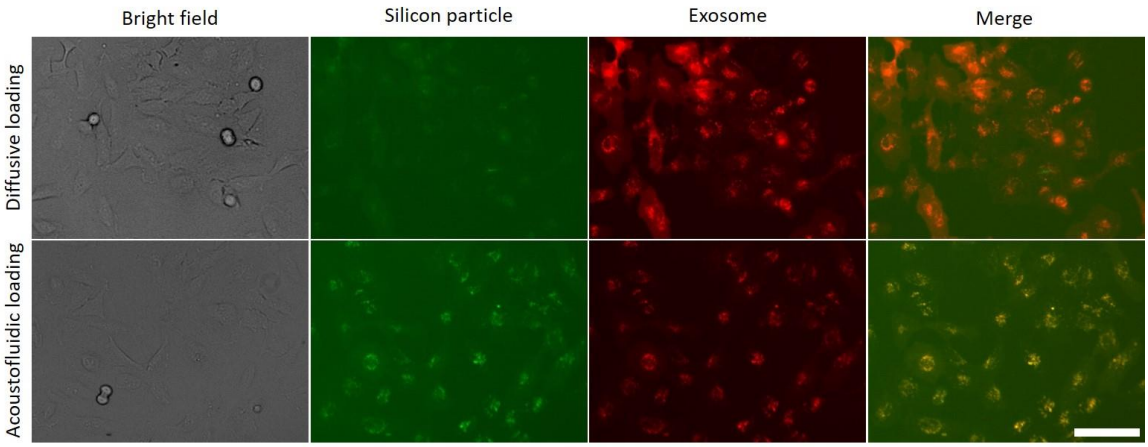

Figure 6-7: HeLa endocytosis of 50 nm silicon rod nanoparticles is enhanced after acoustic droplet rotation induced exosome encapsulation. Compared with nanoparticles and exosomes before fusion, which show lower strength of green fluorescence of silicon nanoparticles, the after fusion group shows higher strength of silicon particles' fluorescence that overlapped with exosomes' red fluorescence, indicates silicon nanoparticles are intake with exosomes enhanced.

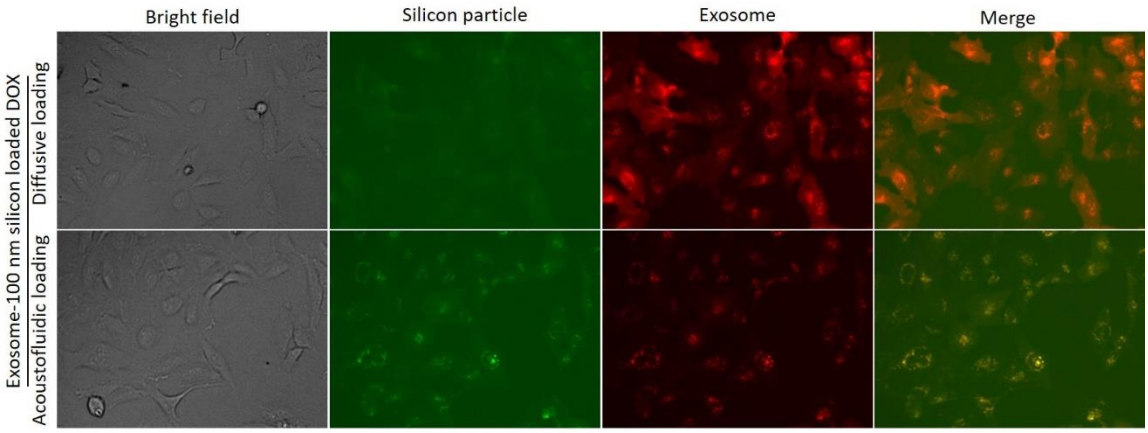

Figure 6-8: HeLa endocytosis of 100 nm silicon rod nanoparticles is enhanced after acoustic droplet rotation induced exosome encapsulation. Compared with nanoparticles and exosomes before fusion, which show lower strength of green fluorescence of silicon nanoparticles, the after fusion group shows higher strength of silicon particles' fluorescence that overlapped with exosomes' red fluorescence, indicates silicon nanoparticles are intake with exosomes enhanced.

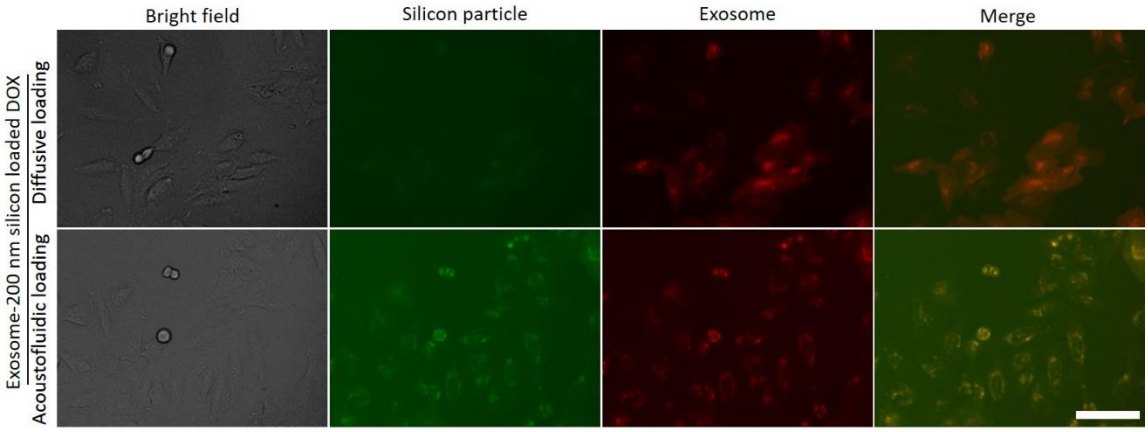

Figure 6-9: HeLa endocytosis of 200 nm silicon rod nanoparticles is enhanced after acoustic droplet rotation induced exosome encapsulation. Compared with nanoparticles and exosomes before fusion, which show lower strength of green fluorescence of silicon nanoparticles, the after fusion group shows higher strength of silicon particles' fluorescence that overlapped with exosomes' red fluorescence, indicates silicon nanoparticles are intake with exosomes enhanced.

6.4.6 Drug intake improvement and proliferation inhibition achieved by acoustofluidic droplet rotation derived drug loading and vesicle encapsulation

After evaluating the acoustofluidic droplet rotation device' performance separately on drug loading and vesicle encapsulation aspects, we derived validation on whether the device could achieve these two functions in the same time and whether the encapsulation and drug loading can improve the drug intake rate of cells. To evaluate the technology's potential in treatment, DOX, exosome, and 50, 100, 200 nm porous silicon nanoparticles were processed by the acoustic droplet rotation and the products were used for culture HeLa and MCF-7 tumor cells. The survival rates of cells, which were evaluated by MTT test, were used for treatment efficiency analysis. The control groups were treated with free DOX, and the final DOX concentration in culture medium is 2.5 μg/mL for both free DOX and acoustic loaded DOX. During 24 hours culture, fluorescent microscopy images demonstrate loaded DOX in 200 nm porous silicon nanoparticles groups shows stronger intracellular DOX fluorescence and lower cell density (Figure 6-10A), and all DOX loaded groups show lower viability than free DOX groups in both HeLa and MCF-7 cells (Figure 6-10C and D). DOX loaded in 50 and 100 nm spheric nanoparticles also shows similar DOX intake enhancement and cell viability decreasing (Figure S3 and S4), indicate exosome encapsulation and silicon nanoparticle promote intake of DOX and inhibit cell proliferation.

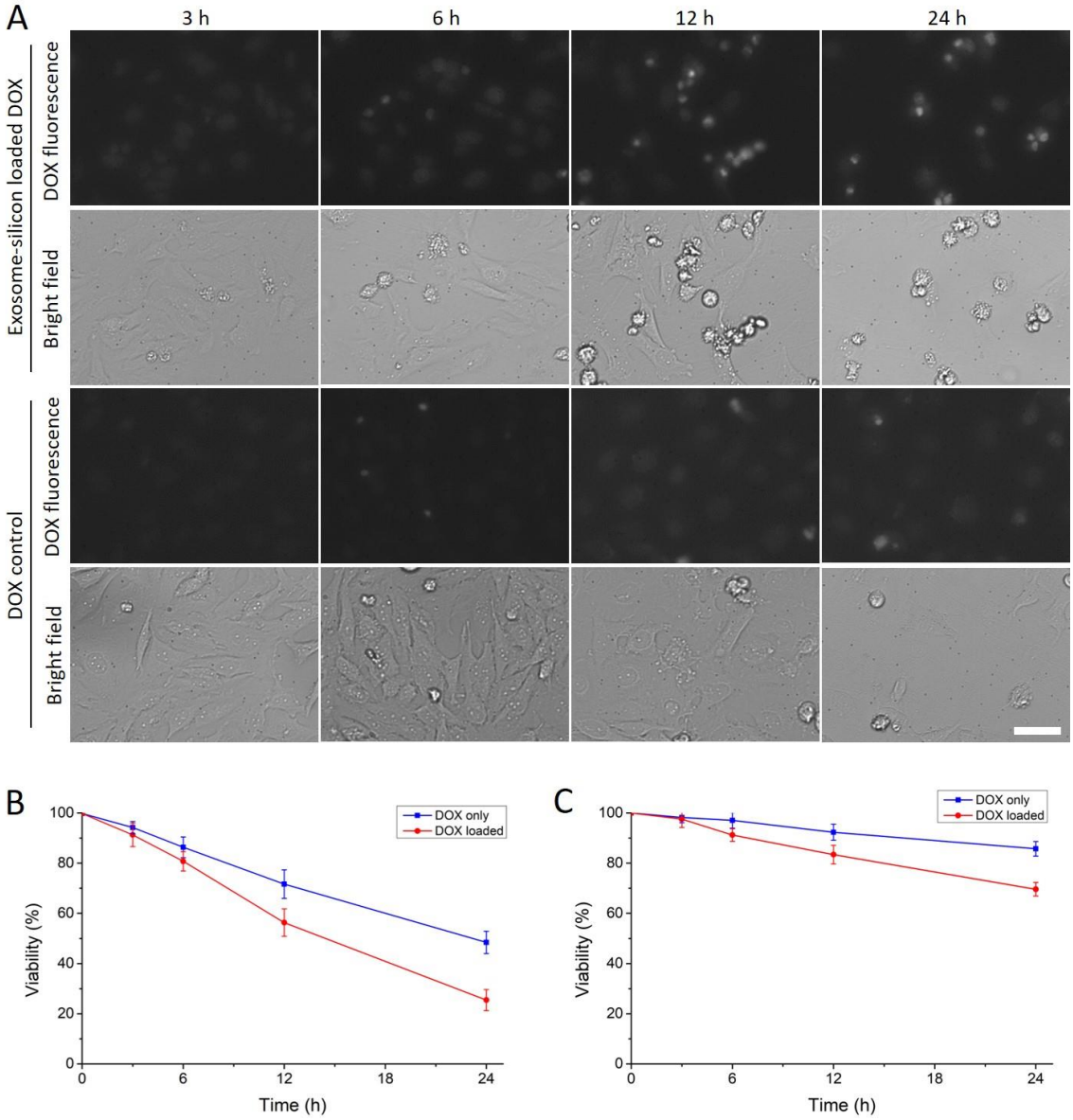

Figure 6-10: Acoustic droplet rotation derived exosome encapsulation and drug loading enhance DOX intake rate and inhibit cell proliferation. (A) HeLa cell intake microscopy, DOX loaded in 50 nm silicon nanoparticles encapsulated by exosomes demonstrate higher intracellular DOX fluorescence than free DOX. (B) MTT viability test indicate loaded and encapsulated DOX cause larger decreasing of viability for HeLa. C) MTT viability test indicate loaded and encapsulated DOX cause larger decreasing of viability for MCF-7.

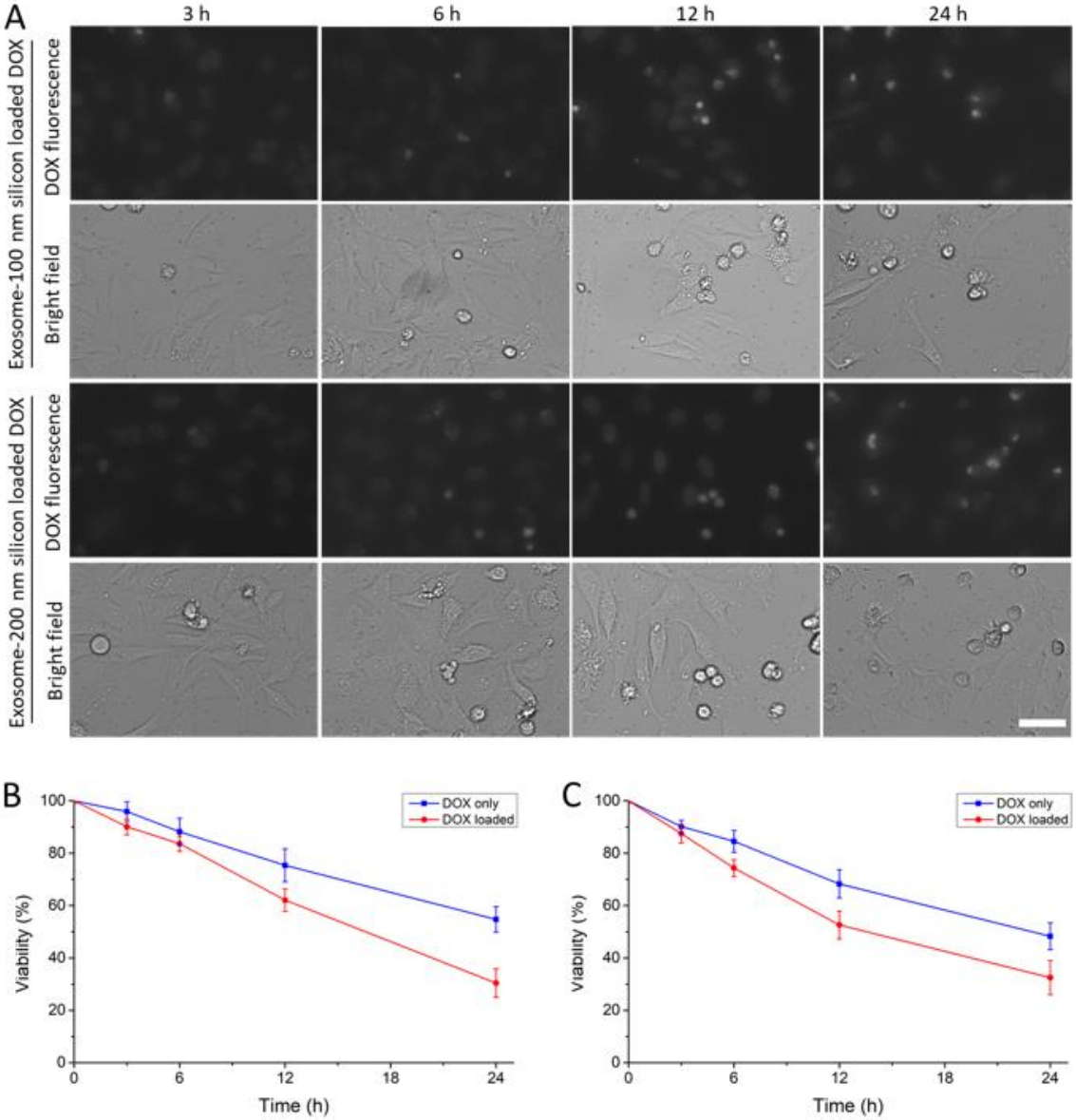

Figure 6-11: Acoustic droplet rotation derived exosome encapsulation and drug loading enhance DOX intake rate and inhibit cell proliferation. (A) HeLa cell intake microscopy, DOX loaded in 100 nm spheric and 200 nm rod silicon nanoparticles encapsulated by exosomes demonstrate higher intracellular DOX fluorescence. (B) MTT viability test indicate 100 nm silicon nanoparticles encapsulated by exosomes induce loaded DOX inhibit HeLa cells' viability. C) MTT viability test indicate 200 nm silicon nanoparticles encapsulated by exosomes induce loaded DOX inhibit HeLa cells' viability.

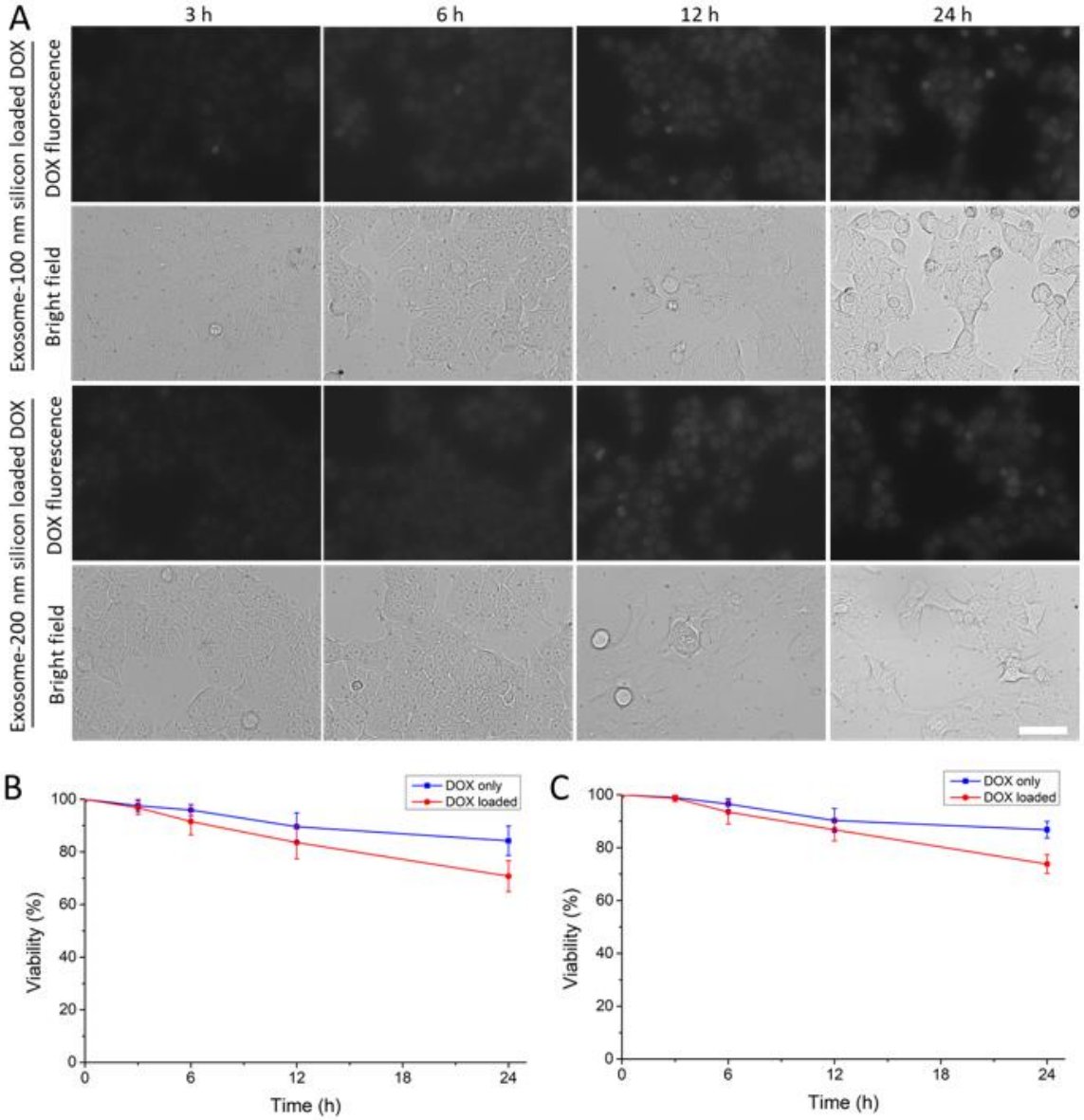

Figure 6-12: Acoustic droplet rotation derived exosome encapsulation and drug loading enhance DOX intake rate and inhibit cell proliferation. (A) MCF-7 cell intake microscopy, DOX loaded in 100 nm spheric and 200 nm rod silicon nanoparticles encapsulated by exosomes demonstrate higher intracellular DOX fluorescence. (B) MTT viability test indicate 100 nm silicon nanoparticles encapsulated by exosomes induce loaded DOX inhibit MCF-7 cells' viability. C) MTT viability test indicate 200 nm silicon nanoparticles encapsulated by exosomes induce loaded DOX inhibit MCF-7 cells' viability.

6.4.7 Pathway of acoustofluidic droplet rotation derived drug delivery

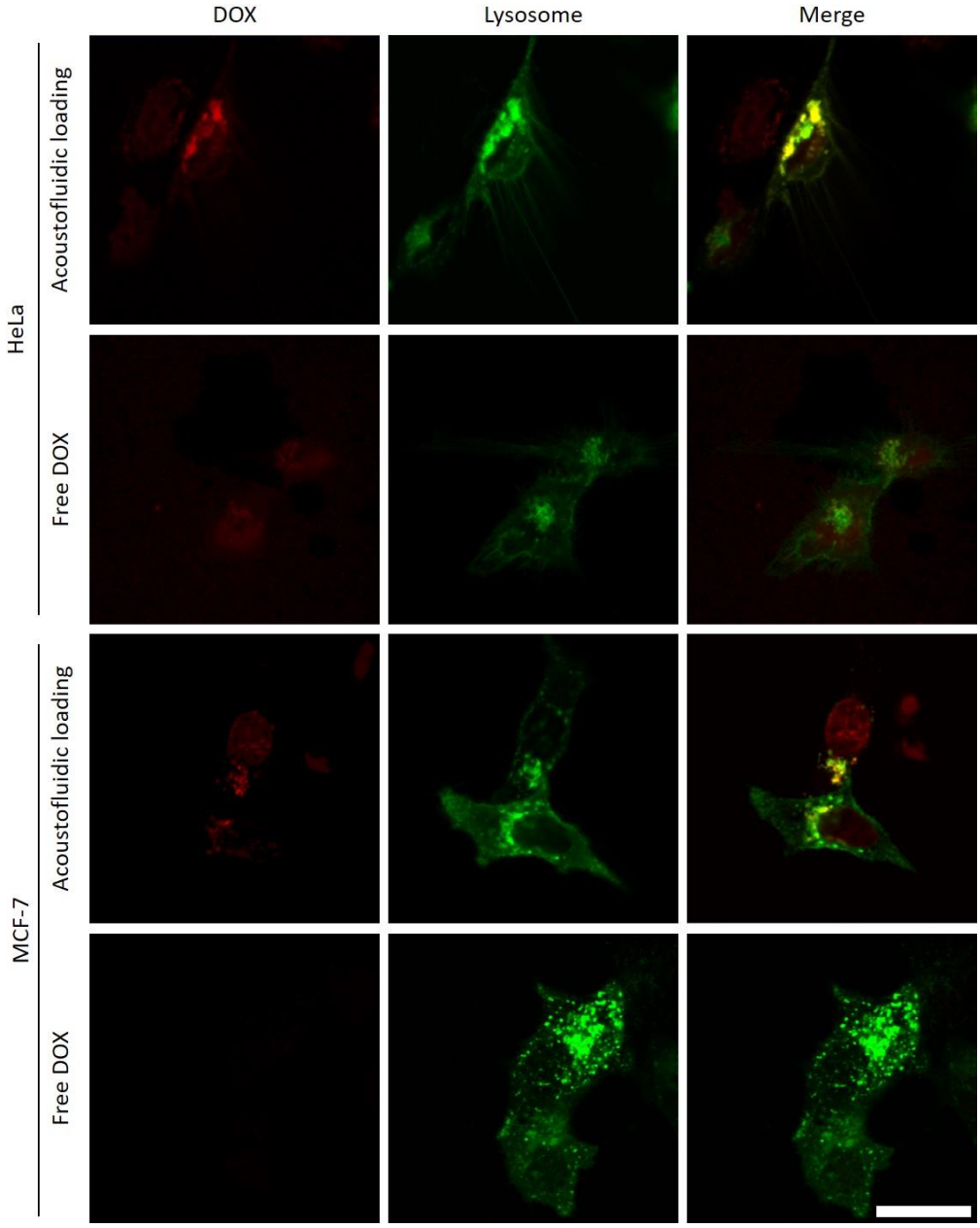

Figure 6-13: DOX loaded in exosome encapsulated silicon nanoparticles through acoustic droplet rotation is intake by endocytosis. Cultured with loaded DOX, both HeLa and MCF cells demonstrated high intracellular red fluorescence of DOX, which demonstrate high overlap with lysosome stained by green fluorescence.

To further investigate the intake mechanism of exosome-silicon-DOX, we derived GFP tagged lysosome tracker prestaining of the cells. Confocal laser scanning microscope images shows for cells cultured with exosome-silicon-DOX, red fluorescence of DOX and green fluorescence of lysosome exist overlaps, while free DOX groups only show DOX fluorescence in nucleic areas (Figure 6-13). These results indicate acoustic droplet rotation device derived drug loading and exosome encapsulation can promote DOX intake by endocytosis and inhibit cancer cell proliferation. The overlap of the fluorescence of DOX and the lysosome indicate for the acoustofluidic droplet rotation treated samples, DOX are intake by endocytosis and exist in the lysosomes, unlike free DOX that exists in nuclei. Since the silicon nanoparticles are intake by the endocytosis pathway, which is the pathway for exosome intake by the cells, it can demonstrate that the exosome encapsulation is the main reason for improving silicon nanoparticle intake rate by cells.

6.5 Conclusion

In summary, by applying SAW derived droplet rotation, we investigate a highly efficient approach that can simultaneously achieve drug loading and exosome encapsulation. The acoustic device generates two effect on the particles in the droplet, which are acoustic radiation force and acoustic derived vortex microstreaming. These effects induce drug molecules, exosomes, and silicon nanoparticles concentrating in the droplet center and actively increase particles' concentration. Since particles are limited in smaller space, higher contacting chance promote drug loading efficiency. Except

concentration derived high loading efficiency, droplet rotation induced microstreaming further induces shear stress that disrupts membrane structure of exosomes and promote exosomes encapsulating silicon particles. The encapsulation successfully coated exosomal specific proteins on the silicon nanoparticles and significantly promote endocytosis rate of the nanoparticle. This method also shows a high drug loading rate and improve the DOX intake rate for cancer cells. Significant improvement of loading rate and encapsulate rate indicate the acoustofluidic technology is promising method for utilization on drug delivery fields.

The acoustic droplet rotation device brings several advantages that can benefit drug deliver study. The concentration and microstreaming shear stress are both physical effects and the whole process do not include any chemical modification, which significantly simplify the synthesis procedure. Compared with conventional physical method including placing and ultrasonication, acoustic droplet rotation method only needs few minutes and significantly increase the loading and encapsulation rate. Furthermore, the acoustic platform also shows tolerance to nanoparticles' morphological properties by enabling drug loading and exosome encapsulation for nanoparticles with different sizes and shapes. These properties bring the acoustic droplet rotation device high flexibility for multiple combination of drugs, nanocarriers, and vesicles. Nanocarriers have been found significantly improving drug deliver efficiency, and exosome encapsulation can enhance endocytosis and provide targeted delivery ability. The

acoustic droplet rotation device provides a simple and one-step method for achieving both nanocarrier loading and exosome encapsulation, and show potential for appliable various of nanocarriers.

7. Conclusions

To provide a summarize of current achievement and future potential of our work on acoustofluidics, in this chapter we will review the efforts made in previous chapters in Section 7.1 and explain the potential applications for the acoustofluidic manipulation and separation technologies in Section 7.2.

7.1 Achievement

In this dissertation, we have brought acoustofluidic separation technology to a status that is closer to application end and evaluated the technology's performance in potential application situations. Since the acoustofluidic technology achieves separation through acoustic radiation force and fluid dragging force, which are physical effects, it is potentially be interfered by environmental condition changes such as fluid density and viscosity fluctuation. However, in real application situation it is impossible for making the acoustofluidic device always working in ideal conditions. Differences on sample collection approaches, storage conditions, and donors' body status can all be variables and influence the physical properties of samples that are processed by the acoustofluidic device. To evaluate the acoustofluidic exosome separation device's performance on different samples, we used conditioned solutions for simulating virous viscosities fluids. Although the fluid properties change induced different performance, the acoustofluidic device keeps separation ability. A more application side validation further firstly demonstrated the acoustofluidic exosome separation technology is eligible for saliva

exosome separation that fit for saliva samples collected by different methods. These results indicate acoustofluidic separation technology having wide applications for different types of samples.

In the dissertation, the acoustofluidic exosome separation technology's expandability, which is the ability for integrating with downstream analytical methods, has also been proved. The ultimate purpose of developing acoustofluidic exosome separation technology is benefiting diagnostic application and providing a point-of-care device that can be easily handled and provide early screening reports for disease risks. However, as a separation technology, for achieving rapid diagnosis it is necessary for integrating the acoustofluidic device with detection units. In the exosome based TBI early screening project, we demonstrated this integration is possible by deriving downstream flow cytometry analysis. Although in the project no direct integration between acoustofluidic separation and flow cytometer detection had been established, since both technologies are microfluidic based system, the integration of the separation and detection part is achievable. Furthermore, the rapid diagnosis potential of the acoustofluidic technology was proved by the successful detection of TBI pathology related exosomes.

During the exploration of application potential of acoustofluidic separation technology, we also improved the device's performance on decreasing the size threshold of the separation. Acoustofluidic separation is achieved by radiation force, which show positive relation with the size increasement of the particle. Previously the lowest

separation threshold of our acoustofluidic device is 200 nm, which is eligible for separating particles larger than 200 nm out from the sample. This threshold is eligible for eliminating interferences from large particle contaminations but the smaller contaminations, including solvable proteins and free nuclei acids, are still in the isolated samples. To increasing the purity of the isolated samples, the acoustofluidic device need to manipulate the target particles, indicate higher frequency for generating higher acoustic radiation force is necessary. However, simply increasing frequency on normal IDT design bring problem of uneven acoustic field, which have low acoustic field strength in the center area and cause gaps in the pressure node lines. To achieve continuous acoustic field for separation, we introduce the dummy finger design. The higher frequency and uniform acoustic field generated by dummy finger IDT decrease the separation threshold to 100 nm, enables the separation of virus particles. The isolated virus keeps infection ability, indicating the dummy finger acoustofluidic technology is biocompatible and is eligible for applications including live virus study.

We further studied the acoustic streaming effect in the acoustofluidic device, which is a different branch with the acoustofluidic separation which is majorly achieved by the acoustic radiation force. In the two projects using bulk acoustic wave generated acoustic streaming and surface acoustic wave generated acoustic streaming, we successful utilized the acoustic streaming shear stress for inducing membrane distribution and used the effects for different applications. The bulk wave derived acoustic streaming derive

shear stress on micrometer level particles. Using this effect, we demonstrated a reagent free approach for high efficient cell lysis that can be integrated with multiple downstream analysis. The acoustic streaming derived by surface acoustic wave generates a coupling effect with acoustic radiation force and enable the concentration of nanometer particles. By using this phenomenon, we designed an acoustofluidic device that can high efficient synchronously derive drug loading and vesicle encapsulation, since the concentration effect increasing contact chance between drug molecules and drug carriers, and acoustic streaming disrupt exosome membrane and enable the membrane coating on the drug carrier nanoparticles. Although the mechanism of acoustic streaming's effect on these applications still needs further study, current results demonstrate by utilizing acoustic streaming, acoustofluidic technology could have more functions that enable its application on a wider field.

7.2 Prospect

Acoustofluidic separation technology has demonstrated great potential for point-of-care application. Since using disease related samples revealed the acoustofluidic exosome separation device can isolated pathology related exosomes, the further work could be focused on the integration of the separation technology and detection technology for constructing a complete system that is eligible for deriving independent separation and detection. Since acoustofluidic technology is a microfluidic form technology, it is naturally feasible for integrating with microfluidic based detection approaches. Methods

including optical detection and electrochemical detection could provide the acoustofluidic technology detection ability and make it evolve to the product phase waiting for real application.

Except the direction of developing the acoustofluidic separation technology into product, the separation threshold of the device could be further improved. The success of using dummy finger design demonstrate the possibility for increasing IDT working frequency. Ability of eliminate protein and nuclei acid contaminations could benefit more sensitive analysis methods including mass spectrum and liquid chromatography. Isolated vesicles or virus with higher purity also benefit the dynamic study of their functions. The acoustofluidic separation technology could still be developed on the technology end for achieving higher throughput and lower isolation threshold.

The direction of utilizing acoustic streaming in acoustofluidic device expands the application fields of the technology. On the cell level, bulk acoustic wave-based membrane lysis enables the development of an all-in-one platform for cell lysis and analysis. The surface acoustic wave-based acoustic streaming technology is more comprehensive. The coupling mechanism between acoustic streaming and acoustic radiation wave need to be studied. On the vesicle membrane disruption aspect, it is also necessary for identifying the membrane encapsulation is caused by vesicle lysis or concentration of the vesicles and nanoparticles. If the acoustic streaming can induce nano size vesicle lysis, it can provide a new method for fast analysis of vesicle cargoes.

References

Abgrall, P. and Gue, A. (2007). Lab-on-chip technologies: making a microfluidic network and coupling it into a complete microsystem—a review. Journal of micromechanics and microengineering, 17(5): R15.

Adams, J. D., Ebbesen, C. L., Barnkob, R., Yang, A. H., Soh, H. T. and Bruus, H. (2012). High-throughput, temperature-controlled microchannel acoustophoresis device made with rapid prototyping. Journal of Micromechanics and Microengineering, 22(7): 075017.

Ahmed, D., Baasch, T., Blondel, N., Läubli, N., Dual, J. and Nelson, B. J. (2017). Neutrophil-inspired propulsion in a combined acoustic and magnetic field. Nature communications, 8(1): 1-8.

Andaloussi, S. E., Mäger, I., Breakefield, X. O. and Wood, M. J. (2013). Extracellular vesicles: biology and emerging therapeutic opportunities. Nature reviews Drug discovery, 12(5): 347-357.

Anglin, E. J., Cheng, L., Freeman, W. R. and Sailor, M. J. (2008). Porous silicon in drug delivery devices and materials. Advanced drug delivery reviews, 60(11): 1266-1277.

Antfolk, M., Kim, S. H., Koizumi, S., Fujii, T. and Laurell, T. (2017). Label-free single-cell separation and imaging of cancer cells using an integrated microfluidic system. Scientific reports, 7(1): 1-12.

Antfolk, M., Magnusson, C., Augustsson, P., Lilja, H. and Laurell, T. (2015). Acoustofluidic, label-free separation and simultaneous concentration of rare tumor cells from white blood cells. Analytical chemistry, 87(18): 9322-9328.

Au, Y., Ahmad, E., Dmytriiev, O., Dvornik, M., Davison, T. and Kruglyak, V. (2012). Resonant microwave-to-spin-wave transducer. Applied Physics Letters, 100(18): 182404.

Augustsson, P., Karlsen, J. T., Su, H.-W., Bruus, H. and Voldman, J. (2016). Iso-acoustic focusing of cells for size-insensitive acousto-mechanical phenotyping. Nature communications, 7(1): 1-9.

Augustsson, P., Magnusson, C., Nordin, M., Lilja, H. and Laurell, T. (2012). Microfluidic, label-free enrichment of prostate cancer cells in blood based on acoustophoresis. Analytical chemistry, 84(18): 7954-7962.

Azmi, A. S., Bao, B. and Sarkar, F. H. (2013). Exosomes in cancer development, metastasis, and drug resistance: a comprehensive review. Cancer and Metastasis Reviews, 32(3-4): 623-642.

Bachman, H., Huang, P.-H., Zhao, S., Yang, S., Zhang, P., Fu, H. and Huang, T. J. (2018). Acoustofluidic devices controlled by cell phones. Lab on a Chip, 18(3): 433-441.

Bahn, J. H., Zhang, Q., Li, F., Chan, T.-M., Lin, X., Kim, Y., Wong, D. T. and Xiao, X. (2015). The landscape of microRNA, Piwi-interacting RNA, and circular RNA in human saliva. Clinical chemistry, 61(1): 221-230.

Bardelli, A. and Pantel, K. (2017). Liquid biopsies, what we do not know (yet). Cancer cell, 31(2): 172-179.

Barnkob, R., Augustsson, P., Laurell, T. and Bruus, H. (2012). Acoustic radiation-and streaming-induced microparticle velocities determined by microparticle image velocimetry in an ultrasound symmetry plane. Physical Review E, 86(5): 056307.

Bhagat, A. A. S., Bow, H., Hou, H. W., Tan, S. J., Han, J. and Lim, C. T. (2010). Microfluidics for cell separation. Medical & biological engineering & computing, 48(10): 999-1014.

Bhagat, A. A. S., Kuntaegowdanahalli, S. S. and Papautsky, I. (2009). Inertial microfluidics for continuous particle filtration and extraction. Microfluidics and nanofluidics, 7(2): 217-226.

Bigler, E. D. and Maxwell, W. L. (2011). Neuroimaging and neuropathology of TBI. NeuroRehabilitation, 28(2): 63-74.

Blanco, E., Shen, H. and Ferrari, M. (2015). Principles of nanoparticle design for overcoming biological barriers to drug delivery. Nature biotechnology, 33(9): 941.

Blyth, B. J., Farhavar, A., Gee, C., Hawthorn, B., He, H., Nayak, A., Stöcklein, V. and Bazarian, J. J. (2009). Validation of serum markers for blood-brain barrier disruption in traumatic brain injury. Journal of neurotrauma, 26(9): 1497-1507.

Bobrie, A., Colombo, M., Raposo, G. and Théry, C. (2011). Exosome secretion: molecular mechanisms and roles in immune responses. Traffic, 12(12): 1659-1668.

Borsetto, D., Cheng, J., Payne, K., Nankivell, P., Batis, N., Rao, K., Bhide, S., Li, F., Kim, Y., Mehanna, H. and Wong, D. (2018). Surveillance of HPV-Positive Head and Neck Squamous Cell Carcinoma with Circulating and Salivary DNA Biomarkers. Crit Rev Oncog, 23(3-4): 235-245 DOI: 10.1615/CritRevOncog.2018027689.

Boyer, P. L., Sarafianos, S. G., Arnold, E. and Hughes, S. H. (2001). Selective excision of AZTMP by drug-resistant human immunodeficiency virus reverse transcriptase. Journal of virology, 75(10): 4832-4842.

Brocklehurst, P., Kujan, O., O'Malley, L. A., Ogden, G., Shepherd, S. and Glenny, A. M. (2013). Screening programmes for the early detection and prevention of oral cancer. Cochrane database of systematic reviews,(11).

Brown, R. B. and Audet, J. (2008). Current techniques for single-cell lysis. Journal of the Royal Society Interface, 5(Suppl 2): S131-S138.

Çetin, B. and Li, D. (2011). Dielectrophoresis in microfluidics technology. Electrophoresis, 32(18): 2410-2427.

Chaplin, D. D. (2010). Overview of the immune response. Journal of Allergy and Clinical Immunology, 125(2): S3-S23.

Chaturvedi, A. K., Engels, E. A., Pfeiffer, R. M., Hernandez, B. Y., Xiao, W., Kim, E., Jiang, B., Goodman, M. T., Sibug-Saber, M. and Cozen, W. (2011). Human papillomavirus and rising oropharyngeal cancer incidence in the United States. Journal of clinical oncology, 29(32): 4294.

Chen, X., Liu, C. C. and Li, H. (2008). Microfluidic chip for blood cell separation and collection based on crossflow filtration. Sensors and Actuators B: Chemical, 130(1): 216-221.

Chen, Y., Wu, M., Ren, L., Liu, J., Whitley, P. H., Wang, L. and Huang, T. J. (2016). High-throughput acoustic separation of platelets from whole blood. Lab on a Chip, 16(18): 3466-3472.

Cheung, T. K. and Poon, L. L. (2007). Biology of influenza a virus. Annals of the New York Academy of Sciences, 1102(1): 1-25.

Choi, S., Song, S., Choi, C. and Park, J.-K. (2007). Continuous blood cell separation by hydrophoretic filtration. Lab on a Chip, 7(11): 1532-1538.

Chokkalingam, V., Tel, J., Wimmers, F., Liu, X., Semenov, S., Thiele, J., Figdor, C. G. and Huck, W. T. (2013). Probing cellular heterogeneity in cytokine-secreting immune cells using droplet-based microfluidics. Lab on a Chip, 13(24): 4740-4744.

Christersson, C. E., Lindh, L. and Arnebrant, T. (2000). Film - forming properties and viscosities of saliva substitutes and human whole saliva. European journal of oral sciences, 108(5): 418-425.

Clarke, M. F. and Hass, A. T. (2006). Cancer stem cells. Reviews in Cell Biology and Molecular Medicine.

Collins, D. J., Ma, Z., Han, J. and Ai, Y. (2017). Continuous micro-vortex-based nanoparticle manipulation via focused surface acoustic waves. Lab on a Chip, 17(1): 91-103.

Collis, J., Manasseh, R., Liovic, P., Tho, P., Ooi, A., Petkovic-Duran, K. and Zhu, Y. (2010). Cavitation microstreaming and stress fields created by microbubbles. Ultrasonics, 50(2): 273-279.

Control, C. f. D. and Prevention (2013). CDC grand rounds: reducing severe traumatic brain injury in the United States. MMWR. Morbidity and mortality weekly report, 62(27): 549.

Dash, P. K., Zhao, J., Hergenroeder, G. and Moore, A. N. (2010). Biomarkers for the diagnosis, prognosis, and evaluation of treatment efficacy for traumatic brain injury. Neurotherapeutics, 7(1): 100-114.

Dawes, C. (2008). Salivary flow patterns and the health of hard and soft oral tissues. The Journal of the American Dental Association, 139: 18S-24S.

Destgeer, G., Ha, B. H., Jung, J. H. and Sung, H. J. (2014). Submicron separation of microspheres via travelling surface acoustic waves. Lab on a Chip, 14(24): 4665-4672.

Destgeer, G., Lee, K. H., Jung, J. H., Alazzam, A. and Sung, H. J. (2013). Continuous separation of particles in a PDMS microfluidic channel via travelling surface acoustic waves (TSAW). Lab on a Chip, 13(21): 4210-4216.

Di Carlo, D., Jeong, K.-H. and Lee, L. P. (2003). Reagentless mechanical cell lysis by nanoscale barbs in microchannels for sample preparation. Lab on a Chip, 3(4): 287-291.

Ding, X., Shi, J., Lin, S.-C. S., Yazdi, S., Kiraly, B. and Huang, T. J. (2012). Tunable patterning of microparticles and cells using standing surface acoustic waves. Lab on a Chip, 12(14): 2491-2497.

Dirix, P., Nuyts, S. and Van den Bogaert, W. (2006). Radiation - induced xerostomia in patients with head and neck cancer: a literature review. Cancer: Interdisciplinary International Journal of the American Cancer Society, 107(11): 2525-2534.

Doinikov, A. A. (1996). Theory of acoustic radiation pressure for actual fluids. Physical Review E, 54(6): 6297.

Dong, Y., Skelley, A. M., Merdek, K. D., Sprott, K. M., Jiang, C., Pierceall, W. E., Lin, J., Stocum, M., Carney, W. P. and Smirnov, D. A. (2013). Microfluidics and circulating tumor cells. The Journal of Molecular Diagnostics, 15(2): 149-157.

Drinkwater, B. W. and Wilcox, P. D. (2006). Ultrasonic arrays for non-destructive evaluation: A review. NDT & e International, 39(7): 525-541.

Epstein, J. B., Thariat, J., Bensadoun, R. J., Barasch, A., Murphy, B. A., Kolnick, L., Popplewell, L. and Maghami, E. (2012). Oral complications of cancer and cancer therapy: from cancer treatment to survivorship. CA: a cancer journal for clinicians, 62(6): 400-422.

Eustice, R. M., Whitcomb, L. L., Singh, H. and Grund, M. (2007). Experimental results in synchronous-clock one-way-travel-time acoustic navigation for autonomous underwater vehicles. Proceedings 2007 IEEE International Conference on Robotics and Automation, IEEE.

Faul, M., Wald, M. M., Xu, L. and Coronado, V. G. (2010). Traumatic brain injury in the United States; emergency department visits, hospitalizations, and deaths, 2002-2006.

Fayad, Z. and Fuster, V. (2001). Clinical imaging of the high-risk or vulnerable atherosclerotic plaque. Circulation research, 89(4): 305-316.

Friend, J. and Yeo, L. Y. (2011). Microscale acoustofluidics: Microfluidics driven via acoustics and ultrasonics. Reviews of Modern Physics, 83(2): 647.

Gallo, A., Tandon, M., Alevizos, I. and Illei, G. G. (2012). The majority of microRNAs detectable in serum and saliva is concentrated in exosomes. PloS one, 7(3): e30679.

Gardner, R. C., Dams-O'Connor, K., Morrissey, M. R. and Manley, G. T. (2018). Geriatric traumatic brain injury: epidemiology, outcomes, knowledge gaps, and future directions. Journal of neurotrauma, 35(7): 889-906.

Gasco, M. and Crook, T. (2003). The p53 network in head and neck cancer. Oral oncology, 39(3): 222-231.

Gavett, B. E., Stern, R. A., Cantu, R. C., Nowinski, C. J. and McKee, A. C. (2010). Mild traumatic brain injury: a risk factor for neurodegeneration. Alzheimer's research & therapy, 2(3): 18.

Giddings, J. C. (1985). A system based on split-flow lateral-transport thin (SPLITT) separation cells for rapid and continuous particle fractionation. Separation Science and Technology, 20(9-10): 749-768.

Goetzl, L., Merabova, N., Darbinian, N., Martirosyan, D., Poletto, E., Fugarolas, K. and Menkiti, O. (2018). Diagnostic potential of neural exosome cargo as biomarkers for acute brain injury. Annals of clinical and translational neurology, 5(1): 4-10.

González-Fernández, C., Sialve, B., Bernet, N. and Steyer, J. (2012). Comparison of ultrasound and thermal pretreatment of Scenedesmus biomass on methane production. Bioresource Technology, 110: 610-616.

Gossett, D. R., Weaver, W. M., Mach, A. J., Hur, S. C., Tse, H. T. K., Lee, W., Amini, H. and Di Carlo, D. (2010). Label-free cell separation and sorting in microfluidic systems. Analytical and bioanalytical chemistry, 397(8): 3249-3267.

Goy, J., Hall, S. F., Feldman - Stewart, D. and Groome, P. A. (2009). Diagnostic delay and disease stage in head and neck cancer: a systematic review. The Laryngoscope, 119(5): 889-898.

Gravesen, P., Branebjerg, J. and Jensen, O. S. (1993). Microfluidics-a review. Journal of micromechanics and microengineering, 3(4): 168.

Grubaugh, N. D., Hanage, W. P. and Rasmussen, A. L. (2020). Making sense of mutation: what D614G means for the COVID-19 pandemic remains unclear. Cell, 182(4): 794-795.

Gu, Y., Chen, C., Mao, Z., Bachman, H., Becker, R., Rufo, J., Wang, Z., Zhang, P., Mai, J. and Yang, S. (2021). Acoustofluidic centrifuge for nanoparticle enrichment and separation. Science Advances, 7(1): eabc0467.

Guan, Y., Zheng, B., He, Y., Liu, X., Zhuang, Z., Cheung, C., Luo, S., Li, P., Zhang, L. and Guan, Y. (2003). Isolation and characterization of viruses related to the SARS coronavirus from animals in southern China. Science, 302(5643): 276-278.

Guo, F., Mao, Z., Chen, Y., Xie, Z., Lata, J. P., Li, P., Ren, L., Liu, J., Yang, J. and Dao, M. (2016). Three-dimensional manipulation of single cells using surface acoustic waves. Proceedings of the National Academy of Sciences, 113(6): 1522-1527.

György, B., Szabó, T. G., Pásztói, M., Pál, Z., Misják, P., Aradi, B., László, V., Pállinger, E., Pap, E. and Kittel, A. (2011). Membrane vesicles, current state-of-the-art: emerging role of extracellular vesicles. Cellular and molecular life sciences, 68(16): 2667-2688.

Hamlett, E. D., Goetzl, E. J., Ledreux, A., Vasilevko, V., Boger, H. A., LaRosa, A., Clark, D., Carroll, S. L., Carmona-Iragui, M. and Fortea, J. (2017). Neuronal exosomes reveal Alzheimer's disease biomarkers in Down syndrome. Alzheimer's & Dementia, 13(5): 541-549.

He, F., Deng, Y. and Li, W. (2020). Coronavirus disease 2019: What we know? Journal of medical virology, 92(7): 719-725.

Herrero, R., Castellsagué, X., Pawlita, M., Lissowska, J., Kee, F., Balaram, P., Rajkumar, T., Sridhar, H., Rose, B. and Pintos, J. (2003). Human papillomavirus and oral cancer: the International Agency for Research on Cancer multicenter study. Journal of the National Cancer Institute, 95(23): 1772-1783.

Hessvik, N. P. and Llorente, A. (2018). Current knowledge on exosome biogenesis and release. Cellular and Molecular Life Sciences, 75(2): 193-208.

Hoshino, A., Costa-Silva, B., Shen, T.-L., Rodrigues, G., Hashimoto, A., Mark, M. T., Molina, H., Kohsaka, S., Di Giannatale, A. and Ceder, S. (2015). Tumour exosome integrins determine organotropic metastasis. Nature, 527(7578): 329.

Hou, H. W., Warkiani, M. E., Khoo, B. L., Li, Z. R., Soo, R. A., Tan, D. S.-W., Lim, W.-T., Han, J., Bhagat, A. A. S. and Lim, C. T. (2013). Isolation and retrieval of circulating tumor cells using centrifugal forces. Scientific reports, 3(1): 1-8.

Hu, S., Arellano, M., Boontheung, P., Wang, J., Zhou, H., Jiang, J., Elashoff, D., Wei, R., Loo, J. A. and Wong, D. T. (2008). Salivary proteomics for oral cancer biomarker discovery. Clinical Cancer Research, 14(19): 6246-6252.

Huang, L. R., Cox, E. C., Austin, R. H. and Sturm, J. C. (2004). Continuous particle separation through deterministic lateral displacement. Science, 304(5673): 987-990.

Huang, P.-H., Chan, C. Y., Li, P., Nama, N., Xie, Y., Wei, C.-H., Chen, Y., Ahmed, D. and Huang, T. J. (2015). A spatiotemporally controllable chemical gradient generator via acoustically oscillating sharp-edge structures. Lab on a Chip, 15(21): 4166-4176.

Huang, P.-H., Nama, N., Mao, Z., Li, P., Rufo, J., Chen, Y., Xie, Y., Wei, C.-H., Wang, L. and Huang, T. J. (2014). A reliable and programmable acoustofluidic pump powered by oscillating sharp-edge structures. Lab on a Chip, 14(22): 4319-4323.

Huang, S.-H., Hung, L.-Y. and Lee, G.-B. (2016). Continuous nucleus extraction by optically-induced cell lysis on a batch-type microfluidic platform. Lab on a Chip, 16(8): 1447-1456.

Hui, Y., Yi, X., Hou, F., Wibowo, D., Zhang, F., Zhao, D., Gao, H. and Zhao, C.-X. (2019). Role of nanoparticle mechanical properties in cancer drug delivery. ACS nano, 13(7): 7410-7424.

Hyder, A. A., Wunderlich, C. A., Puvanachandra, P., Gururaj, G. and Kobusingye, O. C. (2007). The impact of traumatic brain injuries: a global perspective. NeuroRehabilitation, 22(5): 341-353.

Illes, B., Hirschle, P., Barnert, S., Cauda, V., Wuttke, S. and Engelke, H. (2017). Exosome-coated metal–organic framework nanoparticles: an efficient drug delivery platform. Chemistry of Materials, 29(19): 8042-8046.

Jeelani, P. G., Mulay, P., Venkat, R. and Ramalingam, C. (2020). Multifaceted application of silica nanoparticles. A review. Silicon, 12(6): 1337-1354.

Jensen, K. F. (2001). Microreaction engineering—is small better? Chemical Engineering Science, 56(2): 293-303.

Jones, W. and Whitelaw, J. (1982). Calculation methods for reacting turbulent flows: a review. Combustion and flame, 48: 1-26.

Jung, W., Han, J., Choi, J.-W. and Ahn, C. H. (2015). Point-of-care testing (POCT) diagnostic systems using microfluidic lab-on-a-chip technologies. Microelectronic Engineering, 132: 46-57.

Kahlert, C. and Kalluri, R. (2013). Exosomes in tumor microenvironment influence cancer progression and metastasis. Journal of molecular medicine, 91(4): 431-437.

Kang, P., Tian, Z., Yang, S., Yu, W., Zhu, H., Bachman, H., Zhao, S., Zhang, P., Wang, Z. and Zhong, R. (2020). Acoustic tweezers based on circular, slanted-finger interdigital transducers for dynamic manipulation of micro-objects. Lab on a Chip.

Kaplan, A. (2012). Complications of apheresis. Seminars in dialysis, Wiley Online Library.

Kaput, J. and Rodriguez, R. L. (2004). Nutritional genomics: the next frontier in the postgenomic era. Physiological genomics, 16(2): 166-177.

Kelly, R. T., Li, Y. and Woolley, A. T. (2006). Phase-changing sacrificial materials for interfacing microfluidics with ion-permeable membranes to create on-chip preconcentrators and electric field gradient focusing microchips. Analytical chemistry, 78(8): 2565-2570.

Késmárky, G., Kenyeres, P., Rábai, M. and Tóth, K. (2008). Plasma viscosity: a forgotten variable. Clinical hemorheology and microcirculation, 39(1–4): 243-246.

Kim, J., Jang, S. H., Jia, G., Zoval, J. V., Da Silva, N. A. and Madou, M. J. (2004). Cell lysis on a microfluidic CD (compact disc). Lab on a Chip, 4(5): 516-522.

Kim, J., Johnson, M., Hill, P. and Gale, B. K. (2009). Microfluidic sample preparation: cell lysis and nucleic acid purification. Integrative Biology, 1(10): 574-586.

Kim, J. J. and Gean, A. D. (2011). Imaging for the diagnosis and management of traumatic brain injury. Neurotherapeutics, 8(1): 39-53.

Kim, K. S. and Park, J.-K. (2005). Magnetic force-based multiplexed immunoassay using superparamagnetic nanoparticles in microfluidic channel. Lab on a Chip, 5(6): 657-664.

Kim, S. C., Clark, I. C., Shahi, P. and Abate, A. R. (2018). Single-cell RT-PCR in microfluidic droplets with integrated chemical lysis. Analytical chemistry, 90(2): 1273-1279.

Kim, U., Qian, J., Kenrick, S. A., Daugherty, P. S. and Soh, H. T. (2008). Multitarget dielectrophoresis activated cell sorter. Analytical chemistry, 80(22): 8656-8661.

Klein, A. M., Mazutis, L., Akartuna, I., Tallapragada, N., Veres, A., Li, V., Peshkin, L., Weitz, D. A. and Kirschner, M. W. (2015). Droplet barcoding for single-cell transcriptomics applied to embryonic stem cells. Cell, 161(5): 1187-1201.

Kooijmans, S. A., Vader, P., van Dommelen, S. M., van Solinge, W. W. and Schiffelers, R. M. (2012). Exosome mimetics: a novel class of drug delivery systems. International journal of nanomedicine, 7: 1525.

Lam, B., Fang, Z., Sargent, E. H. and Kelley, S. O. (2011). Polymerase chain reaction-free, sample-to-answer bacterial detection in 30 minutes with integrated cell lysis. Analytical chemistry, 84(1): 21-25.

Landahl, M. T., Mollo - Christensen, E. and Korman, M. S. (1989). Turbulence and random processes in fluid mechanics, Acoustical Society of America.

Lange, B., Chang, C.-Y., Suma, E., Newman, B., Rizzo, A. S. and Bolas, M. (2011). Development and evaluation of low cost game-based balance rehabilitation tool using the Microsoft Kinect sensor. Engineering in medicine and biology society, EMBC, 2011 annual international conference of the IEEE, IEEE.

Laskowitz, D. T., Song, P., Wang, H., Mace, B., Sullivan, P. M., Vitek, M. P. and Dawson, H. N. (2010). Traumatic brain injury exacerbates neurodegenerative pathology: improvement with an apolipoprotein E-based therapeutic. Journal of neurotrauma, 27(11): 1983-1995.

Laurell, T., Petersson, F. and Nilsson, A. (2007). Chip integrated strategies for acoustic separation and manipulation of cells and particles. Chemical Society Reviews, 36(3): 492-506.

Lee, K., Shao, H., Weissleder, R. and Lee, H. (2015). Acoustic purification of extracellular microvesicles. ACS nano, 9(3): 2321-2327.

Lenshof, A., Magnusson, C. and Laurell, T. (2012). Acoustofluidics 8: Applications of acoustophoresis in continuous flow microsystems. Lab on a Chip, 12(7): 1210-1223.

Li, P., Mao, Z., Peng, Z., Zhou, L., Chen, Y., Huang, P.-H., Truica, C. I., Drabick, J. J., El-Deiry, W. S. and Dao, M. (2015). Acoustic separation of circulating tumor cells. Proceedings of the National Academy of Sciences, 112(16): 4970-4975.

Li, S., Ma, F., Bachman, H., Cameron, C. E., Zeng, X. and Huang, T. J. (2016). Acoustofluidic bacteria separation. Journal of Micromechanics and Microengineering, 27(1): 015031.

Lingen, M. W., Kalmar, J. R., Karrison, T. and Speight, P. M. (2008). Critical evaluation of diagnostic aids for the detection of oral cancer. Oral oncology, 44(1): 10-22.

Loscalzo, J., Kohane, I. and Barabasi, A. L. (2007). Human disease classification in the postgenomic era: a complex systems approach to human pathobiology. Molecular systems biology, 3(1): 124.

Löwe, H. and Ehrfeld, W. (1999). State-of-the-art in microreaction technology: concepts, manufacturing and applications. Electrochimica Acta, 44(21-22): 3679-3689.

Lu, H., Schmidt, M. A. and Jensen, K. F. (2005). A microfluidic electroporation device for cell lysis. Lab on a Chip, 5(1): 23-29.

MacDonald, M. P., Spalding, G. C. and Dholakia, K. (2003). Microfluidic sorting in an optical lattice. Nature, 426(6965): 421-424.

Mach, A. J. and Di Carlo, D. (2010). Continuous scalable blood filtration device using inertial microfluidics. Biotechnology and bioengineering, 107(2): 302-311.

Mao, Z., Li, P., Wu, M., Bachman, H., Mesyngier, N., Guo, X., Liu, S., Costanzo, F. and Huang, T. J. (2017). Enriching nanoparticles via acoustofluidics. Acs Nano, 11(1): 603-612.

Masudo, T. and Okada, T. (2006). Particle separation with ultrasound radiation force. Current Analytical Chemistry, 2(2): 213-227.

McGurk, M. and Scott, S. (2010). The reality of identifying early oral cancer in the general dental practice. British dental journal, 208(8): 347.

Meacle, F., Lander, R., Ayazi Shamlou, P. and Titchener - Hooker, N. (2004). Impact of engineering flow conditions on plasmid DNA yield and purity in chemical cell lysis operations. Biotechnology and bioengineering, 87(3): 293-302.

Mernier, G., Piacentini, N., Braschler, T., Demierre, N. and Renaud, P. (2010). Continuous-flow electrical lysis device with integrated control by dielectrophoretic cell sorting. Lab on a Chip, 10(16): 2077-2082.

Michael, A., Bajracharya, S. D., Yuen, P. S., Zhou, H., Star, R. A., Illei, G. G. and Alevizos, I. (2010). Exosomes from human saliva as a source of microRNA biomarkers. Oral diseases, 16(1): 34-38.

Milane, L., Singh, A., Mattheolabakis, G., Suresh, M. and Amiji, M. M. (2015). Exosome mediated communication within the tumor microenvironment. Journal of Controlled Release, 219: 278-294.

Mun, B. P., Jung, S. M., Yoon, S. Y., Kim, S. H., Lee, J. H. and Yang, S. (2010). Continuous cell cross over and lysis in a microfluidic device. Microfluidics and Nanofluidics, 8(5): 695-701.

Nam, J., Lim, H., Kim, D. and Shin, S. (2011). Separation of platelets from whole blood using standing surface acoustic waves in a microchannel. Lab on a Chip, 11(19): 3361-3364.

Nama, N., Huang, P.-H., Huang, T. J. and Costanzo, F. (2014). Investigation of acoustic streaming patterns around oscillating sharp edges. Lab on a Chip, 14(15): 2824-2836.

Nama, N., Huang, P.-H., Huang, T. J. and Costanzo, F. (2016). Investigation of micromixing by acoustically oscillated sharp-edges. Biomicrofluidics, 10(2): 024124.

Narayanan, N., Saldanha, A. and Gale, B. K. (2006). A microfabricated electrical SPLITT system. Lab on a Chip, 6(1): 105-114.

Neville, B. W. and Day, T. A. (2002). Oral cancer and precancerous lesions. CA: a cancer journal for clinicians, 52(4): 195-215.

Niemz, A., Ferguson, T. M. and Boyle, D. S. (2011). Point-of-care nucleic acid testing for infectious diseases. Trends in biotechnology, 29(5): 240-250.

Nishikawa, S.-I., Jakt, L. M. and Era, T. (2007). Embryonic stem-cell culture as a tool for developmental cell biology. Nature reviews Molecular cell biology, 8(6): 502-507.

Nyborg, W. L. (1958). Acoustic streaming near a boundary. The Journal of the Acoustical Society of America, 30(4): 329-339.

Olson, D., Grissom, J. L. and Dombrowski, K. (2011). The evidence base for nursing care and monitoring of patients during therapeutic temperature management. Therapeutic hypothermia and temperature management, 1(4): 209-217.

Ortiz, J. R., Zhou, H., Shay, D. K., Neuzil, K. M., Fowlkes, A. L. and Goss, C. H. (2011). Monitoring influenza activity in the United States: a comparison of traditional surveillance systems with Google Flu Trends. PloS one, 6(4): e18687.

Ozcelik, A., Rufo, J., Guo, F., Gu, Y., Li, P., Lata, J. and Huang, T. J. (2018). Acoustic tweezers for the life sciences. Nature methods, 15(12): 1021-1028.

Paterlini-Brechot, P. and Benali, N. L. (2007). Circulating tumor cells (CTC) detection: clinical impact and future directions. Cancer letters, 253(2): 180-204.

Peltonen, L. and McKusick, V. A. (2001). Dissecting human disease in the postgenomic era. Science, 291(5507): 1224-1229.

Peng, C., Shen, G., Zhang, Y., Li, Y. and Tan, K. (2007). Beepbeep: a high accuracy acoustic ranging system using cots mobile devices. Proceedings of the 5th international conference on Embedded networked sensor systems.

Petersson, F., Nilsson, A., Holm, C., Jönsson, H. and Laurell, T. (2005). Continuous separation of lipid particles from erythrocytes by means of laminar flow and acoustic standing wave forces. Lab on a Chip, 5(1): 20-22.

Petersson, F., Nilsson, A., Jönsson, H. and Laurell, T. (2005). Carrier medium exchange through ultrasonic particle switching in microfluidic channels. Analytical chemistry, 77(5): 1216-1221.

Pickett, J. A. and Edwardson, J. M. (2006). Compound exocytosis: mechanisms and functional significance. Traffic, 7(2): 109-116.

Pierce, A. D. (2019). Acoustics: an introduction to its physical principles and applications, Springer.

Popper, A. N., Salmon, M. and Horch, K. W. (2001). Acoustic detection and communication by decapod crustaceans. Journal of Comparative Physiology A, 187(2): 83-89.

Privorotskaya, N., Liu, Y.-S., Lee, J., Zeng, H., Carlisle, J. A., Radadia, A., Millet, L., Bashir, R. and King, W. P. (2010). Rapid thermal lysis of cells using silicon–diamond microcantilever heaters. Lab on a Chip, 10(9): 1135-1141.

Ramachandraiah, H., Svahn, H. A. and Russom, A. (2017). Inertial microfluidics combined with selective cell lysis for high throughput separation of nucleated cells from whole blood. RSC advances, 7(47): 29505-29514.

Rizvi, S. A. and Saleh, A. M. (2018). Applications of nanoparticle systems in drug delivery technology. Saudi Pharmaceutical Journal, 26(1): 64-70.

Robbins, P. D. and Morelli, A. E. (2014). Regulation of immune responses by extracellular vesicles. Nature Reviews Immunology, 14(3): 195-208.

Rusling, J. F., Kumar, C. V., Gutkind, J. S. and Patel, V. (2010). Measurement of biomarker proteins for point-of-care early detection and monitoring of cancer. Analyst, 135(10): 2496-2511.

Safari, A. and Akdogan, E. K. (2008). Piezoelectric and acoustic materials for transducer applications, Springer Science & Business Media.

Sajeesh, P. and Sen, A. K. (2014). Particle separation and sorting in microfluidic devices: a review. Microfluidics and nanofluidics, 17(1): 1-52.

Salonen, A., Nikkilä, J., Jalanka-Tuovinen, J., Immonen, O., Rajilić-Stojanović, M., Kekkonen, R. A., Palva, A. and de Vos, W. M. (2010). Comparative analysis of fecal DNA extraction methods with phylogenetic microarray: effective recovery of bacterial and archaeal DNA using mechanical cell lysis. Journal of microbiological methods, 81(2): 127-134.

Salonen, J., Kaukonen, A. M., Hirvonen, J. and Lehto, V.-P. (2008). Mesoporous silicon in drug delivery applications. Journal of pharmaceutical sciences, 97(2): 632-653.

Sapatnekar, S., Sharma, G., Downes, K. A., Wiersma, S., McGrath, C. and Yomtovían, R. (2005). Acute hemolytic transfusion reaction in a pediatric patient following transfusion of apheresis platelets. Journal of Clinical Apheresis: The Official Journal of the American Society for Apheresis, 20(4): 225-229.

Sedghizadeh, P. P., Billington, W. D., Paxton, D., Ebeed, R., Mahabady, S., Clark, G. T. and Enciso, R. (2016). Is p16-positive oropharyngeal squamous cell carcinoma associated with favorable prognosis? A systematic review and meta-analysis. Oral oncology, 54: 15-27.

Sethu, P., Sin, A. and Toner, M. (2006). Microfluidic diffusive filter for apheresis (leukapheresis). Lab on a Chip, 6(1): 83-89.

Sharma, S., Zapatero-Rodríguez, J., Estrela, P. and O'Kennedy, R. (2015). Point-of-care diagnostics in low resource settings: present status and future role of microfluidics. Biosensors, 5(3): 577-601.

Shi, J., Ahmed, D., Mao, X., Lin, S.-C. S., Lawit, A. and Huang, T. J. (2009). Acoustic tweezers: patterning cells and microparticles using standing surface acoustic waves (SSAW). Lab on a Chip, 9(20): 2890-2895.

Shields IV, C. W., Reyes, C. D. and López, G. P. (2015). Microfluidic cell sorting: a review of the advances in the separation of cells from debulking to rare cell isolation. Lab on a Chip, 15(5): 1230-1249.

Singh, R. and Lillard Jr, J. W. (2009). Nanoparticle-based targeted drug delivery. Experimental and molecular pathology, 86(3): 215-223.

Smith, S. M., Baskin, G. B. and Marx, P. A. (2000). Estrogen protects against vaginal transmission of simian immunodeficiency virus. The Journal of infectious diseases, 182(3): 708-715.

Smyth, T., Kullberg, M., Malik, N., Smith-Jones, P., Graner, M. W. and Anchordoquy, T. J. (2015). Biodistribution and delivery efficiency of unmodified tumor-derived exosomes. Journal of Controlled Release, 199: 145-155.

So, H., Lee, K., Seo, Y. H., Murthy, N. and Pisano, A. P. (2014). Hierarchical silicon nanospikes membrane for rapid and high-throughput mechanical cell lysis. ACS applied materials & interfaces, 6(10): 6993-6997.

Sokolova, V., Ludwig, A.-K., Hornung, S., Rotan, O., Horn, P. A., Epple, M. and Giebel, B. (2011). Characterisation of exosomes derived from human cells by nanoparticle tracking analysis and scanning electron microscopy. Colloids and Surfaces B: Biointerfaces, 87(1): 146-150.

Stone, H. A. and Kim, S. (2001). Microfluidics: basic issues, applications, and challenges. AIChE Journal, 47(6): 1250-1254.

Taylor, D. D. and Gercel-Taylor, C. (2014). Exosome platform for diagnosis and monitoring of traumatic brain injury. Phil. Trans. R. Soc. B, 369(1652): 20130503.

Taylor, D. D. and Shah, S. (2015). Methods of isolating extracellular vesicles impact down-stream analyses of their cargoes. Methods, 87: 3-10.

Telis, V., Telis-Romero, J., Mazzotti, H. and Gabas, A. (2007). Viscosity of aqueous carbohydrate solutions at different temperatures and concentrations. International Journal of food properties, 10(1): 185-195.

Théry, C., Zitvogel, L. and Amigorena, S. (2002). Exosomes: composition, biogenesis and function. Nature Reviews Immunology, 2(8): 569.

Tkach, M., Kowal, J. and Théry, C. (2018). Why the need and how to approach the functional diversity of extracellular vesicles. Philosophical Transactions of the Royal Society B: Biological Sciences, 373(1737): 20160479.

Torr, G. (1984). The acoustic radiation force. American Journal of Physics, 52(5): 402-408.

Urbansky, A., Ohlsson, P., Lenshof, A., Garofalo, F., Scheding, S. and Laurell, T. (2017). Rapid and effective enrichment of mononuclear cells from blood using acoustophoresis. Scientific reports, 7(1): 1-9.

VanDelinder, V. and Groisman, A. (2006). Separation of plasma from whole human blood in a continuous cross-flow in a molded microfluidic device. Analytical chemistry, 78(11): 3765-3771.

Vary, A. and Bowles, K. J. (1979). An ultrasonic - acoustic technique for nondestructive evaluation of fiber composite quality. Polymer Engineering & Science, 19(5): 373-376.

Verhage, M. and Sørensen, J. B. (2008). Vesicle docking in regulated exocytosis. Traffic, 9(9): 1414-1424.

Volpatti, L. R. and Yetisen, A. K. (2014). Commercialization of microfluidic devices. Trends in biotechnology, 32(7): 347-350.

Wang, M. B., Liu, I. Y., Gornbein, J. A. and Nguyen, C. T. (2015). HPV-positive oropharyngeal carcinoma: a systematic review of treatment and prognosis. Otolaryngology–Head and Neck Surgery, 153(5): 758-769.

Wang, X., Chen, S., Kong, M., Wang, Z., Costa, K. D., Li, R. A. and Sun, D. (2011). Enhanced cell sorting and manipulation with combined optical tweezer and microfluidic chip technologies. Lab on a Chip, 11(21): 3656-3662.

Wang, Y., Springer, S., Mulvey, C. L., Silliman, N., Schaefer, J., Sausen, M., James, N., Rettig, E. M., Guo, T. and Pickering, C. R. (2015). Detection of somatic mutations and HPV in the saliva and plasma of patients with head and neck squamous cell carcinomas. Science translational medicine, 7(293): 293ra104-293ra104.

Wang, Z., Huang, P.-H., Chen, C., Bachman, H., Zhao, S., Yang, S. and Huang, T. J. (2019). Cell lysis via acoustically oscillating sharp edges. Lab on a Chip, 19(24): 4021-4032.

Wang, Z., Li, F., Rufo, J., Chen, C., Yang, S., Li, L., Zhang, J., Cheng, J., Kim, Y. and Wu, M. (2020). Acoustofluidic salivary exosome isolation: A liquid biopsy compatible approach for human papillomavirus–associated oropharyngeal cancer detection. The Journal of Molecular Diagnostics, 22(1): 50-59.

Wang, Z., Wang, H., Becker, R., Rufo, J., Yang, S., Mace, B. E., Wu, M., Zou, J., Laskowitz, D. T. and Huang, T. J. (2021). Acoustofluidic separation enables early diagnosis of traumatic brain injury based on circulating exosomes. Microsystems & Nanoengineering, 7(1): 1-11.

Warkiani, M. E., Tay, A. K. P., Guan, G. and Han, J. (2015). Membrane-less microfiltration using inertial microfluidics. Scientific reports, 5(1): 1-10.

Watanabe, A., Taniguchi, M., Tsujie, H., Hosokawa, M., Fujita, M. and Sasaki, S. (2008). The value of narrow band imaging endoscope for early head and neck cancers. Otolaryngology—Head and Neck Surgery, 138(4): 446-451.

Wells, P. N. (1999). Ultrasonic imaging of the human body. Reports on progress in physics, 62(5): 671.

Wiklund, M., Green, R. and Ohlin, M. (2012). Acoustofluidics 14: Applications of acoustic streaming in microfluidic devices. Lab on a Chip, 12(14): 2438-2451.

Wong, D. T. (2006). Towards a simple, saliva-based test for the detection of oral cancer. 'Oral fluid (saliva), which is the mirror of the body, is a perfect medium to be explored for health and disease surveillance.'. Expert review of molecular diagnostics, 6(3): 267-272.

Wu, J. (2007). Shear stress in cells generated by ultrasound. Progress in biophysics and molecular biology, 93(1-3): 363-373.

Wu, M., Huang, P. H., Zhang, R., Mao, Z., Chen, C., Kemeny, G., Li, P., Lee, A. V., Gyanchandani, R. and Armstrong, A. J. (2018). Circulating Tumor Cell Phenotyping via High - Throughput Acoustic Separation. Small, 14(32): 1801131.

Wu, M., Mao, Z., Chen, K., Bachman, H., Chen, Y., Rufo, J., Ren, L., Li, P., Wang, L. and Huang, T. J. (2017). Acoustic separation of nanoparticles in continuous flow. Advanced functional materials, 27(14): 1606039.

Wu, M., Ouyang, Y., Wang, Z., Zhang, R., Huang, P.-H., Chen, C., Li, H., Li, P., Quinn, D. and Dao, M. (2017). Isolation of exosomes from whole blood by integrating acoustics and microfluidics. Proceedings of the National Academy of Sciences: 201709210.

Wu, M., Ouyang, Y., Wang, Z., Zhang, R., Huang, P.-H., Chen, C., Li, H., Li, P., Quinn, D. and Dao, M. (2017). Isolation of exosomes from whole blood by integrating acoustics and microfluidics. Proceedings of the National Academy of Sciences, 114(40): 10584-10589.

Xiong, Y., Mahmood, A. and Chopp, M. (2017). Emerging potential of exosomes for treatment of traumatic brain injury. Neural regeneration research, 12(1): 19.

Yamada, M., Nakashima, M. and Seki, M. (2004). Pinched flow fractionation: continuous size separation of particles utilizing a laminar flow profile in a pinched microchannel. Analytical chemistry, 76(18): 5465-5471.

Yamada, M. and Seki, M. (2005). Hydrodynamic filtration for on-chip particle concentration and classification utilizing microfluidics. Lab on a Chip, 5(11): 1233-1239.

Yoon, Y., Kim, S., Lee, J., Choi, J., Kim, R.-K., Lee, S.-J., Sul, O. and Lee, S.-B. (2016). Clogging-free microfluidics for continuous size-based separation of microparticles. Scientific reports, 6(1): 1-8.

Yosioka, K. and Kawasima, Y. (1955). Acoustic radiation pressure on a compressible sphere. Acta Acustica united with Acustica, 5(3): 167-173.

Yuh, E. L., Mukherjee, P., Lingsma, H. F., Yue, J. K., Ferguson, A. R., Gordon, W. A., Valadka, A. B., Schnyer, D. M., Okonkwo, D. O. and Maas, A. I. (2013). Magnetic resonance imaging improves 3 - month outcome prediction in mild traumatic brain injury. Annals of neurology, 73(2): 224-235.

Zhan, K. Y., Eskander, A., Kang, S. Y., Old, M. O., Ozer, E., Agrawal, A. A., Carrau, R. L., Rocco, J. W. and Teknos, T. N. (2017). Appraisal of the AJCC 8th edition pathologic staging modifications for HPV− positive oropharyngeal cancer, a study of the National Cancer Data Base. Oral oncology, 73: 152-159.

Zhang, P., Chen, C., Su, X., Mai, J., Gu, Y., Tian, Z., Zhu, H., Zhong, Z., Fu, H. and Yang, S. (2020). Acoustic streaming vortices enable contactless, digital control of droplets. Science Advances, 6(24): eaba0606.

Zhang, P., Zhang, G. and Wang, W. (2007). Ultrasonic treatment of biological sludge: floc disintegration, cell lysis and inactivation. Bioresource Technology, 98(1): 207-210.

Zhang, Q. and Austin, R. H. (2012). Applications of microfluidics in stem cell biology. BioNanoScience, 2(4): 277-286.

Zhang, Y., Chopp, M., Meng, Y., Katakowski, M., Xin, H., Mahmood, A. and Xiong, Y. (2015). Effect of exosomes derived from multipluripotent mesenchymal stromal cells on functional recovery and neurovascular plasticity in rats after traumatic brain injury. Journal of neurosurgery, 122(4): 856-867.

Zhang, Y. and Nguyen, N.-T. (2017). Magnetic digital microfluidics–a review. Lab on a Chip, 17(6): 994-1008.

Zhao, Z., Yang, Y., Zeng, Y. and He, M. (2016). A microfluidic ExoSearch chip for multiplexed exosome detection towards blood-based ovarian cancer diagnosis. Lab on a Chip, 16(3): 489-496.

Zhu, M., Cohen, S. R., Hicok, K. C., Shanahan, R. K., Strem, B. M., Johnson, C. Y., Arm, D. M. and Fraser, J. K. (2013). Comparison of three different fat graft preparation methods: gravity separation, centrifugation, and simultaneous washing with filtration in a closed system. Plastic and reconstructive surgery, 131(4): 873-880.

Abgrall, P. and Gue, A. (2007). Lab-on-chip technologies: making a microfluidic network and coupling it into a complete microsystem—a review. Journal of micromechanics and microengineering, 17(5): R15.

Gravesen, P., Branebjerg, J. and Jensen, O. S. (1993). Microfluidics-a review. Journal of micromechanics and microengineering, 3(4): 168.

Jensen, K. F. (2001). Microreaction engineering—is small better? Chemical Engineering Science, 56(2): 293-303.

Jones, W. and Whitelaw, J. (1982). Calculation methods for reacting turbulent flows: a review. Combustion and flame, 48: 1-26.

Landahl, M. T., Mollo‐Christensen, E. and Korman, M. S. (1989). Turbulence and random processes in fluid mechanics, Acoustical Society of America.

Ozcelik, A., Rufo, J., Guo, F., Gu, Y., Li, P., Lata, J. and Huang, T. J. (2018). Acoustic tweezers for the life sciences. Nature methods, 15(12): 1021-1028.

Biography

Zeyu Wang earned his bachelor's degree of science in 2013 from Harbin Institute of Technology, Heilongjiang, China. In 2015, he obtained his master's degree of science in biology from Harbin Institute of Technology. After that, he joined the Acoustofluidic Lab in the Department of Mechanical Engineering and Materials Science at Duke University. Following is a list of his publications:

1. **Zeyu Wang**, Haichen Wang, Ryan Becker, Joseph Rufo, Shujie Yang, Brian Mace, Mengxi Wu, Jun Zou, Daniel T. Laskowitz*, and Tony Jun Huang*, Acoustofluidic separation enables early diagnosis of traumatic brain injury based on circulating exosomes, Microsystems & Nanoengineering, Vol. 7, pp. 20, 2021.
2. **Zeyu Wang**, Feng Li, Joseph Rufo, Chuyi Chen, Shujie Yang, Liang Li, Jinxing Zhang, Yong Kim, Mengxi Wu, Elliot Abemayor, Michael Tu, David Chia, Jordan Cheng, Rachel Spruce, Nikolaos Batis, Hisham Mehanna, David T.W. Wong, and Tony Jun Huang, Acoustofluidic Salivary Exosome Isolation: A Liquid Biopsy Compatible Approach for Cancer Detection, The Journal of Molecular Diagnostics, Vol. 22, pp. 50-59, 2020.
3. **Zeyu Wang**, Po-Hsun Huang, Chuyi Chen, Hunter Bachman, Shuaiguo Zhao, Shujie Yang, and Tony Jun Huang, Cell lysis via acoustically oscillating sharp edges, Lab on a Chip, Vol. 19, pp. 4021-4032, 2019.

4. Zhenhua Tian, **Zeyu Wang**, Peiran Zhang, Ty Downing Naquin, John Mai, Yuqi Wu, Shujie Yang, Yuyang Gu, Hunter Bachman, Yaosi Liang, Zhiming Yu, and Tony Jun Huang, Generating Multifunctional Acoustic Tweezers in Petri Dishes for Contactless, Precise Manipulation of Bioparticles, Science Advances, Vol. 6, No. 37, eabb0494, 2020.
5. Mengxi Wu, Chuyi Chen, **Zeyu Wang**, Hunter Bachman, Yingshi Ouyang, Po-Hsun Huang, Yoel Sadvskyc and Tony Jun Huang, Separating Extracellular Vesicles and Lipoproteins via Acoustofluidics, Lab on a Chip, Vol. 19, pp. 1174-1182, 2019.
6. Yuyang Gu, Chuyi Chen, **Zeyu Wang**, Po-Hsun Huang, Hai Fu, Lin Wang, Mengxi Wu, Yuchao Chen, Tieyu Gao, Jianying Gong, Jean Kwun, Gowthami M. Arepally, and Tony Jun Huang, Plastic-based acoustofluidic devices for high-throughput, biocompatible platelet separation, Lab on a Chip, Vol. 19, pp. 394-402, 2019.
7. Mengxi Wu, Yingshi Ouyang, **Zeyu Wang**, Rui Zhang, Po-Hsun Huang, Chuyi Chen, Hui Li, Peng Li, David Quinn, Ming Dao, Subra Suresh, Yoel Sadovsky, and Tony Jun Huang, Isolation of exosomes from whole blood by integrating acoustics and microfluidics, Proceedings of the National Academy of Sciences of the United States of America (PNAS), Vol. 114, pp. 10584-10589, 2017.
8. Zhenhua Tian*, Shujie Yang*, Po-Hsun Huang, **Zeyu Wang**, Peiran Zhang, Yuyang Gu, Hunter Bachman, Chuyi Chen, Mengxi Wu, Yangbo Xie and Tony Jun Huang,

Wavenumber-spiral acoustic tweezers for dynamic and reconfigurable manipulation of particles and cells, Science Advances, Vol. 5, No. 5, eaau6062, 2019.

9. Mengxi Wu, Kejie Chen, Shujie Yang, **Zeyu Wang**, Po-Hsun Huang, John Mai, Zeng-Yao Li, and Tony Jun Huang, High-throughput cell focusing and separation via acoustofluidic tweezers, Lab on a Chip, Vol. 18, pp. 3003-3010, 2018.
10. Yuyang Gu, Chuyi Chen, Joseph Rufo, Chen Shen, **Zeyu Wang**, Po-Hsun Huang, Hai Fu, Peiran Zhang, Steven Cummer, Zhenhua Tian, and Tony Jun Huang, Acoustofluidic Holography for Micro- to Nano- Scale Particle Manipulation, ACS Nano, Vol. 14, pp. 14635-14645, 2020.
11. Yuyang Gu, Chuyi Chen, Zhangming Mao, Hunter Bachman, Ryan Becker, Joseph Rufo, **Zeyu Wang**, Peiran Zhang, John Mai, Shujie Yang, Jinxin Zhang, Shuaiguo Zhao, Yingshi Ouyang, David T.W. Wong, Yoel Sadovsky, and Tony Jun Huang*, Acoustofluidic centrifuge for nanoparticle enrichment and separation, Science Advances, Vol. 7, No. 1, eabc0467, 2021.
12. Nanjing Hao, Pengzhan Liu, Hunter Bachman, Zhichao Pei, Peiran Zhang, Joseph Rufo, **Zeyu Wang**, Shuaiguo Zhao, and Tony Jun Huang*, Acoustofluidics-Assisted Engineering of Multifunctional Three-Dimensional Zinc Oxide Nanoarrays, ACS Nano, Vol 14, pp. 6150-6163, 2020.
13. Putong Kang*, Zhenhua Tian*,Shujie Yang*,Wenzhuo Yu, Haodong Zhu, Hunter Bachman, Shuaiguo Zhao, Peiran Zhang, **Zeyu Wang**, Ruoyu Zhong, and Tony Jun

Huang, Acoustic tweezers based on circular, slanted - finger interdigital transducers for dynamic manipulation of micro - objects, Lab on a Chip, Vol. 20, pp. 987-994, 2020.

14. Shuaiguo Zhao, Weihua He, Zhehan Ma, Peiyao Liu, Po-Hsun Huang, Hunter Bachman, Lin Wang, Shujie Yang, Zhenhua Tian, **Zeyu Wang**, Yuyang Gu, Zhemiao Xie, and Tony Jun Huang, On-Chip stool liquefaction via acoustofluidics, Lab on a Chip, Vol. 19, pp. 941-947, 2019.